Evaluating and Controlling Glioblastoma Infiltration

by

Joseph F. Georges

A Dissertation Presented in Partial Fulfillment
of the Requirements for the Degree
Doctor of Philosophy

Approved March 2014 by the
Graduate Supervisory Committee:

Burt Feuerstein, Co-Chair
Brian Smith, Co-Chair
Kendall Van Keuren-Jensen
Pierre Deviche
Kevin Bennett

ARIZONA STATE UNIVERSITY

May 2014

ABSTRACT

Glioblastoma (GBM) is the most common primary brain tumor with an incidence of approximately 11,000 Americans. Despite decades of research, average survival for GBM patients is a modest 15 months. Increasing the extent of GBM resection increases patient survival. However, extending neurosurgical margins also threatens the removal of eloquent brain. For this reason, the infiltrative nature of GBM is an obstacle to its complete resection. The central hypothesis of this dissertation is that targeting genes and proteins that regulate GBM motility, and developing techniques that safely enhance extent of surgical resection, will improve GBM patient survival by decreasing infiltration into eloquent brain regions and enhancing tumor cytoreduction during surgery. Chapter 2 of this dissertation describes a gene and protein; aquaporin-1 (aqp1) that enhances infiltration of GBM. In chapter 3, a method is developed for enhancing the diagnostic yield of GBM patient biopsies which will assist in identifying future molecular targets for GBM therapies. In chapter 4, an intraoperative optical imaging technique is developed for improving identification of GBM and its infiltrative margins during surgical resection. This dissertation aims to target glioblastoma infiltration from molecular and cellular biology and neurosurgical disciplines. In the introduction; 1. A background of GBM and current therapies is provided. 2. A protein that decreases GBM survival is discussed. 3. An imaging modality utilized for improving the quality of accrued GBM patient samples is described. 4. An overview of intraoperative contrast agents available for neurosurgical resection of GBM, and discussion of a new agent for intraoperative visualization of GBM is provided.

ACKNOWLEDGMENTS

I would like to express the greatest appreciation to my advisor, Burt Feuerstein MD/PhD. Burt selflessly prioritized my training as a graduate student, and spent substantial time mentoring me in experiment design, data analysis, scientific writing, and grantsmanship. He taught me the value of collaborative research, and helped me acquire training at highly regarded research institutes. Burt always had a plan for my continued growth as a physician-scientist. This was evident in the numerous educational opportunities he provided for me in clinical neuroscience. Without Burt's mentoring and support, this dissertation would not have been possible.

I would also like to thank my committee for supporting my development as a scientist, and creating opportunities for my continued learning. I thank Kendall Van Keuren-Jensen for the countless times she allowed me to interrupt her work to casually chat about neuroscience and experiment design. I also thank Kevin Bennett for providing me opportunities to learn MRI, and for the great memories of working with him and his students. I am grateful to Pierre Deviche for serving as my undergraduate research mentor beginning in 2003, providing me opportunities to work on neuroendocrine projects, and making graduate school a possibility for me. I would also like to thank Brian Smith for his part in creating the interdisciplinary neuroscience program between Arizona State University and Barrow Neurological Institute (ASU-BNI), and for his personal support during graduate school.

Additionally, I thank Trent Anderson and Peter Nakaji for their friendship and mentoring during graduate school. Trent helped me troubleshoot many experiments and always provided great advice towards improving manuscripts. I enjoyed working with

Peter Nakaji at BNI. Dr Nakaji strongly mentored me in clinical neurosurgery research, and he provided me endless opportunities to design and implement molecular imaging projects.

My training as a physician-scientist would not have been possible without the infrastructure and research opportunities created by faculty at ASU-BNI. I would like to thank the researchers who have made this program a great educational experience for myself and fellow classmates.

I would also like to thank the labmates I have enjoyed working with in graduate school. I am grateful for your support during my training and the great times we shared working together. Also, I would like thank my wife Jackie and my family who supported and encouraged me throughout medical and graduate school.

TABLE OF CONTENTS

Page

LIST OF TABLES

LIST OF FIGURES

Figure Page

CHAPTER 1

INTRODUCTION

New brain tumors are diagnosed in more than 40,000 Americans each year . They are the second most common cause of cancer death up to age 35, with a slight peak among children between 6 and 9 years old; but these tumors are most common among middle-aged and older adults. About half of brain tumors are primary - i.e. their origin is intracranial, the remaining tumors are metastases to the brain (Schneider, Mawrin et al. 2010).

Initial efforts to characterize brain tumors were made by Rudolph Virchow in the mid-nineteenth century. His work identified gliomas as a major class of brain tumors (Ferguson and Lesniak 2005). In1926 Percival Bailey and Harvey Cushing published a landmark paper classifying gliomas into 13 unique groups. Bailey later refined this classification into 10 groups. These initial studies showed that each type of brain tumor produced a unique prognosis (Bailey 1985, Ferguson and Lesniak 2005).

Cell Types

Glial cells provide the support structure of the brain. These cells include oligodendrocytes, microglia, ependymal cells, and astrocytes. Oligodendrocytes modulate salutatory conduction in the central nervous system (CNS) through axonal myelination. Microglia are the macrophages of the brain, and respond to pathogens within the CNS. Ependymal cells line ventricles within the CNS and are the source of cerebrospinal fluid. Astrocytes provide structural and biochemical support, are involved in synaptic transmission, and respond to brain injuries (Kandel, Schwartz et al. 2000, McCoy and

Sontheimer 2010, Clarke and Barres 2013). Glial cell interaction is currently a heavily studied field in neuroscience.

Brain Tumors

Primary brain tumors, tumors that arise from cells within the brain, can be classified as benign or malignant. Non-diffuse tumors, such as low grade meningiomas, schwannomas, and pituitary adenomas typically grow slowly and discreetly. These tumors can often be removed by surgery. In contrast, malignant tumors such as high grade gliomas diffusely invade the brain (Louis, Deutsches Krebsforschungszentrum Heidelberg. et al. 2007). These tumors present a challenge to surgical resection and detection of their infiltrative elements (Roberts, Valdes et al. 2012).

Clinical prognostic factors for gliomas include tumor grade, patient age, and performance status (DP Byar 1983, Mahaley, Mettlin et al. 1990, Daumas-Duport 1992, Barker, Prados et al. 1996). The most important current criteria for diagnosis and treatment of human infiltrative gliomas are histologic subtype and grade. Subtype is based on visual and molecular similarity of neoplastic cells to normal cells in the central nervous system. Thus, astrocytomas look like cells of astrocytic lineage and express markers linked to normal astrocytes, and oligodendrogliomas look like cells of oligodendroglial lineage, etc. Histologic grade is scored by the degree of endothelial hyperplasia, necrosis, nuclear atypia, and mitotic activity with low grade tumors exhibiting cellular atypia. High grade gliomas, which tend to be the most infiltrative, exhibit 3 to 4 of these criteria (Daumas-Duport, Scheithauer et al. 1987, Daumas-Duport, Scheithauer et al. 1988, Daumas-Duport 1992).

Current Therapy

Glioblastoma is the most common primary brain tumor. Average GBM survival is 12-15 months. Less than 30% of the 27,000 patients diagnosed with GBM each year will survive beyond 2 years (Schneider, Mawrin et al. 2010, Teodorczyk and Martin-Villalba 2010). In 1980, the post-resection median survival of GBM patients was six months. If chemotherapy and radiation were included at the time the median survival increased to approximately twelve months (Salcman 1980). Decades of focused research have improved GBM characterization and diagnosis. However, current median survival for GBM after aggressive treatment is a modest 12-15 months (Georges, Zehri et al. 2014). Thirty years of research has only increased survival approximately 3 months.

Standard GBM treatment is surgical resection followed by radiation and treatment with the alkylating agent, temozolomide (Hegi, Diserens et al. 2005). GBM resection is aimed at maximal safe resection as aggressive surgery prolongs patient survival. However, in some cases, GBM may reside in critical regions that preclude resection (Sanai and Berger 2008, Sanai and Berger 2009, Sanai and Berger 2011, Sanai, Polley et al. 2011, Bloch, Han et al. 2012). Regardless of completeness of resection, infiltrative cells always remain following surgical cytoreduction leading to recurrence (Di, Mattox et al. 2010). Controlling and/or targeting infiltrative tumor cells may improve the extent of surgical resection and improve patient survival.

Temozolomide (TMZ), a chemotherapeutic agent introduced in 1999, has increased GBM patient survival approximately 3 months. This cytotoxic agent, once converted to its active form in the alkaline tumor environment, damages DNA by methylating DNA guanine bases at the N7, N3, and O-6 positions. TMZ's cytotoxic

effects are mediated by its methylation of guanine at the O6 position (O6-MeG). This prohibits DNA strand elongation by a persistent mismatch of O6-MeG to thymine rather than cystine. Missmatch repair results in a persistent O6-MeG in the template strand and futile cycling of DNA repair which leads to cessation of cell replication and death. However, some tumor cells express MGMT; an enzyme that can efficiently repair O6-MeG. Tumors with this enzyme respond poorly to TMZ (Zhang, Stevens et al. 2012, Hart, Garside et al. 2013). Infiltrative tumor cells may also be less responsive to TMZ since these cells have decreased mitotic activity and may be further away from the alkaline tumor environment (Wolf, Agnihotri et al. 2011, Zhang, Stevens et al. 2012). Therefore, agents specifically targeting infiltrative cells may be required in addition to standard chemotherapeutics.

Radiation is an anti-neoplastic therapeutic typically used with chemotherapy. Radiation damages DNA in mitotically active cells. Cancer cells are less capable of dealing with DNA damage and eventually decrease in mitotic activity or die. Radiation therapy relies on generation of free radicals in oxygen-rich environments. Infiltrative cells undergo a change known as the Warburg effect. Once infiltrative cells migrate away from vasculature their oxygen access diminishes and they switch from aerobic to anaerobic metabolism (Warburg effect).This altered environment and metabolism may attenuate the effects of radiation on infiltrative tumor cells (Wolf, Agnihotri et al. 2010, Wolf, Agnihotri et al. 2011).

Surgical resection, TMZ therapy, and radiation are the current standard of care for GBM patients (Schneider, Mawrin et al. 2010, Sanai, Polley et al. 2011, Hart, Garside et al. 2013). However, infiltrative tumor cells may be less receptive to all these therapeutic

approaches by evading resection and altering physiologic properties targeted by chemotherapy and radiation (Wolf, Agnihotri et al. 2010, Wolf, Agnihotri et al. 2011, Mattox, Li et al. 2012). Controlling GBM infiltration may improve patient outcomes by increasing the efficacy of current GBM therapies.

GBM Infiltration

The infiltrative nature of GBM allows tumor regions to evade surgical resection (Orringer, Lau et al. 2012) and may attenuate the effectiveness of tumor-specific therapeutic agents (Wolf, Agnihotri et al. 2011). Identifying genes and proteins that regulate tumor cell motility may improve efficacy of current therapeutics by providing additional clinical targets for GBM therapy. Inhibiting tumor infiltration may also allow GBM to be treated as a chronic disease by controlling its damage to surrounding brain. Secondly, developing methods to identify infiltrative cells during surgical resection could lead to a greater extent of tumor resection and increased patient survival (Sanai and Berger 2008, Sanai, Polley et al. 2011, Bloch, Han et al. 2012).

Aquaporin-1

We recently identified aquaporin-1expression (AQP1 = gene, aqp1 = protein) as a predictor of GBM patient survival. A clinical nine gene predictive indicator of GBM survival suggests AQP1 is independently prognostic (Colman, Zhang et al.). AQP1 expression is linked to increased motility in normal (McCoy and Sontheimer) and neoplastic glial cells (McCoy and Sontheimer 2007). Our experiments with cultured human GBM cells reveal that AQP1 enhanced motility without significantly altering cell

growth or proliferation. Previously, the physiological role of aqp-1 expression in GBM was unknown. Chapter 2 of this thesis addresses a gap in knowledge related to aqp-1's role in GBM motility.

Aquaporins (AQPs) are a family of mammalian transmembrane proteins. They were first identified by Peter Agre in 1991 while studying red blood cells. CHIP28, later named Aquaporin 1, was the first aquaporin discovered. These small channel proteins (267 amino acids, 30kDA) are mostly known for water transport. We now know of 13 aquaporin proteins (aqp). Aqps 1-6 have been identified to transport water. AQPs 7-13 have been reported to transport water and glycerol (Gonen and Walz 2006).

Aquaporins are tetramers composed of 4 identical monomers. Each monomer contains two repeating elements that contain an asparagine-proline-alanine (NPA) motif. The NPA motifs align once the monomer folds and effectively form a water channel. The channel forms an hour-glass shape. At its narrowest point, the channel transports individual water molecules (Agre 2006).

Aquaporin-1 and Cell Motility

Several aquaporins - AQP-1, 3, 4, 5, and 9 – have been linked to cell motility (Loitto, Karlsson et al. 2009). AQP1 is overexpressed in migrating endothelial cells and AQP3 increases motility of keratinocytes in the skin and corneal epithelial cells in the eye. Normally, AQP1 is only expressed in ependymal cells within the CNS. However, AQP1 and AQP4 are both overexpressed in migrating reactive astrocytes responding to traumatic injury. AQP1 is also linked to motility in neoplasms of the breast, CNS, and lung (Verkman, Hara-Chikuma et al. 2008).

The mechanism of AQP1-mediated motility in GBM and other neoplasms is unknown. Proposed mechanisms of AQP-1 mediated motility include: 1) Rapid water flux may promote cell morphological changes during migration through narrow spaces, 2) Water flux through AQP1 may generate a propulsive force to facilitate directional movement, 3) Local increases in hydrostatic pressure may detach the cell membrane from the cytoskeleton resulting in repolymerization of the cytoskeleton to support the protruded membrane. However, these mechanisms have not been rigorously tested. Assembly of aquaporins' 4 subunits creates a central pore in the protein that transports K^+ ions (Yool and Campbell 2012). Hypotheses of AQP1 mediated motility have focused on water transport, while the functional role of AQP1's potassium ion transport in motility has been generally overlooked. Increased potassium conductance has been shown to enhance the motility of GBM cells (Catacuzzeno, Aiello et al. 2011). If AQP1 overexpression similarly alters K^+ conductance, its role in cell motility may be independent of water transport.

Aquaporin-1 Water Transport Inhibition

Independent study of aqp1-mediated water transport or ion transport on cell motility is not possible with current aqp1 inhibitors. The commonly used aqp1 inhibitors in basic science are mercurial compounds such as HgCl2 and tetraethylammonium (TEA). Unfortunately, these agents are toxic and/or nonspecific for independent testing of AQP1's water transport function (Brooks, Regan et al. 2000, Farina, Rocha et al. 2011).

$HgCl_2$ inhibits AQP1-facilitated water transport by forming a covalent bond with its cysteine 189 residue. C189 is in the pore forming region of loop E, and binding of $HgCl_2$ to this region effectively blocks the water channel (Yool, Brown et al. 2010). Unfortunately, $HgCl_2$ is cytotoxic. It inhibits enzymatic processes, blocks sulfur oxidation processes, enzymatic processes involving B6 and B12, alters cytochrome C processes, and affects cellular mineral levels of Ca, Mg, Zn, and Li. In humans it can cause allergic, immune, and autoimmune responses. Therefore, independent study of aqp1-mediated water transport is problematic with $HgCl_2$ (Sutton and Tchounwou 2006).

TEA may be a less toxic alternative to Hg for inhibiting AQP1 water transport. This compound reversibly binds Tyrosine 186 in AQP1. TEA appears more specific to AQP1 than Hg and may be less cytotoxic. However, this agent also blocks some K+ channels. This precludes its use as a specific agent targeting the water transport function of AQP1 without influencing K+ conductance (Brooks, Regan et al. 2000).

Independent of water transport, aqp1 promotes cation conductance when expressed in oocytes (Boassa, Stamer et al. 2006). Targeted substitution of asparagine for glutamate in the first transmembrane portion of AQP1 has generated a water-impermeable aqp-1 mutant (e17n). Tested in oocytes, e17n failed to produce water flux, but produced cation conductance. Though specific inhibitors of AQP1-mediated water transport are under development (Antonio Frigeri 2007), their antineoplastic activity has not been rigorously studied. Non-water permeating aqp1 mutants, such as e17n, allow for immediate study of specific inhibition of aqp1's water channel.

Chapter 2 of this thesis investigates the relationship between AQP1 water transport and GBM invasion *in vitro* and *in vivo*. Our results suggest aqp1 harbors a

undocumented function that promotes tumor cell motility independent of water transport. This suggests novel inhibitors of aqp1-mediated GBM motility must target regions outside of the water channel.

Cellular Screening of Biospecimens

Our work identifying AQP1 as a prognostic factor was made possible by studying biobanked samples of human GBM. During surgical resection of tumors, tumor samples are immediately frozen and stored for future diagnostic or analytical use (Vaught, Henderson et al. 2012). The necrotic nature of GBM is an obstacle for this technique, as many biobanked samples do not contain the cellularity to appropriately re-capitulate the features of the original tumor. Incorporated into neuro-oncology studies, necrotic tissues could produce erroneous results for researchers (Botling and Micke 2011, Lim, Dickherber et al. 2011, Basik, Aguilar-Mahecha et al. 2013). In clinical trials, GBM patient responses are correlated with molecular characteristics of the participants' tumors. Therefore, storage of necrotic tissue could be detrimental to collecting useful information during a clinical trial. A method for screening biospecimens prior to storage could improve the quality of tissue samples collected for research and clinical use.

Confocal Reflectance Microscopy

Confocal reflectance microscopy (CRM) is an optical imaging modality that can sample thick tissue without the application of contrast agents. CRM generates contrast by raster-scanning a laser across a sample and collecting back-scattered photons after they have passed through a confocal aperture. Similar to fluorescence confocal microscopy,

this technique can generate thin optical sections from examined tissues. However, CRM does not excite fluorophores or cause a detectable Stokes shift (Wirth, Snuderl et al. 2012, Georges, Zehri et al. 2014). Therefore, CRM introduces a small fraction of potentially damaging laser energy into sampled tissue and does not require application of exogenous contrast agents.

In chapter 3, we evaluate the effectiveness of CRM for determining the cellularity of GBM tissue samples prior to biobanking. Secondly, we test if this imaging technique alters the molecular characteristics of examined tissue. We believe CRM will provide means for increasing the diagnostic yield of GBM biospecimens by assessing their cytoarchitecture prior to biobanking.

Visualizing Surgical Margins

Extent of glioblastoma surgical resection and survival are directly correlated. Maximum survival benefit is achieved at greater than 98% tumor volume reduction (Lacroix, Abi-Said et al. 2001, Tonn, Thon et al. 2012). However, high degrees of resection are difficult to achieve due to the infiltrative nature of GBM and the Neurosurgeon's goal of preserving eloquent brain. A means for intraoperative examination of glioma tissue at a cellular level could increase tumor cytoreduction by allowing immediate detailed differentiation between tumor and normal brain (Sanai 2012). Neurosurgeons are equipped with MRI, ultrasonography, and macroscopic fluorescence guided-surgery, but these technologies do not provide visualization of detailed infiltrative tumor margins. In chapter 4, we show the use of a novel contrast

agent can immediately provide specific intraoperative visualization of astrocytic tumors, such as GBM, at the cellular level.

Sulforhodamine 101

Advancing optical technologies such as a laser scanning confocal micropscopy (LSCM) may provide real time histopathological information of GBM *in vivo* and *ex vivo* (Foersch, Heimann et al. 2012). LSCM allows microscopic tissue analysis with cellular and subcellular detail. Contrast of morphological details is typically generated with the application of exogenous fluorescent dyes (Udovich, Besselsen et al. 2009). This technology has recently been studied in the neurosurgical setting to improve resection by providing immediate histological assessment of tumor margins (Sanai, Eschbacher et al. 2011). Currently, three fluorescent contrast agents are approved for *in vivo* neurosurgical applications, these include fluorescein sodium (FNa), indocyanine green (ICG), and aminolevulinic acid (5-ALA). Unfortunately, FNa and ICG only provide non-specific staining, and 5ALA photobleaches too quickly for cellular imaging (Mooney, Zehri et al. 2014). The development of new fluorescent contrast agents that specifically stain astrocytic tumors could provide specific intraoperative diagnoses and allow better identification of the infiltrative margin of brain tumors.

Sulforhodamine 101 (SR101) is a red fluorescent contrast agent that rapidly labels astrocytes with glial fibrillary acidic protein (GFAP)-like specificity; the target for immunohistochemistry staining of astrocytes and astrocytomas (Berens, Bjotvedt et al. 1993, Nimmerjahn, Kirchhoff et al. 2004). However, SR101 is capable of labeling astrocytic cells in minutes, whereas conventional GFAP staining requires a minimum of

24 hours (Nimmerjahn and Helmchen 2012). SR101's potential for neurosurgical use has not been studied. In chapter 4 of this dissertation, we hypothesized that if SR101 similarly labels tumors of astrocytic lineage, such as GBM, it could provide a rapid alternative to GFAP for intraoperative identification of GBM and its infiltrative margins. Unlike fluorescein and indocyanine green, SR101 is capable of providing specific intracellular staining of astrocytic cells. Due to its strong quantum yield and resilience to photobleaching, SR101 can provide real-time visualization of astrocytic cells at the cellular level, which is not possible with 5-ALA.

In chapter 4 of this thesis, we aim to establish whether the selective staining of astrocytic tumors with SR101 is a reliable and reproducible method for rapidly identifying human astrocytoma cells in cell culture, animal models, and fresh human brain tumor biopsies. We hypothesize that combined use of live-cell imaging with SR101 could provide a rapid method for identifying GBM and its infiltrative margins.

Summary

Infiltrative tumor cells provide a challenge to the clinical and surgical treatment of GBM. This dissertation addresses a means for clinically targeting the infiltration of GBM by:

1. Identifying AQP1 as a gene and protein that enhances the infiltration of GBM.
2. Developing a GBM biospecimen screening technique that will aide in discovering future GBM molecular targets.
3. Identifying a new GBM-specific contrast agent that can intraoperatively assess GBM and its margins.

In chapter two, we study the role of AQP1 overexpression in GBM. We identify the prognostic role of this gene and protein from human biospecimens and test its physiological effects in cell culture and animal models of GBM. Next, we develop GBM cells expressing mutants of this protein to determine if its role in GBM cell migration is mediated by water transport. We find aqp1 overexpression can upregulate GBM cell motility independently of water transport.

In chapter three we recognize the current problem of over-sampling necrotic tissue in GBM biobanking. We test confocal reflectance microscopy as a means for screening GBM tissue prior to biobanking. We further evaluate the influence this imaging modality has on downstream molecular analysis of the GBM biospecimens. We find CRM can immediately differentiate cellular from non-cellular GBM biospecimens without altering their molecular characteristics.

Lastly, in chapter four we identify a new intraoperative contrast agent that may assist the identification of GBM and tumor margins during resection. We test this contrast agent in cell culture, animal models of GBM, and fresh human *ex vivo* brain tumor biopsies. As a negative control, we also test this contrast agent on an animal model of central nervous system lymphoma and non-astrocytic human brain tumor biopsies. We find SR101 can provide intraoperative specific visualization of astrocytic tumors and their margins.

CHAPTER 2A

AQUAPORIN 1 PREDICTS SURVIVAL OF MALIGNANT GLIOMA PATIENTS AND INCREASES GLIOMA CELL INVASIVENESS

Glioblastoma (World Health Organization grade 4 glioma; GBM) are highly vascular, infiltrative tumors with 12-15 month median patient survival. Standard treatment is surgical resection, radiation and chemotherapy, but provides modest survival benefit. Since GBM are infiltrative, local therapies do not remove all neoplastic elements, and appropriate therapeutic alternatives for infiltrative cells are not available. These studies address a potential therapeutic target, the water channel protein aquaporin 1 (aqp1). Literature suggests expression of the aquaporin 1 gene (AQP1) correlates negatively with patient survival, and links the protein to cell movement. Our clinical data indicate AQP1 RNA and aqp1 protein are independently prognostic. We developed *ex vivo,* and *in vivo* assays to model likely mechanisms underlying the clinical effects of AQP1. The results suggest that AQP1 decreases GBM patient survival by altering the motility of GBM, but not cell proliferation or survival. Our results suggest that aqp1 protein is a viable therapeutic target.

Introduction

Malignant gliomas represent a treatment challenge for the neuro-oncology team. Patients with the most malignant and common glioma, World Health Organization (WHO) grade 4 or glioblastoma multiforme (GBM), most often die within 2 years of diagnosis, and fewer than 10% become long-term survivors (Stupp, Mason et al. 2005). Even when the surgeon achieves a gross total resection of tumor, microscopic residual cells nearly always remain. Standard therapy treats residual tumor with radiation and chemotherapy, but poor patient survival highlights the challenges of tumor cell invasion for GBM therapy.

Although GBM patient survival is not favorable, clinical-pathologic and molecular approaches suggest there are several forms of disease, and these affect patient outcome. Clinical-pathologic prognostic factors indicate that GBM behavior depends on patient age at diagnosis and performance status, in addition to grade (Scott, Scarantino et al. 1998, Li, Wang et al. 2011). We recently developed a 9-gene molecular indicator of survival that is independent of patient age and tumor grade for patients treated with surgery, radiotherapy, and the alkylating agent temozolamide (Colman, Zhang et al. 2010). One of the mRNA indicators, aquaporin 1 (AQP1), is a major contributor to this signature of GBM gene expression marking poor survival (Phillips, Kharbanda et al. 2006). The work we report here investigates whether a biologic function of AQP1 underlies its relationship to survival, and determines whether its expression marks prognosis.

Aquaporins quickly conduct water across membranes and prevent movement of various ions and other solutes (Gonen and Walz 2006). There are 14 known aquaporins in humans (Verkman 2005, Papadopoulos and Verkman 2013). AQP1, 4, and 9 are found in

the central nervous system. AQP1 is expressed in cerebrospinal fluid-producing cells lining the ventricles, and highly expressed in migrating reactive astrocytes. AQP4 is expressed in endothelial cells and astrocytes throughout the brain. AQP9 is found in the retina.

Aqp1 is a 28 KDa cell membrane channel protein that allows rapid water movement in response to osmotic gradients. It is a 28KDa member of a large protein family (MIP – major intrinsic proteins) that forms pores in cell membranes. Aqp1 functions in water movement across membrane barriers in kidney, brain, eye, erythrocytes, GI tract, sweat glands, and vascular endothelia (Agre, King et al. 2002, Saadoun, Papadopoulos et al. 2002, McCoy and Sontheimer 2007, Hara-Chikuma and Verkman 2008, Papadopoulos, Saadoun et al. 2008). Expression in the central nervous system is typically limited to cells lining the ventricles, and extraventricular expression typically relates to pathological processes (Papadopoulos and Verkman 2013).

Oncology literature suggests aqp1 is related to the malignant phenotype. Recent work indicates AQP1 is a prognostic indicator for clear-cell renal cell carcinoma(Huang, Murakami et al. 2009), and neoplastic cells of several cancers, including GBM, highly express AQP1 RNA (Markert, Fuller et al. 2001, Saadoun, Papadopoulos et al. 2002, Hoque, Soria et al. 2006). One report indicates that aqp1 overexpression allows anchorage independent growth in NIH 3T3 cells (Hoque, Liu et al. 2000), and others suggest it enhances migration and localizes to cell processes associated with movement (Nagashima, Fujimoto et al. 2006, Verkman, Hara-Chikuma et al. 2008). Sontheimer et. al. showed that reactive astrocytes responding to brain injury express AQP1(McCoy and Sontheimer

2010), and that protein kinase C regulates aqp4 water permeability, which is rate limiting for glioma invasion(McCoy, Haas et al. 2010).

We hypothesized both aquaporin 1 protein (aqp and mRNA (AQP1) are prognostic markers for GBM patients based on AQP1's presence in a survival-associated mesenchymal gene signature (Phillips, Kharbanda et al. 2006, Huang, Murakami et al. 2009)and in a multi-gene predictor of survival (Colman, Zhang et al. 2010). This manuscript builds on existing AQP1 mRNA microarray data by validating both protein and mRNA as prognostic in formalin-fixed, paraffin-embedded (FFPE) tissue sections of human tumors, and by suggesting that their relationship to invasion and motility underlies aquaporin1's negative impact on glioma patient survival.

Materials and Methods

Human Patient selection

We collected clinical data on patients with primary WHO grade IV GBM resected at the University of Texas M. D. Anderson Cancer Center from 1993 to 2005. Accessible electronic and/or written clinical records, and formalin fixed, paraffin embedded (FFPE) tumor tissue were other selection criteria. We excluded recurrent tumors. We (K.D.A.) re-reviewed the histopathologic diagnosis of all tumors to confirm grading and evaluate tissue suitability for immunohistochemical (IHC) staining. We collected patient clinical data, including age at diagnosis, date of surgery, date of last follow-up/death, vital status, and date of radiographic progression. The University of Texas M. D. Anderson Cancer Center Institutional Review Board approved all clinical studies.

Human Immunohistochemistry

We carried out IHC staining of FFPE tissue with anti-human Aquaporin 1, clone 1/22 mouse monoclonal antibody (Abcam,Cambridge, MA). We incubated tissue in primary antibody at 4°C overnight at 1:7500 dilution. Two independent reviewers scored IHC blinded to clinical data with a 3-tier system: high, strongly positive in the majority of tumor cells in at least 1 medium power (100 X) microscopic field; intermediate, weak/patchy staining in tumor cells; negative, no staining. We repeated the assay and reached consensus for cases with scoring discrepancy. We re-coded cases scored as intermediate and high as "positive" for multivariate analysis because univariate analysis did not distinguish between intermediate and high staining patient outcomes.

Real-time, reverse transcription polymerase chain reaction (qRT-PCR)

A neuropathologist (K.D.A.) selected FFPE tumor tissue for qRT-PCR by macro-dissection based on representative hematoxylin and eosin stained sections. We isolated total RNA with the MasterPure Complete RNA Purification kit (Epicentre Biotechnologies, Madison, WI) according to the manufacturer's instructions for paraffin-embedded tissue. We reverse transcribed 10 µg of total RNA with random hexamers using TaqMan Reverse Transcription reagents (Applied Biosystems, Foster City, CA). We performed and reported qRT-PCR results as previously described (Colman, Zhang et al. 2010).

Statistical Analysis of GBM Cases

The primary clinical endpoints for analysis were overall survival, progression-free survival, and response to radiotherapy. We measured follow-up intervals from date of surgical resection to date of death or last contact. We defined time to progression from the date of surgery to the date of tumor recurrence or growth as first documented by MRI. We used the method of Kaplan and Meier (Kaplan and Meier 1958) for survival analysis and made comparisons using the logrank test. We determined univariate associations by χ^2 test or, when appropriate, the Fisher exact test (Fisher 1922) for categorical variables and the Wilcoxon rank sum test (Wilcoxon 1945) or Student t-test, when appropriate, for associations with continuous variables. We carried out multivariate analysis using the Cox proportional hazards model (Cox 1972) for survival or Spearman's rank sum test (Spearman 1904). We determined the AQP1 qRT-PCR threshold best able to partition patients by vital status into high and low AQP1 expression by recursive partitioning. Analysis was in JMP 6.0.3 for Macintosh (SAS Institute, Cary, NC).

AQP1 U251 Glioma Model.

We cloned human AQP1 cDNA and red fluorescent protein (RFP) into mammalian retroviral expression vector pLXSN (Clonetech, Mountain View, CA). We generated and packaged pLXSN-AQP1, pLXSN-RFP, and pLXSN-EV (empty vector) virus with Phoenix A cells (American Type Culture Collection, Manassas, VA). We infected U251 glioma cells (American Type Culture Collection) and selected with appropriate antibiotics and by fluorescence activated cell sorting for RFP to generate stable nonclonal cell lines: *U251 parental*: U251 cells infected with pLSXN-RFP. *U251-AQP1*: U251 cells infected

with pLSXN-RFP and pLXSN-AQP1. *U251-EV*: U251 infected with pLSXN-RFP and pLXSN. We incubated all lines in Dulbecco's Minimal Essential Medium (DMEM) with pyruvate, supplemented with 10% FBS, 1% non essential amino acids, and 1% L-glutamine (all from Invitrogen, Grand Island, NY), at 37^0C at 100% relative humidity (Jung, Kim et al.) under 5%CO_2. In some experiments, we treated the cultures overnight with tetraethylammonium chloride (TEA, TOCRIS, Ellisville, MO).

Immunocytochemistry on Cell Lines

We grew U251 derivative lines to 80% confluence on laminin coated coverslips, fixed with 4% paraformaldehyde for 10 min at room temperature, and washed 3X with phosphate buffered saline (PBS). We permeabilized with 0.2% Triton X-100/PBS (Invitrogen, Grand Island, NY), blocked with 3% horse serum/PBS for 1hr at room temperature, and incubated at 4°C overnight with rabbit primary polyclonal antibody to aqp1 (Millipore, Billerica, MA) diluted 1:1000 in PBS. Following three PBS washes, we incubated with secondary Fluorescein-5-Isothiocyanate (FITC) Donkey anti rabbit antibody (Millipore) diluted 1:500 with PBS on the coverslips for 2hr at room temperature. After washing 3X with PBS, we mounted the coverslips on slides with 4', 6-diamidino-2-phenylindole (DAPI)/Prolong Gold (Invitrogen, Grand Island, NY), and imaged with a 63X/1.4NA oil immersion objective on a Zeiss 710 confocal microscope. We visualized the FITC by exciting with 488nm diode laser and collecting 505-525nm emission. We visualized DAPI by exciting with a 405nm diode laser and collecting emission at 450-475nm. Supplemental Figure 5 indicates Aqp1 localizes to apparent

lamellipodia of U251-AQP1. This confirms previous literature (Papadopoulos, Saadoun et al. 2008), and suggests normal physiological localization of aqp1 in U251-AQP1 cells.

Immunofluorescent Confocal Microscopy of Rat Brain Tumor Slices

We permeablized Serial 40um brain sections with PBS containing 0.3% triton, blocked with CAS block (Invitrogen), and incubated overnight in anti-aqp1 primary antibody (Millipore). The next day, we rinsed and incubated sections with Alexa488 anti-rabbit secondary and DAPI (invitrogen). Following immunofluorescent labeling, we mounted sections on slides with Vectashield (Vector labs) and coverslipped with No:1.5 glass.

We imaged slides on a Zeiss LSM710 laser scanning confocal microscrope using a 405nm laser to excite Dapi and a 488nm laser to excite Alexa488. Lasers were raster scanned sequentially to minimize overlap between emission spectra. We tiled low magnification images with a 10x/0.3NA air objective with the confocal aperature set to collect fluorescence from a 30um thick focal plane. For other magnifications, we set the confocal aperature to one Airy unit to minimize photon collection outside the focal plane. We acquired 20x images with a 20x/0.8NA objective, and 63x images with a 63x/1.4NA objective. We used NIH Image J linear functions for all image processing.

Ki67 Cell Proliferation Assay

We immunostained serial 4um paraffin-embedded sections from AQP1 overexpressing (n=5) and Control (n=5) xenograft tumors for Ki67 (MIB-1) and lightly counterstained with hematoxylin. A neuropathologist (JE) calculated the MIB-1 labeling indices.

Cell Counting Proliferation Assay

We plated 10^5 cells into 6 well plates (VWR, Radnor, PA) harvested in triplicate every day for 8 days and counted with a Z2™ Coulter Counter (Beckman Coulter, Inc., Hialeah, FL.).

Cell Survival Assay

We plated 50-100 single cells/well of a 6 well plate, incubated for 10-20 days, and counted colonies in triplicate wells after staining with methylene blue. We define a colony as an aggregate of at least 50 cells (Franken, Rodermond et al. 2006).

Wound closure assay.

We plated ~10^5 cells in 6 well plates, incubated to 100% confluence in 2-3 days, cleared a standard area with a pipette tip, and measured the gap with a Zeiss Axiovert 200 inverted microscope using the Zeiss software line tool to define upper and lower boundaries. We typically measured 5 random sites/time point/cell type, and calculated means, standard deviation, and % gap closure based on differences between time of observation and time at start. We obtained similar wound closure results using cell proliferation inhibitor hydroxyurea (5mM) (Sigma, St. Louis, MO), previously described as an inhibitor of cell proliferation (Jung, Kim et al. 2002).

Water flux assay

We plated five thousand U251-AQP1 cells into each well of a 96 well plate. After two hours, we reduced the volume of each well to 30ul and transferred the plate to the

stage of a DIC-capable Zeiss 710 LSM equipped with a transmitted light PMT. While imaging at 2hz, we added 200ul of hypotonic (150mOsm) artificial cerebrospinal fluid (aCSF) to each well at ~130ul/second (Normotonic aCSF: 126 mM NaCl, 26 mM $NaHCO_3$, 2.5 mM KCl, 1.25 mM NaH_2PO_4, 2 mM $MgSO_4$, 2 mM $CaCl_2$ and 10 mM glucose, pH 7.4). We measured changes in cell cross-sectional area over time with image J software to estimate rate of cell swelling after hypotonic shock. We used a one-way ANOVA followed by a Fisher's LSD multiple comparisons test to detect differences in cell cross sectional area among doses TEA.

Boyden Chamber Migration Assay

We starved cell suspensions of 0.5-1 x 10^6 cells/ml in serum free media overnight, added 300µl to the upper well of a Boyden Chamber (McCoy and Sontheimer 2007) with CytoSelect Cell Migration 8µm pore size polycarbonate membrane inserts (Cell Biolabs, San Diego, CA) and 500µl of media containing 10% fetal bovine serum to the lower wells. We incubated 5hr at 37°C, 5% $C0_2$, aspirated the media inside the insert, transferred the insert to a clean well and quantitated migratory cells at the bottom of the insert with CyQuant® GR Dye (Jones, Gray et al. 2001) Kit (Invitrogen, Grand Island, NY) by detaching the cells, incubating in dye and reading on a fluorescent plate reader (Beckman Coulter, Brea, CA) at 520nm.

Matrigel Invasion

We cultured cells on glass-bottomed 35mm culture dishes with #1.5 optical glass coated with poly L Lysine (MatTek, Ashland, MA), aspirated media following adhesion,

covered cells with 100ul of matrigel (BD Bioscience, San Diego, CA), and incubated 15-20min at 37°C to solidify. We replaced media above the matrigel, and incubated 36 hrs at 37°C, 95% RH, 5% C02. We measured invasion with a Zeiss 710 inverted confocal microscope using Zeiss Zen software in z stack mode taking six readings on x/z and y/z line scans at 3 locations per dish.

Murine Brain Slice Invasion

All animal experiments reported in this manuscript were performed in accordance with the guidelines and regulations set forth by the National Institutes of Health Guide for the Care and Use of Laboratory Animals and were approved by the Institutional Animal Care and Use Committee of the Barrow Neurological Institute of St. Joseph's Hospital and Medical Center, Phoenix, Arizona.

We decapitated a deeply anesthetized rat using 0.1-0.2 ml/250 g of 75.8mg/ml Ketamine and 4.8mg/ml of Xylazine, excised the brain, and placed it in cold sterile PBS. We cut a 4-5mm slice with a 1mm metal template, attached it to a platen in a Vibratome 1500 (Vibratome, St. Louis, MO), cut 300µm coronal slices, floated each in a chamber slide in slice medium (DMEM, 10% FBS, 1% NEAA, 1% L-gluNH2, 1X Penicillin/streptomycin (Invitrogen, Grand Island, NY), and finally removed the medium, leaving a flat, centrally located slice. We injected approximately 1 x 10^5 cells in 1µl on the caudate/putamen of the slice, adhered by incubating 1hr at 37°C, 95% RH, 5% C02, and incubated the preparation in slice medium. We measured invasion with a Zeiss 710 confocal microscope using Zeiss Zen software in z stack mode using six readings on x/z and y/z line scans at 3 locations per slice.

Human Xenograft in Nude Rat

Twenty-six male Crl:NIH-Foxn1^{rnu} rats (5 weeks age) from The Charles River Laboratories International, Inc. (Wilmington, MA) were anesthetized by intramuscular injection of of 10 mg/kg xylazine and 80 mg/kg ketamine (Wyeth, Madison, NJ) and placed in a rodent stereotactic headframe (Model 900, David Kopf Instruments, Tujunga, CA). A 10-mm incision was made to expose bregma. A bur hole was made 3.5 mm lateral to bregma. U251 (n=13 rats) or U251-AQP1 cells (n=13 rats) were infused at a depth of 4.5 mm below the surface of the brain after the syringe (Hamilton) was advanced 5.0 mm to create a 0.5-mm pocket. The cell suspension was infused using a UMP3-1 UltraMicroPump microinjector (WPI, Sarasota, FL) set to a volume of 10 µL with an infusion rate of 3.00 µL/minute. The needle was withdrawn 2 minutes after the injection to minimize backflow of the cell suspension. The bur hole was covered with bone wax, the skin incision was sutured, and the rats were allowed to recover. Rodents were monitored daily for dietary and behavioral changes, and were euthanized at first sign of morbidity.

Results

Aquaporin1 protein predicts poor GBM patient survival

We evaluated 186 GBMs for aqp1 expression and correlated to patient outcome. Table 1 indicates patient characteristics. ***Progression-free survival.*** At a median follow-up of 57 weeks, aqp1 was prognostic for progression-free survival (Figure 1A). The median actuarial time to progression was 36 weeks in the low expressing group compared

to 16 weeks in the high-expressing groups. The 6-month PFS was 18% vs. 37% in the low -expressing groups. ***Overall survival.*** The median overall survival in the aqp1 high-expressing group was 50 wks vs. 97 wks in the low-expressing group ($p<0.0001$, log-rank test) (Figure 1B). Recursive, split-sample validation achieved significance in all iterations by univariate analysis. Patients with high aqp1 expression had a nearly two fold increased risk of death compared to those with low expression. Multivariate analysis including age and extent of surgical resection demonstrated aqp1 was an independent prognostic factor (Table 2).

AQP1 mRNA levels predict patient survival

We reverse transcribed total RNA derived from 67 formalin-fixed paraffin embedded (FFPE) GBM with sufficient available tissue and quantitated AQP1 cDNA via qRT-PCR to support our IHC data. Tumors from patients with < 2yr survival had 2.9-fold higher median expression than tumors from patients with > 2yr survival ($p=0.0069$, Wilcoxon rank sum test) (Figure 1C). Two yr survival for high vs. low tumor AQP1 expression was 67% vs. 29%, consistent with IHC data ($p=0.0001$, log-rank test) (Figure 1D)

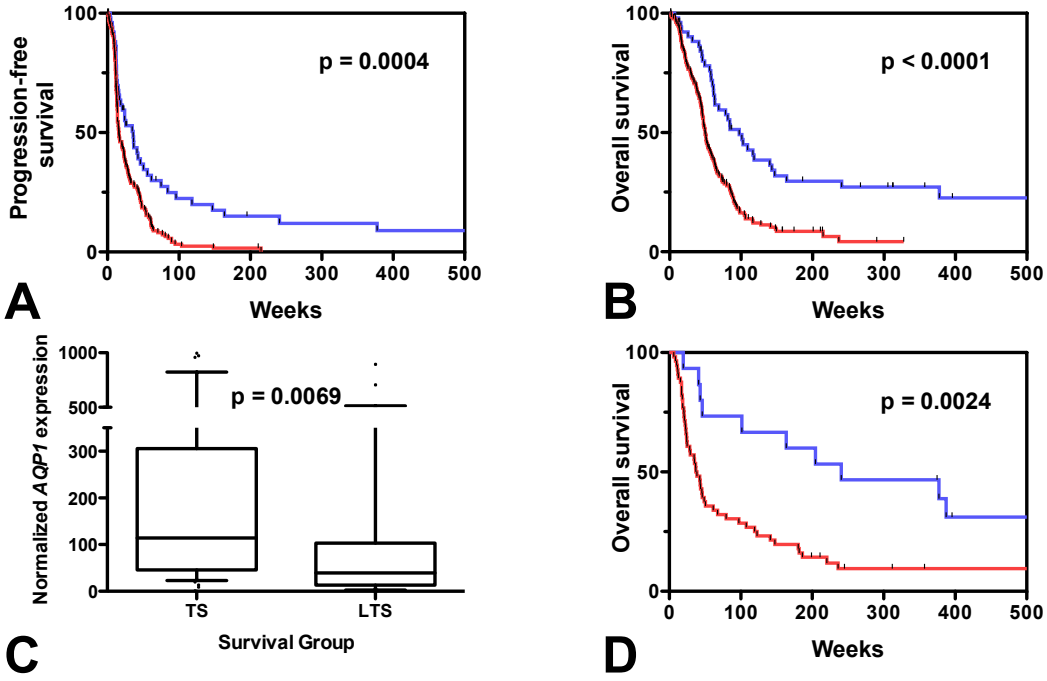

Figure 1: Aquaporin-1 expression is prognostic in GBM. (A) *Progression-free survival.* Kaplan-Meier curves demonstrate progression-free survival (PFS) probability for 186 GBM patients as a function of aqp1 staining by IHC. The data show that high aqp1 expression (red) is associated with poor PFS for patients with GBM. Kaplan-Meier curves demonstrate better PFS among patients with low aqp1 expression by IHC. (B) *Overall survival.* Low aquaporin-1 expression (blue) associated with improved overall survival. (C) qRT-PCR AQP1 on 71 FFPE GBM tumors. Values represent fold change ($2^{-\Delta\Delta Ct}$) normalized to the tumor with lowest expression among all cases. Significantly higher RNA levels in tumors from typical GBM survivors (TS, <2yrs) compared to long-term survivors (LTS, >/= 2yrs) (Wilcoxon rank sum test). (D) Recursive partitioning identified a cut-off for AQP1 expression that best separates survivors from deceased. Stratification ("low" <24.7 fold (blue); "high" >/= 24.7 fold (red)) correlated with OS.

Aqp1 overexpression stimulates glioma cell movement.

In vitro wound closure (Figure 2A- 2C) and migration (Figure 2D) assays indicate direct correlation between AQP1 expression and glioma movement in the absence of host tissue. At two days, wound closure rate was ~3 fold and migration rate ~4 fold faster in aqp1 overexpressors.

Experiments in murine brain slices confirm increased invasion of U251-AQP1 overexpressors over U251-EV empty vector controls (Figure 2E). At day 2, controls invade approximately 35 um, but U251-AQP1 overexpressors invade approximately 51 um. Similarly, cultures under matrigel indicate that AQP1 overexpressers bleb more and migrate faster than U251-EV empty vector controls at 36 hr (29.9 +/- 12.0*um* vs. 19.27+/- 9.5*um*; p=0.02). (Supplemental Figure 1).

Experiments with the putative inhibitor of Aqp1-mediated water diffusion, TEA (Figure 2E) suggest motility is related to aqp1 function. The dose response curve for U251-AQP1 indicates 100 µM TEA limits wound closure to 10%. Literature (Brooks, Regan et al. 2000) suggests that tetraethylammonium chloride (TEA) blocks aqp1 channels at this concentration. Water flux studies indicate a dose dependent relationship between TEA and Aqp1-mediated water transport in our cells, and confirms that our TEA concentrations inhibit water transport (Supplemental Figure 2). The motility increase in empty vector controls at 0.03 mM TEA and in U251-AQP1 at higher TEA concentrations suggest that TEA action – and U251 motility - are not simple functions of aqp1 water transport activity.

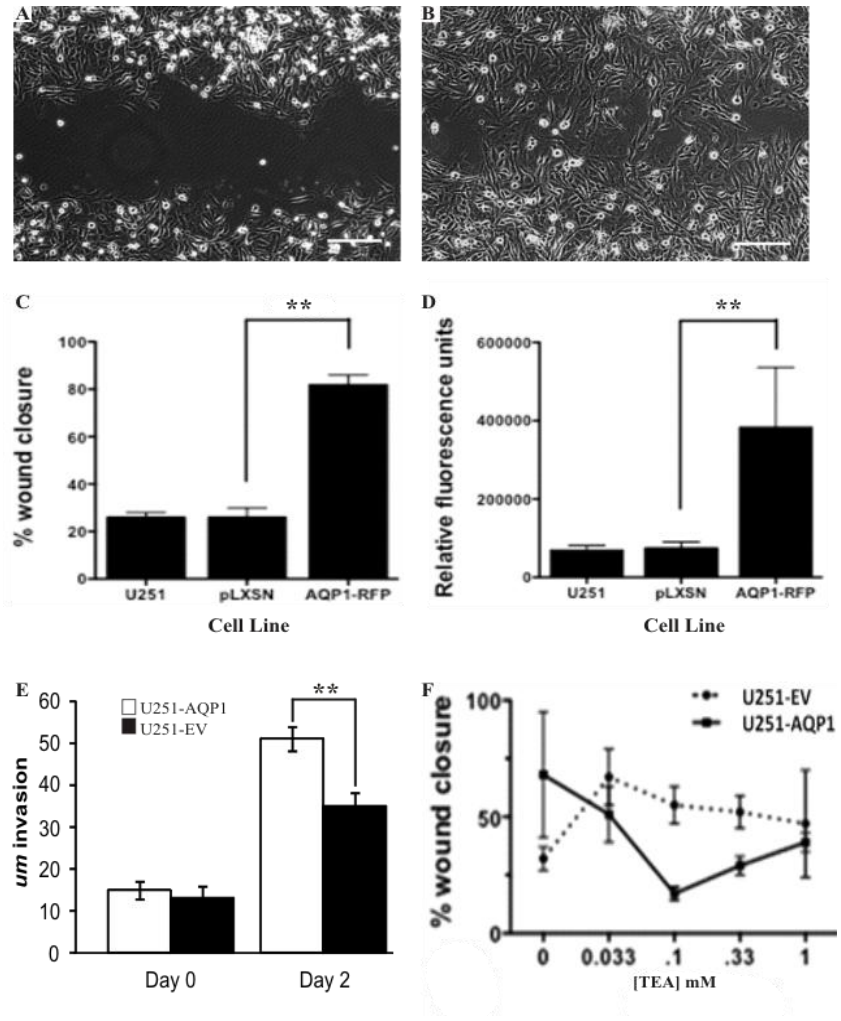

Figure 2: AQP1 overexpression enhances U251 motility. (**A**) Wound closure of U251-EV with empty vector expression at 2 days **(B)** Wound closure of U251 with AQP1 overexpression at 2 days; note greater wound closure compared to U251-EV. **(C)** U251-AQP1 close wounds faster than U251-EV and parental controls 2 days after scratch; p= 0.0008. (**D**) U251-AQP1 overexpression increases migratory activity in a Boyden chamber assay. Parental U251 and U251-EV are negative controls. Relative fluorescence units are proportional to the number of cells moving across a membrane in the chamber. Stable AQP1 overexpressors (AQP1-U251) migrated more quickly than either control (p= 0.037). ((**E**) U251-AQP1 is more invasive than U251-EV in Thy1-YFP mouse brain slice. (Day 2 p-value is 9.9E-09) (**F**) Putative Aqp1 inhibitor tetraethyl ammonium chloride (TEA) inhibits wound closure. TEA inhibits wound closure of AQP1-U251 but not controls in a dose dependent fashion. The error bars reflect +/- 1SD. Scale bars equal 200*um*.

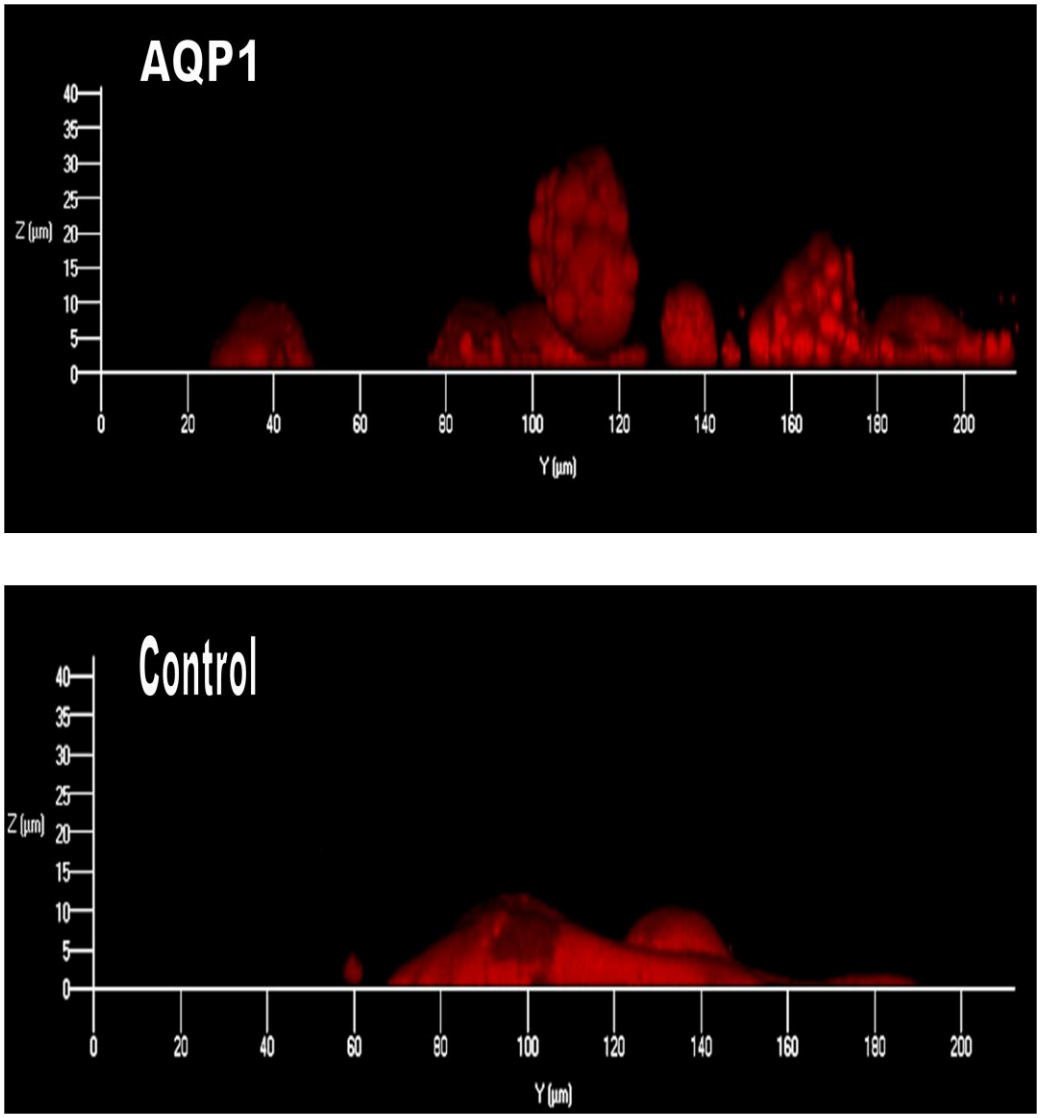

Supplemental Figure 1: U251-AQP1 Migrates faster in Matrigel than control, U251-EV at 24 hr. Confocal images of cells growing into matrigel layered onto cultured cell monolayer. Z Axis indicates matrigel depth. Note blebbing in U251-AQP1 (AQP1) are absent in U251-EV (Control).

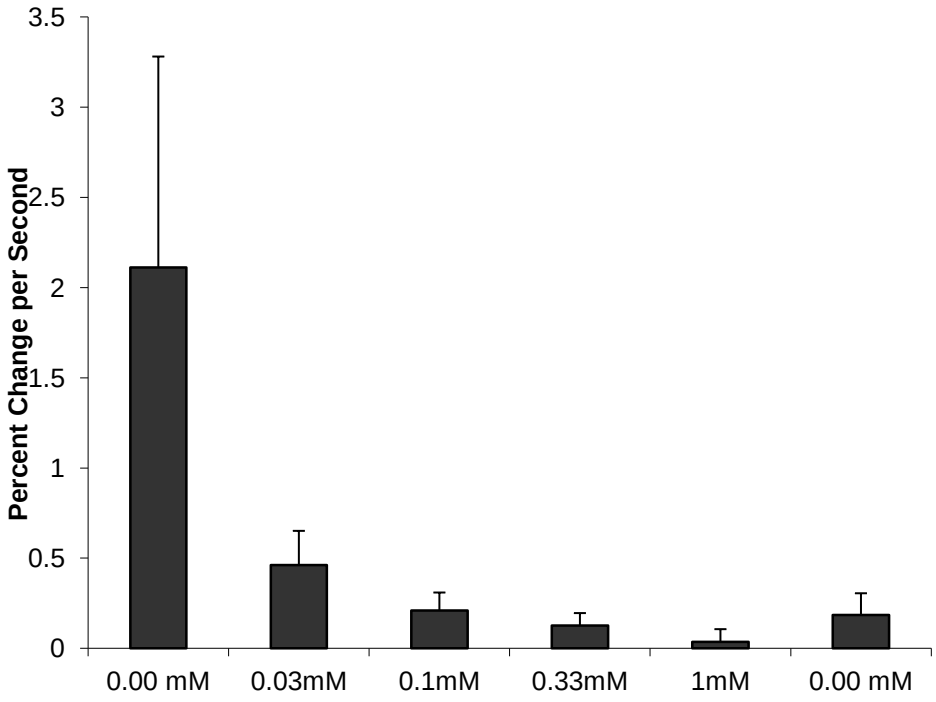

Supplemental 2: TEA attenuates AQP1 mediated water transport. After 150mOSM hypoosmolar exposure, U251-aqp1 cells' cross-sectional area increased at a rate at least four-fold greater than control cells (pLXSN) and TEA treated cells. Cross sectional area of U251-aqp1 cells dosed with 0.03mM TEA increased significantly faster than higher TEA doses, but were significantly slower than U251-aqp1cells not treated with TEA. This suggests a dose response relationship between apparent water transport as measured by cell swelling and concentration of the putative channel blocker TEA.

Control experiments suggest that aquaporin overexpression does not affect proliferation or cell survival in U251-AQP1 overexpressors and U251-EV controls in culture. Our xenograft data confirm this: the MIB-1 labeling index in the most proliferative areas was 49.5% for control tumors and 51% for AQP1 over-expressing tumors (Supplemental Fig 3). The results indicate equivalent cell proliferation in U251-AQP1 overexpressors and U251-EV controls.

Aqp1 immunohistochemistry and confocal fluorescence imaging in rodent xenografts confirm that U251-AQP1 tumors are more invasive than U251-EV controls (Figure 3). The AQP1 cells created a tumor edge with cell clusters/cords that appeared infiltrative (Fig 3A-3E), whereas the controls produced a circumscribed tumor with a more solid edge (Fig 3F-J). Furthermore, we identified U251-AQP1 cells migrating in white matter tracts and in corpus callosum, where Aqp1 expression was directed toward the contralateral hemisphere (Supplemental Fig 4). Controls did not exhibit this invasive behavior. However, both Aqp1 overexpressors and empty vector controls had pleomorphic nuclei.

Glioblastoma AQP1 overexpression decreases survival in rodent xenografts

We produced rodent orthotopic xenografts from human control U251 and U251-AQP1 glioma cells (n= 13 rodents per group). Kaplan-Meier curve and log rank test show median survival for rodents implanted with control U251 glioma cells is 36 days compared to 29 days for U251-AQP1 rodents; p=0.0002 (Figure 4).

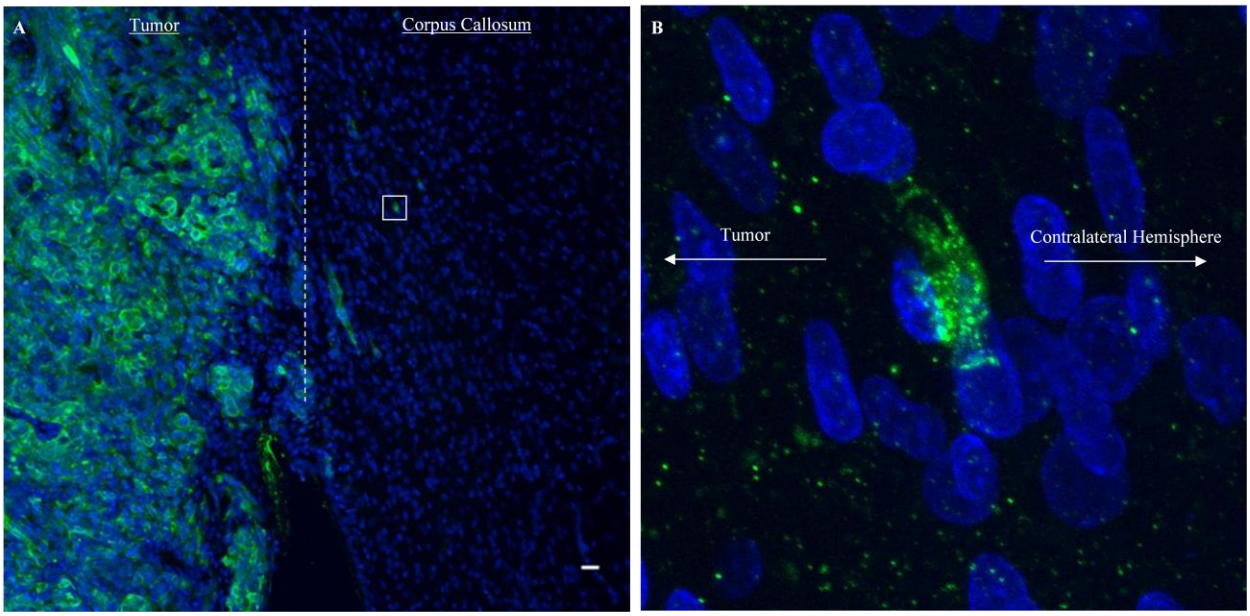

Supplemental figure 4: U251-AQP1 cells in white matter tract orient Aqp1 expression towards contralateral hemisphere. Confocal image of immunostained brain section from rodent xenograft implanted with U251-AQP1. Section stained for Aqp1 (green) and cell nuclei (blue). (A) Low magnification of tumor margin near the corpus callosum. Dashed line indicates location of brain hemispheric separation. (B) Inset from A with AQP1-expressing cell in the corpus callosum. Note AQP1 expression oriented away from tumor and toward contralateral hemisphere. Scale bar equals 50*um*

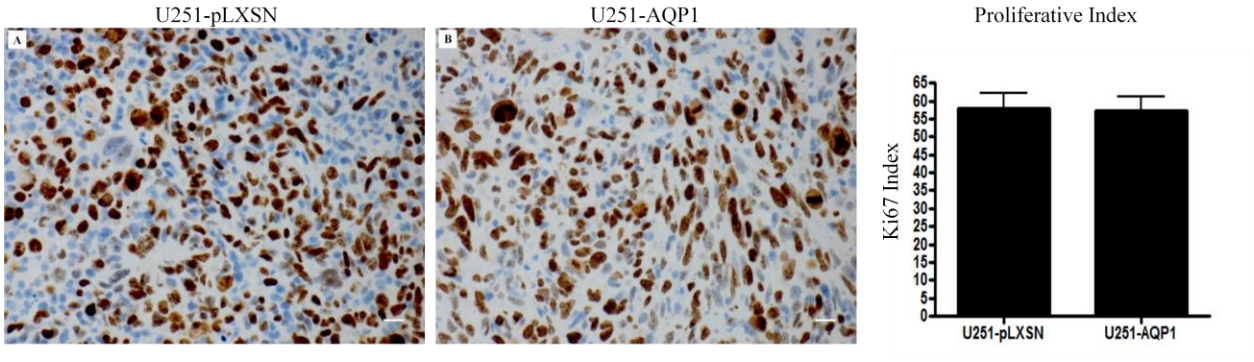

Supplemental Figure 3: AQP1 expression does not alter in vivo tumor proliferation. (A-B)Sections from rodent xenografts immunostained with the proliferative marker Ki67 and counterstained with hematoxylin. (C) U251-pLXSN tumors and U251-AQP1 tumors do not have significantly different Ki67 proliferative indices (p=0.42).

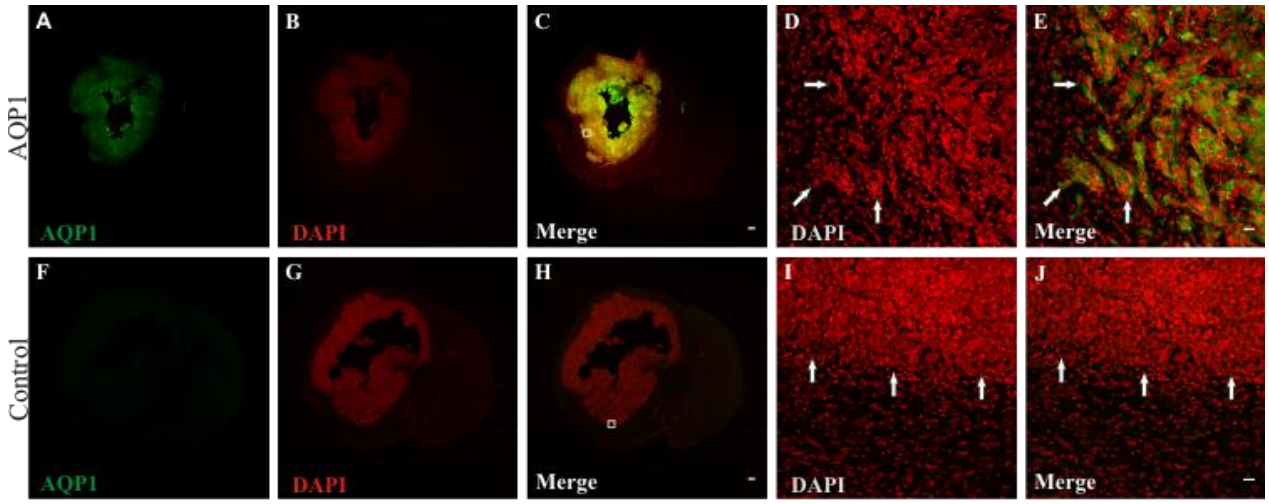

Figure 3: Aquaporin-1 expression enhances infiltration at the tumor margin. Confocal fluorescence images of Aqp1- overexpressing (A-E) and control (F-J) xenograft tumors stained for Aqp1 (green). DAPI counterstain (red) indicates cell nuclei. (A) Aqp1 staining shows expression maintained *in vivo*. (B) DAPI staining of Aqp1-expressing brain section reveals hypercellular tumor.(C) DAPI and Aqp1 staining merged. Note overlap between Aqp1 and tumor. (D) DAPI staining at inset in Fig 3C; DAPI stained nuclei of infiltrative U251 cell clusters/cords at the tumor margin (arrows). (E) Aqp1 expression in infiltrative cell clusters/cords in Fig 3D (F) Minimal aqp1 staining in control tumor. (G) DAPI staining of brain section reveals hypercellular control tumor. (H) Merged image. (I) Inset from Fig 3H; note well-defined tumor border with solid tumor structure (arrows). (J) Merged image from fig 3H shows minimal Aqp1 staining. Scale bars equal 500um (C & H) and 20um (E & J).

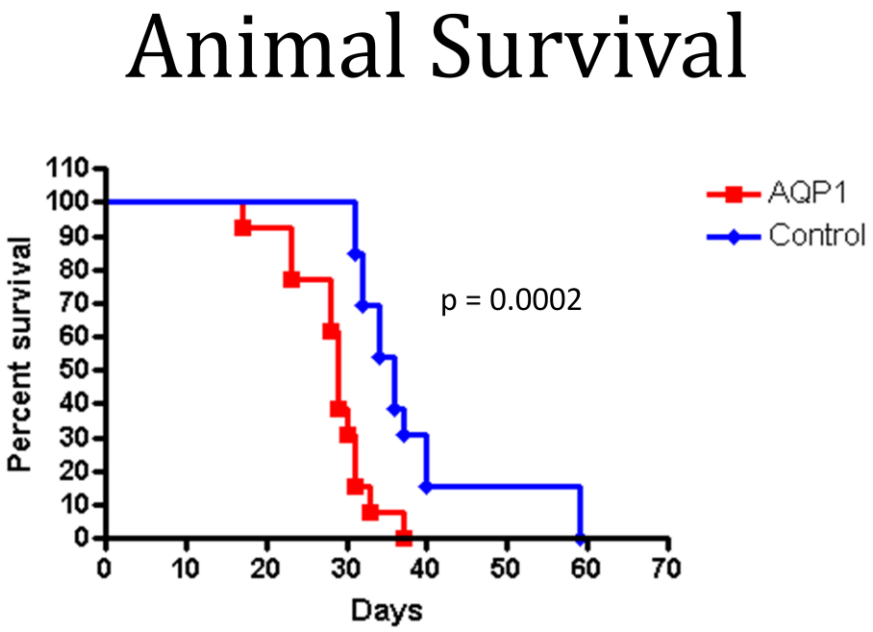

Figure 4: Aquaporin-1 overexpression decreases survival of rodent xenografts. Kaplan-Meier comparison of rodents intracranially implanted with human U251-AQP1 glioma cells to rodents implanted with control U251 glioma cells. Mean survival of U251-AQP1 xenografts is 29 days versus 36 days for control xenografts; p = 0.0002.

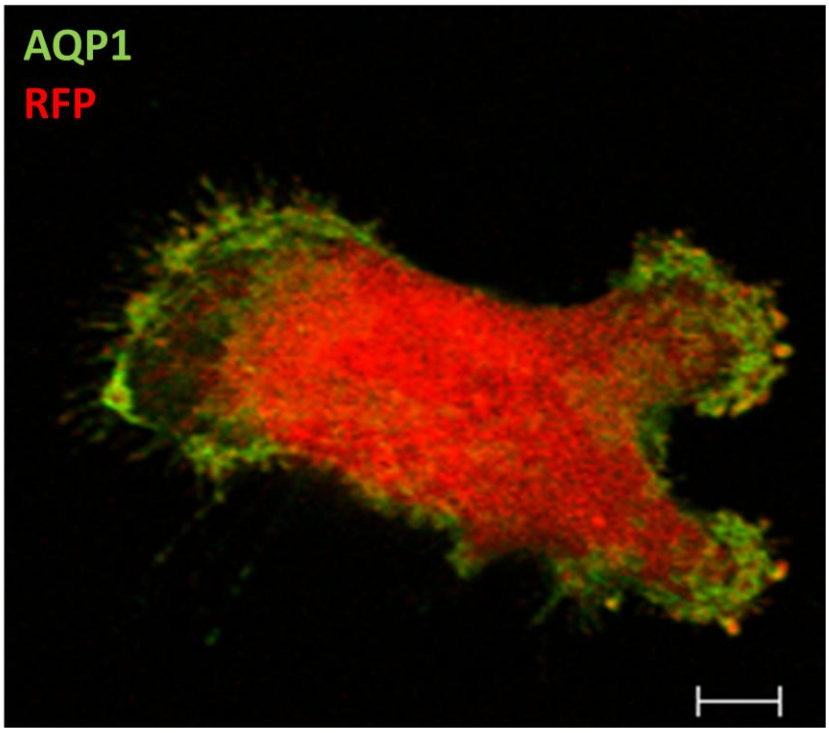

Supplemental 5: Aqp1 Immunocytochemistry. We grew RFP-expressing U251-AQP1 cells on coverslips to ~70% confluence. Polyclonal antibody to Aqp1 and FITC conjugate secondary antibody confirm membrane bound Aqp1 (green) in edge extensions (1). Scale bar equals *5um*.

Discussion

Our data indicate aquaporin 1 protein (aqp1) and message (AQP1) gauge GBM patient outcome, play a critical role in invasion, but do not affect cell proliferation or cell survival. The data suggest aqp1's clinical effects are related to its effects on motility, and not on cell growth or survival.

Median overall and progression free survival doubled when GBM had low aqp1, median survival quadrupled when tumor had low AQP1, and tumors from long term survivors (> 2 yr OS) expressed about 50% less AQP1 than tumors from typical survivors. This prognostic power is independent of age, performance status, or extent of resection (Fig 1, Table 2). The results mirror previous descriptions of a mesenchymal GBM group associated with poor survival (Phillips, Kharbanda et al. 2006) and a nine gene predictor of survival after standard therapy (Colman, Zhang et al. 2010). AQP1 was the leading prognostic indicator in the nine gene predictor series.

We show in Supplemental Figure 5 that aqp1 localizes to edge processes of the cell called lamellipodia (Saadoun, Papadopoulos et al. 2005). Lamellipodia are sheetlike extensions of cytoplasm forming transient adhesion to the cell substrate enabling movement. The data indicate that aqp1 protein is closely associated with cell movement.

Our data demonstrate that AQP1 expression correlates directly with cell migration and invasion as shown by wound closure, Boyden Chamber, brain slice, and matrigel assays (Figure 2 and Supplemental Figure 1). The wound closure rate tripled for U251-AQP1 compared to U251-EV controls and migration rate in a Boyden chamber quadrupled for U251-AQP1 compared to U251-EV control. The murine brain slice assay

indicates much greater invasion for U251-AQP1 than U251EV. The matrigel invasion data support the wound and Boyden chamber data. Invasion of U251-AQP1 is 2-3X the rate of U251-EV in matrigel after 24hr incubation. The results indicate that aqp1 protein is closely associated with cell movement.

Literature supports our wound and Boyden Chamber assay results. Stable transfection of non-endothelial cells with AQP1 accelerated cell migration(Saadoun, Papadopoulos et al. 2005) and aqp1-deficient kidney epithelial cells slowed migration measured by *in vivo* wound healing, and by Boyden chamber assay (Hara-Chikuma and Verkman 2006). AQP1 and AQP5 levels also correlated with invasion in human corneal epithelial cells (HCEC) and cell lines (CEP117) (Shankardas, Patil et al. 2010).

Verkman hypothesizes (Verkman 2005) that aqp1 expression on lamellipodia of migrating cells allows alterations in osmolality following actin depolymerization and ion influx to drive water flux, increasing local hydrostatic pressure and regulating membrane protrusion. Data suggest that aqp1 localizes to lamellipodia and allows quick changes in lamellipodial volume (Verkman, Hara-Chikuma et al. 2008). The hypothesis predicts greater water diffusion mediated by aqp1 results in faster cell movement. Our IHC data support this hypothesis by localizing aqp1 to the lamellipodia involved in migration. This typical aqp1 pattern of distribution also suggests that overexpressed aqp1 in our model emulates natural protein distribution after translation, and suggests that relationships between aqp1 and motility in our model represent physiologic aqp1 function.

Central nervous system AQP1 expression is typically limited to ependymal cells of the choroid plexus (Oshio, Watanabe et al. 2005, Papadopoulos and Verkman 2013).

Therefore, AQP1 overexpression within glioma cells suggests tumor cell genetic instability and/or presence of a different cell type.

Our nude rat xenograft model demonstrates aggressive behavior of U251-AQP1 cells. Figure 3 and supplemental 4 indicate an infiltrative growth pattern at the tumor margin compared to the well-delineated tumor in U251-EV controls. Figure 4 shows the effect of GBM AQP1 overexpression on rodent survival. The results suggest the relationship between poor survival and aqp1 expression in human disease results from aqp1's effects on tumor motility. Histologically, nuclei were equally pleomorphic in control and AQP1 overexpressors and the proliferative index was similar between both groups (Supplemental Figure 3). Our data suggest aqp1 expression does not affect cell proliferation or colony formation, consistent with other reports (Saadoun, Papadopoulos et al. 2005, Hara-Chikuma and Verkman 2006) .

Water penetration across tissue compartments is an important function of aqp1. The relationship between motility and TEA treatment (Figure 2E) suggests aqp1-mediated motility is not entirely regulated by water movement, and confirms that TEA concentrations we use for the experiment reported in fig 2E inhibit water transport in our system. The motility increase in empty vector controls at 0.03 mM TEA and in U251-AQP1 at higher TEA concentrations suggest that TEA action – and U251 motility - are not simple functions of aqp1 water transport activity. TEA's ability to inhibit aqp1-mediated water permeation was originally established and then validated by mutagenizing loop E of aqp1(Jung, Kim et al. 2002). Our data indicate that TEA inhibits Aqp1 mediated water transport and wound closure in a dose dependent manner – 100 uM is the optimal inhibitory concentration for wound closure. The small motility increases in

U251-AQP1 overexpressors at higher TEA concentrations suggest TEA also affects other processes associated with motility. Its ability to increase motility in control U251 cells strengthen this likelihood. In our experiments, controlling for TEA's nonspecific effects on motility strengthen aqp1's relationship to motility. One well-known activity of TEA is to inhibit K+ channel function (Post, Hume et al. 1992); perhaps this or other effects of TEA are a basis for the behavior we document in Figure 2E. Literature suggests TEA inhibition of Cl- and K+ channels result in inhibition of human malignant glioma cell invasion(Soroceanu, Manning et al. 1999) although increases in the motility of control cells (Figure 3E) suggest this is not the case in our system.

Conclusion

Aqp1 is an independent prognostic factor in GBM patients. Our studies of aqp1 overexpression suggest its effects on cell migration form the basis of this protein's ability to affect patient outcome. These data suggest aqp1 is a candidate for therapeutic intervention.

Table 1. Characteristics of patients examined for aqp1 expression

	Value	N	(%)
Total patients		187	(100)
Median age, years	59		
Age range 19-84			
Number <50y		47	(25)
Number ≥50y		140	(75)
Median follow-up, weeks	55		
Follow-up range, weeks	1-394		
Median survival (weeks)			
Overall	58		
Progression-free	26		
Vital Status			
Alive		36	(19)
Deceased		151	(81)
Karnofsky Performance Status			
<70		5	(3)
70 – 80		82	(44)
90 – 100		100	(53)
RTOG RPA Class (Scott, Scarantino et al. 1998)			
III		29	(16)
IV		134	(73)
V+VI		21	(11)
Surgical Resection			
Gross-total		97	(52)
Subtotal		88	(47)
Biopsy only		2	(1)

Table 2: Aqp1 expression is an independent predictor of survival.

Variable		Hazard Ratio	(95% CI)	p-value
Age	(<50y vs. ≥ 50y)	2.3	(1.5 – 3.7)	0.0001
KPS	(<70 vs. 70-80)	1.1	(0.5 – 1.0)	0.0980
	(70-80 vs ≥90)	1.4	(0.4 – 2.6)	
Surgical resection (GTR vs. STR/biopsy)		1.2	(1.0 – 1.4)	0.0850
Aquaporin-1 (high vs. low)		1.9	(1.3 – 2.9)	0.0001

References

Agre, P., L. S. King, M. Yasui, W. B. Guggino, O. P. Ottersen, Y. Fujiyoshi, A. Engel and S. Nielsen (2002). "Aquaporin water channels--from atomic structure to clinical medicine." J Physiol **542**(Pt 1): 3-16.

Brooks, H. L., J. W. Regan and A. J. Yool (2000). "Inhibition of aquaporin-1 water permeability by tetraethylammonium: involvement of the loop E pore region." Mol Pharmacol **57**(5): 1021-1026.

Colman, H., L. Zhang, E. P. Sulman, J. M. McDonald, N. L. Shooshtari, A. Rivera, S. Popoff, C. L. Nutt, D. N. Louis, J. G. Cairncross, M. R. Gilbert, H. S. Phillips, M. P. Mehta, A. Chakravarti, C. E. Pelloski, K. Bhat, B. G. Feuerstein, R. B. Jenkins and K. Aldape (2010). "A multigene predictor of outcome in glioblastoma." Neuro Oncol **12**(1): 49-57.

Cox, D. R. (1972). "Regression models and life tables." J Royal Stat Soc **34**: 187-220.

Fisher, R. A. (1922). "On the interpretation of $\chi 2$ from contingency tables, and the calculation of P." J Royal Stat Soc **85**(1): 87-94.

Franken, N. A., H. M. Rodermond, J. Stap, J. Haveman and C. van Bree (2006). "Clonogenic assay of cells in vitro." Nat Protoc **1**(5): 2315-2319.

Gonen, T. and T. Walz (2006). "The structure of aquaporins." Q Rev Biophys **39**(4): 361-396.

Hara-Chikuma, M. and A. S. Verkman (2006). "Aquaporin-1 facilitates epithelial cell migration in kidney proximal tubule." J Am Soc Nephrol **17**(1): 39-45.

Hara-Chikuma, M. and A. S. Verkman (2008). "Aquaporin-3 facilitates epidermal cell migration and proliferation during wound healing." J Mol Med **86**(2): 221-231.

Hoque, A. T., X. Liu, H. Kagami, W. D. Swaim, R. B. Wellner, B. C. O'Connell, I. S. Ambudkar and B. J. Baum (2000). "Construction and function of a recombinant adenovirus encoding a human aquaporin 1-green fluorescent protein fusion product." Cancer Gene Ther **7**(3): 476-485.

Hoque, M. O., J. C. Soria, J. Woo, T. Lee, J. Lee, S. J. Jang, S. Upadhyay, B. Trink, C. Monitto, C. Desmaze, L. Mao, D. Sidransky and C. Moon (2006). "Aquaporin 1 is overexpressed in lung cancer and stimulates NIH-3T3 cell proliferation and anchorage-independent growth." Am J Pathol **168**(4): 1345-1353.

Huang, Y., T. Murakami, F. Sano, K. Kondo, N. Nakaigawa, T. Kishida, Y. Kubota, Y. Nagashima and M. Yao (2009). "Expression of aquaporin 1 in primary renal tumors: a prognostic indicator for clear-cell renal cell carcinoma." Eur Urol **56**(4): 690-698.

Jones, L. J., M. Gray, S. T. Yue, R. P. Haugland and V. L. Singer (2001). "Sensitive determination of cell number using the CyQUANT cell proliferation assay." J Immunol Methods **254**(1-2): 85-98.

Jung, S., H. W. Kim, J. H. Lee, S. S. Kang, H. H. Rhu, Y. I. Jeong, S. Y. Yang, H. Y. Chung, C. S. Bae, C. Choi, B. A. Shin, K. K. Kim and K. Y. Ahn (2002). "Brain tumor invasion model system using organotypic brain-slice culture as an alternative to in vivo model." J Cancer Res Clin Oncol **128**(9): 469-476.

Kaplan, E. and P. Meier (1958). "Nonparametric estimation from incomplete observations." J Am Stat Assoc **53**: 457-481.

Li, J., M. Wang, M. Won, E. G. Shaw, C. Coughlin, W. J. Curran, Jr. and M. P. Mehta (2011). "Validation and Simplification of the Radiation Therapy Oncology Group Recursive Partitioning Analysis Classification for Glioblastoma." Int J Radiat Oncol Biol Phys.

Markert, J. M., C. M. Fuller, G. Y. Gillespie, J. K. Bubien, L. A. McLean, R. L. Hong, K. Lee, S. R. Gullans, T. B. Mapstone and D. J. Benos (2001). "Differential gene expression profiling in human brain tumors." Physiol Genomics **5**(1): 21-33.

McCoy, E. and H. Sontheimer (2007). "Expression and function of water channels (aquaporins) in migrating malignant astrocytes." Glia **55**(10): 1034-1043.

McCoy, E. and H. Sontheimer (2010). "MAPK induces AQP1 expression in astrocytes following injury." Glia **58**(2): 209-217.

McCoy, E. S., B. R. Haas and H. Sontheimer (2010). "Water permeability through aquaporin-4 is regulated by protein kinase C and becomes rate-limiting for glioma invasion." Neuroscience **168**(4): 971-981.

Nagashima, G., T. Fujimoto, R. Suzuki, J. Asai, H. Itokawa and M. Noda (2006). "Dural invasion of meningioma: a histological and immunohistochemical study." Brain Tumor Pathol **23**(1): 13-17.

Oshio, K., H. Watanabe, Y. Song, A. S. Verkman and G. T. Manley (2005). "Reduced cerebrospinal fluid production and intracranial pressure in mice lacking choroid plexus water channel Aquaporin-1." FASEB J **19**(1): 76-78.

Papadopoulos, M. C., S. Saadoun and A. S. Verkman (2008). "Aquaporins and cell migration." Pflugers Arch **456**(4): 693-700.

Papadopoulos, M. C. and A. S. Verkman (2013). "Aquaporin water channels in the nervous system." Nat Rev Neurosci **14**(4): 265-277.

Phillips, H. S., S. Kharbanda, R. Chen, W. F. Forrest, R. H. Soriano, T. D. Wu, A. Misra, J. M. Nigro, H. Colman, L. Soroceanu, P. M. Williams, Z. Modrusan, B. G. Feuerstein

and K. Aldape (2006). "Molecular subclasses of high-grade glioma predict prognosis, delineate a pattern of disease progression, and resemble stages in neurogenesis." Cancer Cell **9**(3): 157-173.

Post, J. M., J. R. Hume, S. L. Archer and E. K. Weir (1992). "Direct role for potassium channel inhibition in hypoxic pulmonary vasoconstriction." Am J Physiol **262**(4 Pt 1): C882-890.

Saadoun, S., M. C. Papadopoulos, D. C. Davies, B. A. Bell and S. Krishna (2002). "Increased aquaporin 1 water channel expression in human brain tumours." Br J Cancer **87**(6): 621-623.

Saadoun, S., M. C. Papadopoulos, M. Hara-Chikuma and A. S. Verkman (2005). "Impairment of angiogenesis and cell migration by targeted aquaporin-1 gene disruption." Nature **434**(7034): 786-792.

Scott, C. B., C. Scarantino, R. Urtasun, B. Movsas, C. U. Jones, J. R. Simpson, A. J. Fischbach and W. J. Curran, Jr. (1998). "Validation and predictive power of Radiation Therapy Oncology Group (RTOG) recursive partitioning analysis classes for malignant glioma patients: a report using RTOG 90-06." Int J Radiat Oncol Biol Phys **40**(1): 51-55.

Shankardas, J., R. V. Patil and J. K. Vishwanatha (2010). "Effect of down-regulation of aquaporins in human corneal endothelial and epithelial cell lines." Mol Vis **16**: 1538-1548.

Soroceanu, L., T. J. Manning, Jr. and H. Sontheimer (1999). "Modulation of glioma cell migration and invasion using Cl(-) and K(+) ion channel blockers." J Neurosci **19**(14): 5942-5954.

Spearman, C. (1904). ""General intelligence," objectively determined and measured." Am J Psychology **15**: 201-293.

Stupp, R., W. P. Mason, M. J. van den Bent, M. Weller, B. Fisher, M. J. Taphoorn, K. Belanger, A. A. Brandes, C. Marosi, U. Bogdahn, J. Curschmann, R. C. Janzer, S. K. Ludwin, T. Gorlia, A. Allgeier, D. Lacombe, J. G. Cairncross, E. Eisenhauer and R. O. Mirimanoff (2005). "Radiotherapy plus concomitant and adjuvant temozolomide for glioblastoma." N Engl J Med **352**(10): 987-996.

Verkman, A. S. (2005). "More than just water channels: unexpected cellular roles of aquaporins." J Cell Sci **118**(Pt 15): 3225-3232.

Verkman, A. S., M. Hara-Chikuma and M. C. Papadopoulos (2008). "Aquaporins--new players in cancer biology." J Mol Med **86**(5): 523-529.

Wilcoxon, F. (1945). "Individual comparisons by ranking methods." Biometrics Bulletin **1**: 80-83.

CHAPTER 2B

AQUAPORIN-1 OVEREXPRESSION ENHANCES GLIOMA CELL MOTILITY INDEPENDENTLY OF WATER TRANSPORT

Introduction

New brain tumors arise in more than 40,000 Americans each year. They are the second most common cause of cancer death up to age 35, with a slight peak among children between 6 and 9 years old, but these tumors are most common among middle-aged and older adults. About half of brain tumors are primary - i.e. their origin is intracranial; the remaining are metastatic. Clinical prognostic factors for primary brain tumors include tumor grade, patient age, performance status, and radiation response (DP Byar 1983, Mahaley, Mettlin et al. 1990, Daumas-Duport 1992, Barker, Prados et al. 1996). Grade IV glioma (GBM) is the most common primary brain tumor. Standard GBM treatment is surgical resection followed by radiation and temozolomide (Hegi, Diserens et al. 2005). Aggressive resection improves survival (Sanai and Berger 2008). However, infiltrative cells remain following GBM resection leading to recurrence.

We recently reported aquaporin-1 (aqp1) gene and protein as predictors of GBM infiltration and patient survival. A clinical nine gene predictive indicator of GBM survival suggests AQP1 is independently prognostic (Colman, Zhang et al.). AQP1 expression is linked to increased motility in normal and neoplastic glial cells(McCoy and Sontheimer 2007). Our previous work shows that AQP1 promotes GBM migration and invasion. AQP1 is also linked to motility in neoplasms of the breast, CNS, and lung

(Verkman, Hara-Chikuma et al. 2008). Thus, developing an aqp1-targeted GBM therapy may provide a versatile antineoplastic. However, the mechanistic role of aqp1-mediated motility is unknown.

We know of 16 aquaporin proteins (aqp) - water channels that facilitate transmembrane water movement. Some aquaporin genes - AQP-1, 3, 4, 5, and 9 - are implicated in cell motility (Loitto, Karlsson et al. 2009). Functional inhibitors of aquaporin water transport are nonspecific (TEA), and/or toxic (Hg). Thus, independent study of aqp1-mediated water transport on cell motility is not possible with current aqp1 inhibitors.

Non-water permeating aqp1 mutants allow specific study of aqp1's water channel (Yool 2007). Aqp1's 267 amino acid sequence consists of cytosolic loops B and D and extracellular loops A, C, and E. In aqp1's tertiary structure, NPA motifs of loops B and E interact to form the water pore. Mutants alter the alignment of these motifs and restrict water transport. One well-characterized aqp1 mutant substitutes an asparagine for the glutamic acid at the 17 position of the protein (e17n). This mutant functionally inhibits water transport without altering other characteristics of the protein. (Jung, Preston et al. 1994).

Although specific inhibitors of aqp1-mediated water transport are under development (Antonio Frigeri 2007, Yool 2007), their antineoplastic activity has not been rigorously studied. This work investigates the relationship between aqp1 water transport and GBM invasion by studying the effects of e17n overexpression in human GBM cells.

We hypothesize glioma cells overexpressing e17n will have impaired motility compared to glioma cells overexpressing aqp1.

Materials and Methods

Cell lines

We cloned aquaporin-1 (AQP1) and mutant non-water permeating aquaporin-1 (e17n) cDNA into mammalian retroviral vector pLXSN(clonetech), and generated viral particles with PhoenixA cells. We infected two human cell lines (Ln18,U251) with aqp1, e17n, and empty vector cDNA. Cells were selected with 1mg/ml of genticin (Gibco) for three weeks and tested for aqp1 and e17n expression by and immunofluorescence. Cells were maintained in standard DMEM culture media without antibiotic supplementation.

Immunofluorescence

Cells were cultures on No. 1.5 coverslips and fixed with 4% paraformaldehyde then rinsed 3x10 min in PBS, permeabilized with 0.3% triton for 1 hour, and blocked for 1 hour (Cas Block; Invitrogen). Samples were then incubated overnight in 0.1% aqp1 primary antibody (Millipore), rinsed 3x15min with PBS, and incubated with Alexa488 secondary antibody. Samples were incubated for 15 minutes in DAPI and placed on slides with #1.5 coverslips.

We imaged the fluorescently stained cells with a Zeiss710 laser scanning confocal microscope using zen software. DAPI was visualized with 405nm excitation and 450nm emission, and Alexa488 with 488 excitation and 525nm emission. To minimize signal overlap between each fluorophore, we sequentially rastered each laser line during

excitation. We minimized collection of signal from outside the focal plane by setting the confocal aperature to one Airy unit.

Cell Swelling Assay

We placed 1,000 cells into wells of a 96-well glass bottom plate (MatTek). Cell swelling was monitored during immediate 200mOSM hypotonic shock at 2hz using a Zeiss laser scanner confocal microscope (Zeiss LSM710/Live Duo) set for transmitted light microscopy. We quantified the rate of cell swelling by measuring cell cross sectional areas with NIH image J software.

Wound Assay

We seeded 200,000 cells into each well of a six well plate. At 100% confluency, a line of cells was removed from each well with a p200 pipette tip. Five points per scratch were imaged with a Zeiss inverted phase contrast microscope equipped with a motorized stage and mark and find module. Identical regions were imaged every twelve hours for 36 hours and data was analyzed by repeated measures ANOVA followed by Tukeys multiple comparisons test.

Growth Assay

We conducted growth assays on U251 and Ln18 cell lines by seeding 35,000 cells into each well of a twelve well plate. We trypsinized and counted cells from 4 wells per cell type (control, e17n, and aqp1) with a coulter counter at days 1,3,5, and 9. Data was grouped by parental cell line and analyzed by ANOVA and Tukeys multiple comparisons tests.

Rodent xenografts

All animal procedure were approved by ASU/BNI IACUC committees in agreement with NIH standards. Five-week-old male athymic rats were anesthetized with ketamine/xylazine/acepromazine and placed into a stereotaxic frame(Kopf). A 5mm midline incision was made superficial to bregma, and a small burr hole was created at 3.5 lateral to bregma. We infused $1.0x10^6$ cells suspended in 10ul of serum free media 4.5mm deep at 3ul/min (Quintessential Injector;Stoelting). Animals were administered Caprofen to minimize discomfort following surgery and monitored animals daily for morbidity.

Histology

Rodent xenografts were deeply anesthetized and sacrificed by cardiac perfusion of PBS followed by fresh 4% paraformaldehyde (PFA). Brains were excised, fixed overnight in 4degree celsius PFA, and rinsed three times with PBS. Brains were embedded in paraffin, sectioned at *5um* and stained with hematoxylin and eosin.

Results

Immunofluorescence

To study targeted inhibition of aqp1 water transport, we acquired a mutant Aquaporin-1 (e17n) that has restricted water transport (Yool 2007). We infected two gbm cell lines (Ln18 and U251) with aqp1, e17n, and EV viral vectors. We used immunofluorescence to show aqp1 and e17n expression in transduced cells and negligible native aqp1 expression in controls (Figure1: A-F).

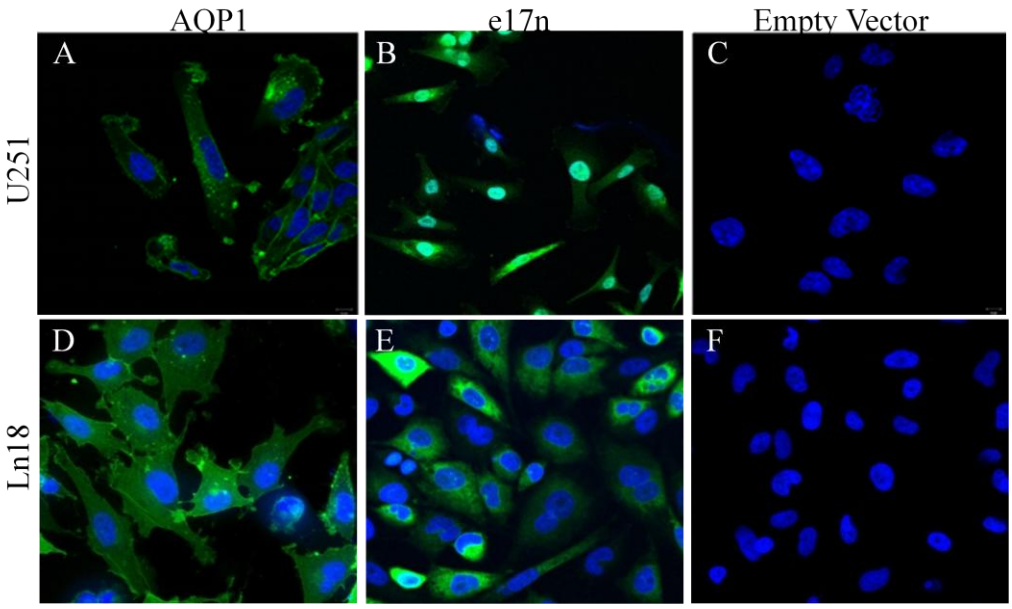

Figure 1: Expression of aquaporin and e17n in two human glioma cell lines. Immunofluorescent images of U251 cells infected to overexpress AQP1 or e17n (DP Byar). Dapi counterstain to visualize cell nuclei. (A,D) U251 and Ln18 cells transduced with AQP1 strongly express the protein in the cytoplasm and cell membrane. (B,E) Cells infected with e17n localize the protein to the plasma membrane and cytoplasm. Note greater cytoplasmic localization for the mutant aqp1 (C,F). Empty vector U251 and Ln18 cells express minimal aqp1.

Water Flux Assay

We utilized a water flux assay to test the function of e17n. We monitored the percent change in cell cross-sectional area by time-lapse imaging after immediate exposure to hypotonic (200 mOsm) aCSF. We found cells expressing aqp1 increased in cross-sectional area at a greater rate than e17n or empty vector control cells which did not differ in rate of increase ($p< 0.0001$). This confirms aqp1 overexpression increases water flux whereas e17n expression does not increase water flux above rate of control cells (Figure 2).

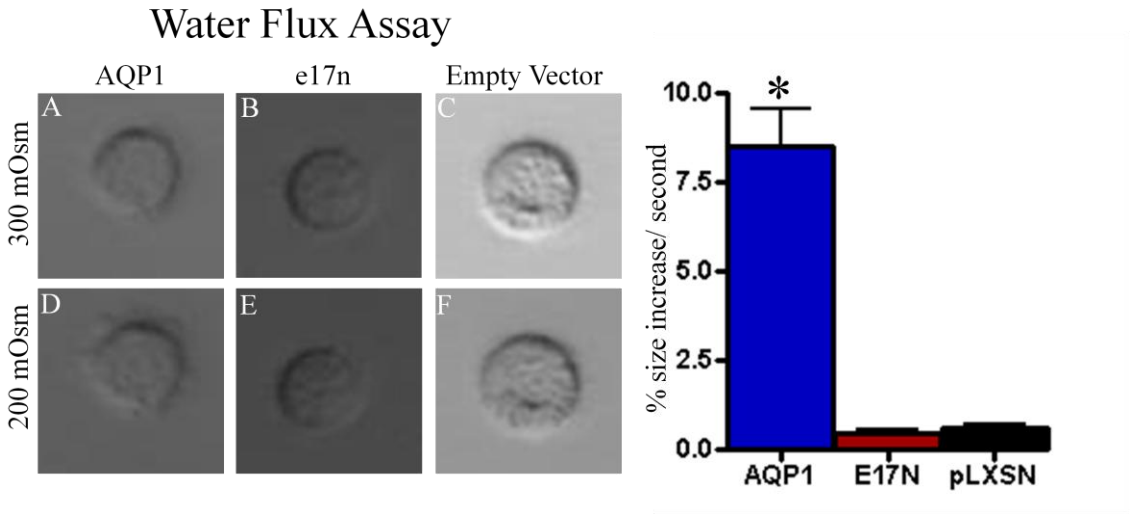

Figure 2: Water flux assay AQP1 overexpressing glioma cells transport water at a greater rate than mutant and empty vector cells. (Verkman, Hara-Chikuma et al.) Cells prior to hypo-osmotic challenge. (D-F) Cells during 200mOsm challenge. Note multiple membrane blebs in AQP1 overexpressing cells. (Bar Graph) AQP1 overexpressing cells transport water at a greater rate than e17n and empty vector cells.

Cell Motility

We tested e17n-mediated motility with a wound assay. Two cell lines engineered to express aqp1, e17n, and empty vectors were cultured. A wound was made in each well once cells reached confluency. We found e17n and aqp1 overexpression both independently promote wound closure in GBM cells compared to control cells ($p< 0.05$) (Figure3: A-E)

Cell Growth

We implanted a growth curve to determine effects of aqp1 and e17n on cell growth. We observed the greatest rate of cell growth occurred between days 3 and 5 for all cell groups. There was no difference between growth of control cells or e17n and aqp1 overexpressing cells at any time point for Ln18 and U251 cell lines ($p> 0.05$)(Figure3: F&G) .

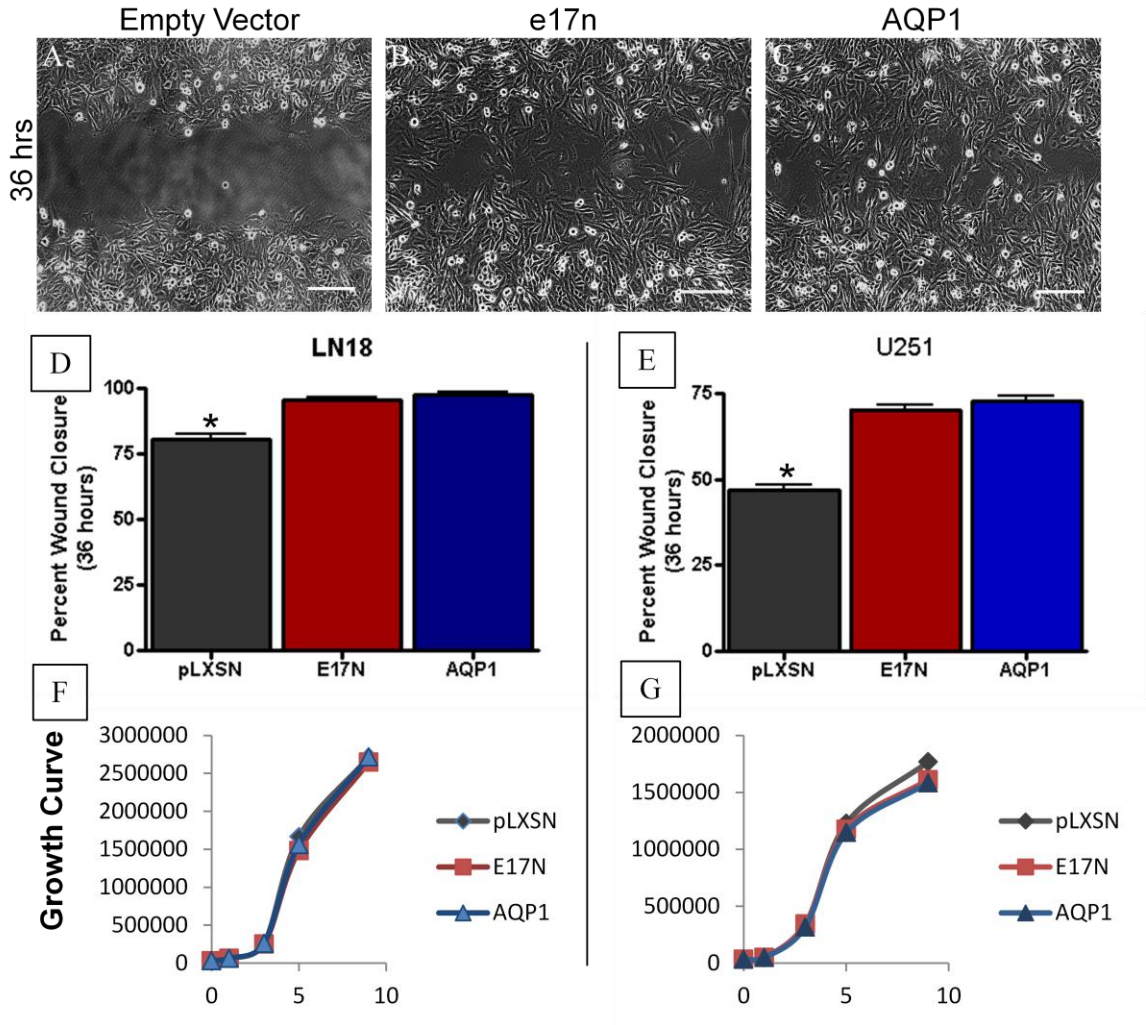

Figure 3: Cell Motility and Growth
Aqp1 upregulates motility independently but does not alter cell proliferation.. (A-E) Wound closure assays. (Verkman, Hara-Chikuma et al.) Phase contrast images of (A) empty vector U251, (B) e17n-U251, and (C) AQP1-U251 after 36hours of wound. (D,E) Empty vector u251 show decreased wound closure at 36 hours compared to e17n and AQP1 expressing glioma cells. (F,G) Cell growth assays. (F)Ln18 and (G) U251 cells overexpressing AQP1 and e17n have similar growth to empty vector control cells. Scale bar equals 200*um*.

Rodent Xenografts

We intracranially injected male nude rats with $1.0x10^6$ newly developed U251 cells expressing aqp1, e17n, and empty vectors. H & E staining of these xenografts contrasts normal tissue with lighter staining, and neoplastic tissue with dark staining. Our data suggest both aqp1 and e17n produce more infiltrative tumor margins than tumors not overexpressing these proteins. (Figure4: A-C).

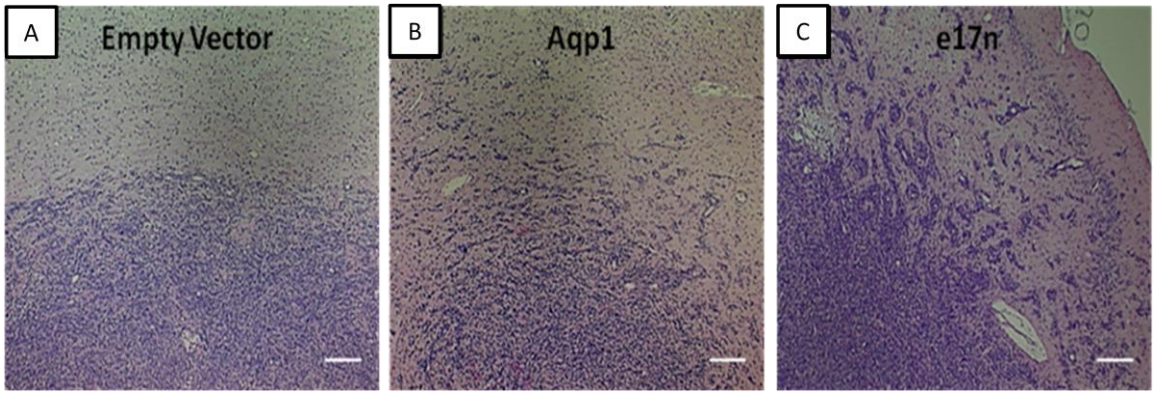

Figure4: Mutant Xenograft Histology
AQP1 enhances brain tumor infiltration and decreases rodent survival. (Verkman, Hara-Chikuma et al.) H and E stained sections from rodent xenografts. (A) Empty vector control human glioma cell tumor border. Note well delineated tumor margin. (B) Aqp1-overexpressing tumor margin with infiltrative cells. (C) Mutant aquaporin tumor with infiltrative tumor margin. Scale bar equals 200*um.*

Discussion

Aquaporin-1 is upregulated in cancers of the breast, colon, and kidney (Otterbach, Callies et al. 2008, Huang, Murakami et al. 2009, Jiang 2009). Our previous work additionally showed AQP1 was overexpressed in glioblastoma (Oshio, Binder et al. 2005). We found aqp1 to be predictive of GBM patient survival, with low aqp1 expressors surviving 97 weeks, and high expressors surviving an average of 50 weeks. In GBM, aqp1 increases the infiltration of tumor cells without effecting their growth or proliferation. A similar hyper-motile phenotype is appreciated in other cancers that over-express aqp1 (Hu and Verkman 2006, Jiang 2009). Current hypotheses attribute changes in motility to water transport (Papadopoulos, Saadoun et al. 2008). However, our findings suggest aqp1 harbors a water transport-independent function that accelerates cell motility.

Therapeutic targeting of AQP1 is hindered by the lack of aqp1-specific agents. To circumvent this, researchers have used non-specific water channel inhibitors such as mercury and tetraethylammonium (TEA). However, these inhibitors block additional channels (ie: TEA) and/or are toxic (ie:Hg) (Brooks, Regan et al. 2000, Farina, Rocha et al. 2011). Therefore, our findings that e17n and aqp1 similarly increase motility in glioma cells suggest pure inhibition of water transport will not necessarily inhibit aqp1-mediated motility.

Our observations suggest aqp1 up-regulates cell motility independently of water transport. Others have eluded to multiple functions for aqp1 (Monzani, Bazzotti et al. 2009, Yool and Campbell 2012). In our studies, we developed glioma cells expressing a mutant aqp1 incapable of water transport (e17n). We verified the lack of water transport

for e17n with hypotonic cell-swelling assays and found e17n-expressing cells to transport water at a similar rate to empty vector control cells; a rate much less than cells expressing aqp1. Our in-vitro assays show that glioma cell lines over-expressing e17n have enhanced motility similar to cells over-expressing wild-type aqp1.

Our previous work with rodent xenografts showed that a typically non-invasive human glioma cell line could become more invasive after aqp1 overexpression. The infilitrative margins we observed in e17n- overexpressing tumors suggest this effect is independent of water transport. This is in contrast to control tumors that produce well-demarcated tumor margins.

We recognize limitations in our work include the use of cell lines that do not fully recapitulate the human form of GBM. Future work exploring the effects of aqp1 and e17n expression in primary tumor cells and neurospheres may provide additional insight towards the mechanism(s) decreasing human survival. However, our data suggest targeting aqp1 molecular regions outside the water channel may be required to control the malignancy of high grade tumors such as glioblastoma.

References

2010, from http://www.castlebiosciences.com/.

National Cancer Institute:
Surveillance, Epidemiology and End Results (SEER) Database.

Antonio Frigeri, G. P. N., Maria Svelto (2007). "Aquaporins as Targets for Drug Discovery." Current Pharmaceutical Design **13**(23): 2421-2427.
Barker, F. G., 2nd, M. D. Prados, S. M. Chang, P. H. Gutin, K. R. Lamborn, D. A. Larson, M. K. Malec, M. W. McDermott, P. K. Sneed, W. M. Wara and C. B. Wilson (1996). "Radiation response and survival time in patients with glioblastoma multiforme." J Neurosurg **84**(3): 442-448.

Brooks, H. L., J. W. Regan and A. J. Yool (2000). "Inhibition of aquaporin-1 water permeability by tetraethylammonium: involvement of the loop E pore region." Mol Pharmacol **57**(5): 1021-1026.

Colman, H., L. Zhang, E. P. Sulman, J. M. McDonald, N. L. Shooshtari, A. Rivera, S. Popoff, C. L. Nutt, D. N. Louis, J. G. Cairncross, M. R. Gilbert, H. S. Phillips, M. P. Mehta, A. Chakravarti, C. E. Pelloski, K. Bhat, B. G. Feuerstein, R. B. Jenkins and K. Aldape "A multigene predictor of outcome in glioblastoma." Neuro Oncol **12**(1): 49-57.

Daumas-Duport, C. (1992). "Histological grading of gliomas." Curr Opin Neurol Neurosurg **5**(6): 924-931.

DP Byar, S. G. a. T. S. (1983). Prognostic Factors For Malignant Gliomas. Oncology of the Nervous System. Boston, Martinus Nijoff.

Farina, M., J. B. Rocha and M. Aschner (2011). "Mechanisms of methylmercury-induced neurotoxicity: evidence from experimental studies." Life Sci **89**(15-16): 555-563.

Hegi, M. E., A. C. Diserens, T. Gorlia, M. F. Hamou, N. de Tribolet, M. Weller, J. M. Kros, J. A. Hainfellner, W. Mason, L. Mariani, J. E. Bromberg, P. Hau, R. O. Mirimanoff, J. G. Cairncross, R. C. Janzer and R. Stupp (2005). "MGMT gene silencing and benefit from temozolomide in glioblastoma." N Engl J Med **352**(10): 997-1003.

Hu, J. and A. S. Verkman (2006). "Increased migration and metastatic potential of tumor cells expressing aquaporin water channels." FASEB J **20**(11): 1892-1894.

Huang, Y., T. Murakami, F. Sano, K. Kondo, N. Nakaigawa, T. Kishida, Y. Kubota, Y. Nagashima and M. Yao (2009). "Expression of aquaporin 1 in primary renal tumors: a prognostic indicator for clear-cell renal cell carcinoma." Eur Urol **56**(4): 690-698.

Jiang, Y. (2009). "Aquaporin-1 activity of plasma membrane affects HT20 colon cancer cell migration." IUBMB Life **61**(10): 1001-1009.

Jung, J. S., G. M. Preston, B. L. Smith, W. B. Guggino and P. Agre (1994). "Molecular structure of the water channel through aquaporin CHIP. The hourglass model." J Biol Chem **269**(20): 14648-14654.

Loitto, V. M., T. Karlsson and K. E. Magnusson (2009). "Water flux in cell motility: expanding the mechanisms of membrane protrusion." Cell Motil Cytoskeleton **66**(5): 237-247.

Mahaley, M. S., Jr., C. Mettlin, N. Natarajan, E. R. Laws, Jr. and B. B. Peace (1990). "Analysis of patterns of care of brain tumor patients in the United States: a study of the Brain Tumor Section of the AANS and the CNS and the Commission on Cancer of the ACS." Clin Neurosurg **36**: 347-352.

McCoy, E. and H. Sontheimer (2007). "Expression and function of water channels (aquaporins) in migrating malignant astrocytes." Glia **55**(10): 1034-1043.

Monzani, E., R. Bazzotti, C. Perego and C. A. La Porta (2009). "AQP1 is not only a water channel: it contributes to cell migration through Lin7/beta-catenin." PLoS One **4**(7): e6167.

Oshio, K., D. K. Binder, Y. Liang, A. Bollen, B. Feuerstein, M. S. Berger and G. T. Manley (2005). "Expression of the aquaporin-1 water channel in human glial tumors." Neurosurgery **56**(2): 375-381; discussion 375-381.

Otterbach, F., R. Callies, R. Kimmig, K. W. Schmid and A. Bankfalvi (2008). "[Aquaporin 1 expression in invasive breast carcinomas]." Pathologe **29 Suppl 2**: 357-362.

Papadopoulos, M. C., S. Saadoun and A. S. Verkman (2008). "Aquaporins and cell migration." Pflugers Arch **456**(4): 693-700.

Sanai, N. and M. S. Berger (2008). "Glioma extent of resection and its impact on patient outcome." Neurosurgery **62**(4): 753-764; discussion 264-756.

Verkman, A. S., M. Hara-Chikuma and M. C. Papadopoulos (2008). "Aquaporins--new players in cancer biology." J Mol Med **86**(5): 523-529.

Yool, A. J. (2007). "Dominant-negative suppression of big brain ion channel activity by mutation of a conserved glutamate in the first transmembrane domain." Gene Expr **13**(6): 329-337.

Yool, A. J. (2007). "Functional domains of aquaporin-1: keys to physiology, and targets for drug discovery." Curr Pharm Des **13**(31): 3212-3221.

Yool, A. J. and E. M. Campbell (2012). "Structure, function and translational relevance of aquaporin dual water and ion channels." Mol Aspects Med **33**(5-6): 553-561.

CHAPTER 3

CONTRAST-FREE MICROSCOPIC ASSESSMENT OF GLIOBLASTOMA BIOSPECIMENS PRIOR TO BIOBANKING

Glioblastoma (World Health Organization grade 4 glioma; GBM) is the most common primary brain tumor with a 12-15 month median patient survival. Improving patient survival involves better understanding the biological mechanisms of GBM tumorgenesis and seeking targeted molecular therapies. Central to furthering these advances is the collection and storage of surgical biopsies (biobanking) for research. Unfortunately, due to the necrotic feature of GBM and our inability to assess tissue prior to biobanking, the majority of biobanked GBM samples lack appropriate cellularity to be utilized in research. This manuscript addresses an imaging modality (confocal reflectance microscopy; CRM) for safely screening GBM biopsies prior to biobanking to increase the quality of tissue provided for research and clinical trials. CRM is a light scattering imaging modality that can generate contrast from cells and tissue without exogenous contrast agents. Our data indicate that CRM can immediately identify cellularity of tissue biopsies from animal models of GBM. When screening fresh human biopsies, CRM can differentiate a cellular GBM biopsy from a necrotic biopsy. Compared to controls, CRM does not alter the DNA, RNA, or protein expression of sampled tissue. Our data illustrate CRM's potential for rapidly and safely screening clinical biopsies prior to biobanking. This information can augment data gained from resected tissue for molecular and translational research, and for determining the eligibility of GBM patients for enrollment into clinical trials. Secondly, this method provides a digital histological record of a biopsy that can be stored along with a biobanked specimen. Our data show CRM to be a

robust screening technique that can improve the quality of tissue biobanked for glioblastoma patients.

Introduction

Each year, over 22,000 Americans are diagnosed with high-grade gliomas. More than half of these brain tumors are Glioblastoma (GBM), the most aggressive and essentially non-curable form of this disease (Dolecek, Propp et al. 2012). Standard treatment for newly diagnosed GBM is surgical resection followed by ionizing radiation and chemotherapy (Lefranc, Brotchi et al.) . However, current therapeutic approaches provide minimal survival benefit with median survival remaining formidably at 12 months and two-year survival remaining less than 30% (Stupp, Mason et al. 2005, Furnari, Fenton et al. 2007).

A key component to improving patient survival involves a better understanding of the biological mechanisms in tumor formation and seeking targeted molecular therapies (Mohyeldin and Chiocca 2012). With recent advances in medical genetics, computational biology, and biotechnology, novel molecular approaches such as immune, vaccine, and gene therapy are being extensively explored in treating brain tumors. Central to furthering these advances requires collecting surgical biopsies (biobanking) to study for gliomagenesis or to assess a patient's eligibility for potential life-prolonging clinical trials. Unfortunately, due to the necrotic feature of malignant gliomas and our inability to assess tissue prior to biobanking, the majority of biobanked GBM samples lack appropriate cellularity to be utilized in these two research arenas. A method for safely

screening tissue biopsies prior to biobanking is needed to increase the quality of tissue provided for research and clinical trials.

Confocal reflectance microscopy (CRM) is an optical imaging modality that can rapidly assesses tissue without physical manipulation or application of exogenous contrast agents (Campo-Ruiz, Ochoa et al. 2002, Tilli, Cabrera et al. 2007). In CRM, a laser is raster-scanned across a specimen without generating a detectable stokes-shift. Photons from the laser are scattered back towards the objective and passed through a confocal aperature. This allows multiple optical sections to be collected from a sample without physical sectioning. When applied to thick tissue samples, CRM can identify individual cells and structural components within the tissue (Campo-Ruiz, Ochoa et al. 2002). Compared to other optical sectioning techniques (ie: fluorescence confocal microscopy, structured illumination, non-linear microscopy), CRM introduces a fraction of energy into tissue samples. Thus, it is least likely to alter tissue characteristics by generation of free radicals or thermal energy.

We hypothesized CRM would provide a safe and rapid means for screening GBM tissue appropriate for biobanking. In this study we first utilize CRM to assess tissue cellularity from rodent glioma models, then evaluate alterations to the molecular integrity of tissue imaged with CRM. Lastly, we test CRM on clinical samples with a pathology-based CRM system. Our data illustrate CRM's potential for screening clinical biopsies prior to biobanking. Though multidiscipline applications for intraoperative CRM exist, our immediate goal is to determine its efficacy as a robust screening technique that will improve the quality of tissues collected and biobanked for brain tumor patients.

Material and Methods

Intracranial implantation

Nude rats were acquired from Charles River Laboratories. Rats (n=5) were anesthetized by intramuscular injection of a mixture of 10 mg/kg xylazine and 80 mg/kg ketamine (Wyeth, Madison, NJ) and placed in a small animal stereotactic headframe (Model 900, David Kopf Instruments, Tujunga, CA). A 10-mm incision was made starting between the animal's eyes to expose bregma. A bur hole was made 3.5 mm lateral to bregma. Human glioma cells (U251; ATCC) were infused at a depth of 4.5 mm below the surface of the brain after the syringe (Hamilton) was advanced 5.0 mm to create a 0.5-mm pocket. The cell suspension was infused using a UMP3-1 UltraMicroPump microinjector (WPI, Sarasota, FL) set to a volume of 10 µL with an infusion rate of 3.00 µL/minute. The needle was withdrawn 2 minutes after the injection to minimize backflow of the cell suspension. The bur hole was covered with bone wax, the skin incision was sutured, and the rats were allowed to recover.

Rodent tissue

Twenty-eight days after implantation, rodent xenografts were deeply anesthetized using xylazine and ketamine (previously described). They were immediately decapitated, and their brains were removed. Immediately, coronal slices (350 µm thick) were cut from the cerebrum on a Leica VT1200 vibratome and placed in artificial cerebrospinal fluid (aCSF) containing the following (in mM): 126 NaCl, 26 $NaHCO_3$, 2.5 KCl, 1.25 NaH_2PO_4, 2 $MgSO_4$, 2 $CaCl_2$ and 10 glucose, pH 7.4. Slices were then fixed in 4% paraformaldehyde at 4 degrees Celsius overnight and washed three times with phosphate

buffered saline (PBS). Three tumor containing slices per animal were incubated with DAPI for 45 minutes at room temperature, rinsed three times with PBS, and placed into number 1.5 glass bottom dishes (MatTek) for imaging. A coefficient of determination analysis was used to compare cells identified with CRM to cells labeled with DAPI.

Rodents utilized for molecular experiments (n=2) were deeply anesthetized using xylazine and ketamine and rapidly decapitated. Whole brains were placed in ice cold aCSF and sectioned into 1mm coronal sections using a rodent brain block. The cerebrum from each section was blocked into 4 equivalent sections. Two sections were immediately frozen in liquid nitrogen (LN2) for reference. At 15, 30, 45, 60, 90, and 120minutes two sections were placed into glass bottom dishes. At each time point, the cortex, corpus callosum, and caudate/putamen from one section was imaged with CRM. As a control, one section was simultaneously placed on the stage of the microscope but not imaged. Each section was frozen in LN2 and stored at -80° C for assessment of DNA, RNA, and protein.

Imaging

All samples were imaged in uncoated No.1.5 glass-bottom dishes (MatTek corp). CRM was conducted with a Zeiss invereted 710 laser scanning confocal microscope equipped with a 40x/1.2NA water emersion objective. For reflectance imaging, a 633-nm diode laser was raster scanned across the sample and reflected photons were collected by tuning the emission filters to allow photons with the same wavelength of the incident laser passage to the photomultiplier tube. For DAPI imaging, samples were excited with a 405-nm diode laser and 430-490nm emission collected. The confocal aperture was set to

one Airy unit for all imaging. The laser and gain values were set to fill the dynamic range of the photomultiplier tube, and the frame size was set to sample at nyquist. Images were collected in 12-bit format absent of nonlinear processing.

DNA Isolation & Analysis

DNA was isolated from brain tissue using the QIAamp DNA Mini (Qiagen), per manufacter's instructions. DNA was quantified using the Nanodrop Spectrophotometer (Thermo Scientific). Samples were loaded in equal concentrations (100 ng) in a 1% agarose gel with ethidium bromide and imaged on an Alpha Imager (Alpha Imager).

RNA Isolation and Analysis

Tissue was homogenized in 500 ul Ambion's Cell Disruption Buffer (Life Technologies) and subsequently isolated using Ambion's *mir*Vana kit (Life Technologies), per manufacturer's instructions. RNA concentrations were determined using the Nanodrop Spectrophotometer (Thermo Scientific) and provided information for the dilutions necessary to remain within the dynamic range of the Bioanalyzer. The integrity of the RNA was assessed using Agilent 2100 Bioanalyzer Nanochips (Agilent Technologies).

Western Blot Analysis

Frozen tissue was sectioned on dry ice and protein lysate was made by placing brain sections into 750 ul Ambion's Cell Disruption Buffer (Life Technologies); triturated using RNase-free pipettes; and sonicated using Covaris Sonolab at 2 X 5% for 5

seconds; 2 X 20% for 15 seconds; 2 X 20% for 15 seconds; 2 X 5% for 5 seconds (Covaris Inc).

Protein concentrations were quantified by BCA (Pierce, Thermo Scientific) and 18 ug/lane was loaded in 4-12% NuPage Bis-Tris gels (Invitrogen) and run using NuPage electrophoresis reagents (Invitrogen). Protein was transferred onto Novex nitrocellulose membrane (Invitrogen) and thereafter incubated for an hour in blocking solution consisting of 5% bovine serum albumin (Sigma Aldrich) in tris-buffered saline with 0.1% Tween (Thermo Fisher Scientific). Primary antibodies were incubated for 12 hours at 4 C while secondary HRP-conjugated antibodies were incubated for 1 hour at room temperature. Blots were probed for AKT (1:1000; Cell Signaling; Cat#: 9272) and GAPDH (1:60,000; Millipore; Cat#: AB2302). Horseradish peroxidase (HRP)-conjugated secondary antibodies were Anti-Rabbit (1:2000; Cell Signaling; Cat#: 7074**)** and Anti-Chicken (Millipore; Cat#:12-341).

Blots were developed by using Pierce SuperSignal Chemiluminescent Substrate (Thermo Fisher Scientific) per manufacturer's instructions. Protein signal was detected on film (General Electric).

Statistical Analysis

Coefficient of correlation (R^2 value) was determined between DAPI stained nuclei and nuclei detected by RCM using Graphpad Prizm. Differences were considered statistically significant for probability of less than .05. The Agilent 2100 Bioanalyzer provided an RNA integrity number (RIN) calculated algorithmically by including the 28s/18s ribosomal RNA bands, the region before the peaks, signal areas, and intensities.

An elevated threshold baseline and a decreased 28s:18s ratio are both indicative of RNA degradation while high 28S and 18S ribosomal RNA peaks as well as a small amount of 5s RNA or a RNA number of greater than 7.5 are indicative of intact RNA (Fleige and Pfaffl 2006). Image J was used to determine density (intensity) of bands on a western blot. Data analysis consisted of determining relative density. Results will be expressed as the means and mean square error (SEM) data with normal distribution that will be compared by one-way analysis of variance and student's t-test.

Clinical Samples

This research was approved by the Institutional Review Board of St. Joseph's Hospital and Medical Center and Barrow Neurological Institute, Phoenix, Arizona, where all surgery was performed. Preoperatively, patients signed an informed consent for participation. Samples (mean size, 4 x 2 x 2 mm) were obtained at the time of craniotomy from within the tumor mass at a location determined to be safe by the surgeon. Tissue samples were placed in ice-cold aCSF and transported from the operating room to the pathology-based CRM system. There, the samples were immediately placed in #1.5 glass-bottom dishes (MatTek) and imaged. Investigators conducting imaging experiments were unaware of the pathological diagnosis at the time of imaging. Final diagnosis was determined by traditional immunohistochemistry and paraffin-embedded hematoxylin and eosin staining of the sampled tissue. For the purpose of comparisons, the histopathological diagnosis made by a board-certified neuropathologist was accepted as the final diagnosis.

Results

Reflectance imaging differentiates neoplastic cellular tumor from acellular tissue.

To investigate the potential of reflectance imaging for differentiating cellular tumor biopsies from acellular biopsies, we imaged acute slices generated from rodents intracranially implanted with human glioma cells. We incubated slices with DAPI to label all cell nuclei, then sequentially imaged the slices with CRM and LSCM (n=15 slices from 5 animals). We collected five images per acute slice and compared cells identified with CRM to cells identified with DAPI. We found CRM provided definitive contrast between cell nuclei, cytoplasm, and extracellular tissue. Within tumor regions, CRM provided contrast to visualize hypercellular regions and relatively acellular regions with isolated cell populations (Fig1. A-C & E-G). In hypercellular and acellular regions we found CRM contrast correlated with r^2=0.97 and r^2=.098; respectively, to cells labeled with DAPI (Fig1. D&H).

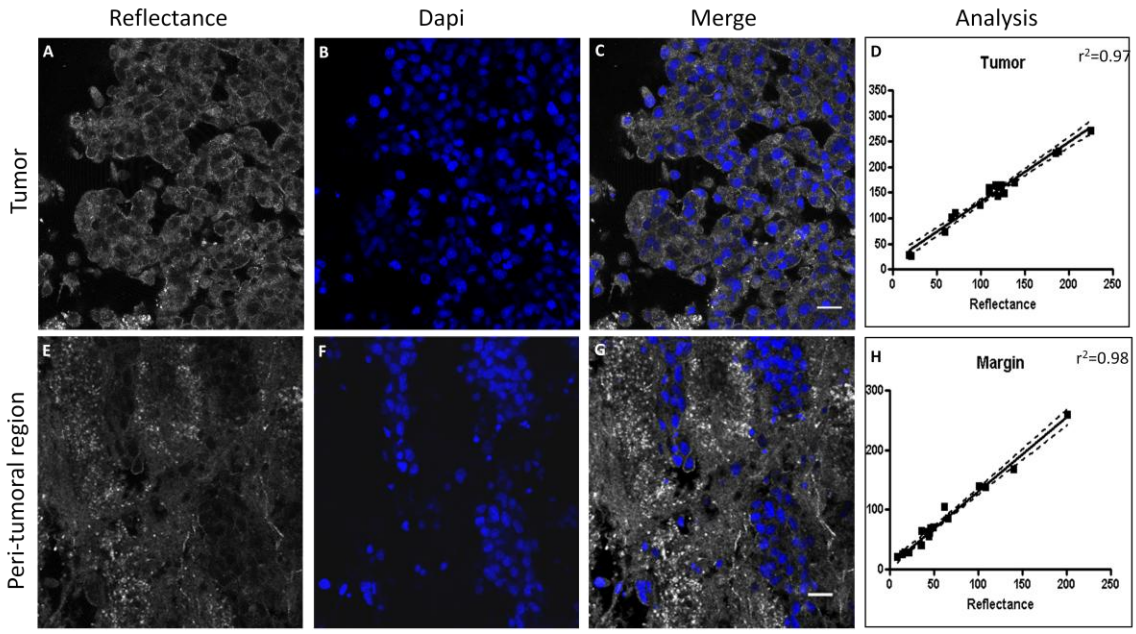

Figure1: Reflectance confocal imaging identifies cellular tumor in rodent acute slices. Cellular Tumor (A-D). (A) Reflectance image of rodent xenograft tumor region; note shading of cell nuclei. (B) Dapi stain of identical tumor region identifies all cells in the field of view. (C) Overlay shows location of cells contrasted by reflectance to cells labeled with dapi. (D) Plot of coefficient of determination and confidence intervals for tumor cells identified by reflectance imaging. r^2=0.97. Cellular tumor and acellular tissue interface (E-H). (E) Reflectance image of cellular tumor and adjacent acellular region from rodent xenograft; note isolated cell populations. (F) Fluorescence confocal image of identical region labeled with dapi. (G) Overlay of reflectance and fluorescence images from tumor and peritumoral tissue interface. (H) Plot of coefficient of determination and confidence intervals for cells identified by reflectance imaging at tumor and interface acellular tissue interface. r^2= 0.98. Scale bar equals 20*um*

Reflectance imaging does not alter the molecular characteristics of examined tissue.

To determine if CRM alters the molecular characteristics of tissue, we examined DNA, RNA, and protein from tissue imaged with CRM to tissue immediately frozen for analysis and compared that with tissue that had reflectance imaging and was left out for varying amount of time. Although the typical time from surgical resection to reception in pathology and assessment using CRM typically takes 15 minutes, we tested out to 180 minutes. Neoplastic tissues are heterzyogous in terms of cellularity and gene and protein expression and may yield inter-specimen molecular variability. Therefore, we conducted these experiments on control tissue harvested from rodent normal brain.

DNA quality was assessed in CRM imaged samples, which showed no difference compared to immediately frozen controls. Discrete DNA bands were detectable up to 180 minutes after extraction (Fig. 2B) suggesting no degradation of DNA elements. RNA integrity number (RIN) was generated to determine the integrity of isolated RNA. RIN number of 1 suggests strong degradation while RIN greater than 8 suggest minimal degradation (Fleige and Pfaffl 2006). RIN number was comparably the same between control and CRM imaged groups (Figure 2C), indicating no effect of CRM on RNA integrity of imaged samples. RNA integrity remained the relatively the same up to 120 minutes post-biopsy. There was a slight decrease over time in RIN value that was similar for both the control and CRM tissue, most likely due to RNases within the tissue over time. Protein kinase B (AKT), a protein involved in GBM pathogenesis, was examined for potential damage post-imaging with CRM. Western blot analysis of extracted tissue showed that up to120 minutes post-extraction, discrete AKT bands were detectable and contained similar density to control samples (Fig. 2E).

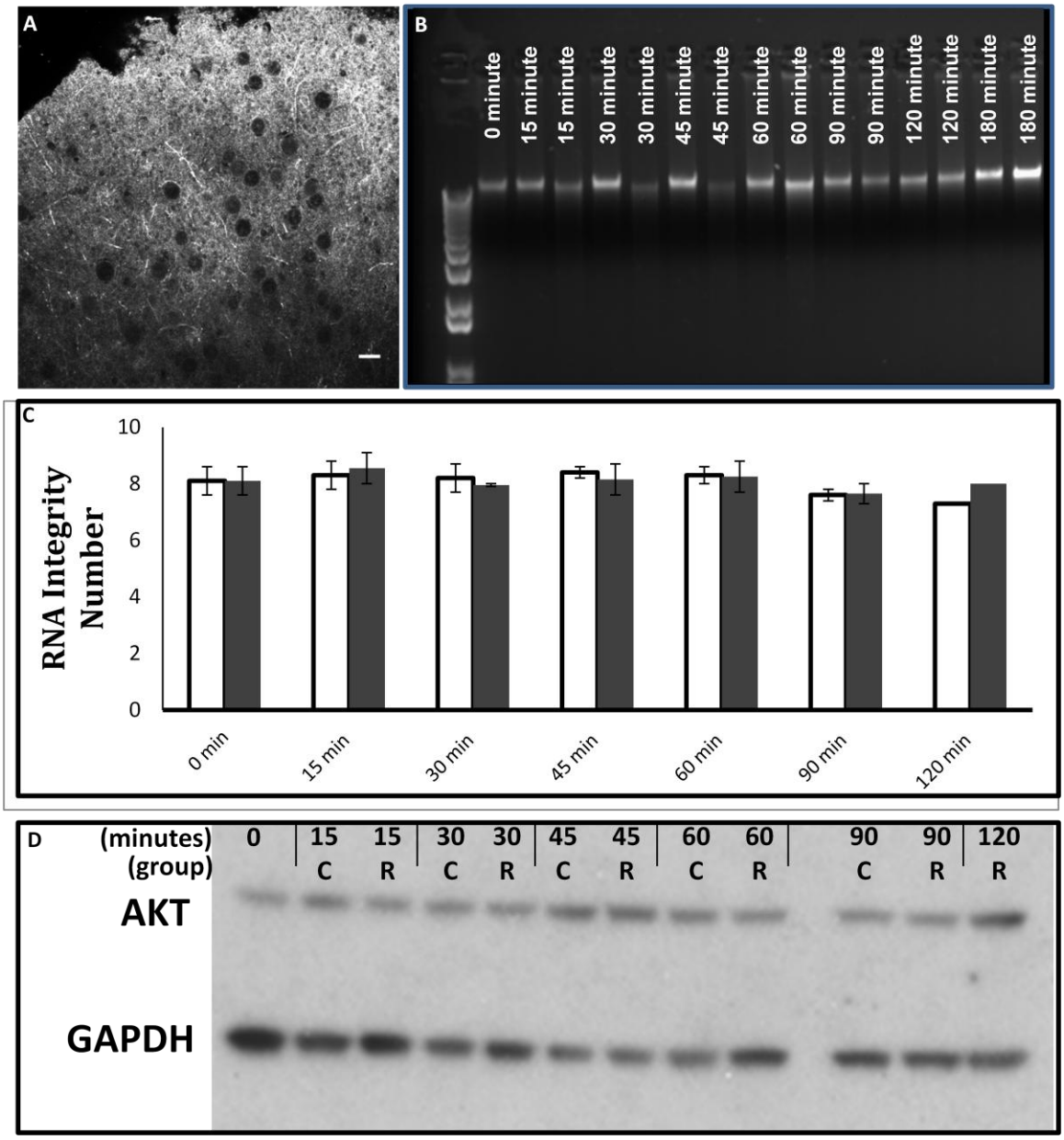

Figure 2: CRM does not alter DNA, RNA, or protein of examined tissue.**A)** CRM image of fresh brain tissue at cerebral cortex 90 minutes post-excision. Scale bar equals 20*um*. **B)** Gel electrophoresis of genomic DNA extracted from control and CRM imaged biopsies; note similar bands across time course. C=control and R= CRM. between imaged and control biopsies. **C)** Time course comparison of RNA integrity for all imaged and control samples; note similar RNA integrity for all samples. **D)** Western blot analysis showing expression of AKT over 120-minute time course. Protein signal did not degrade over time course or when exposed to CRM. R= Confocal Reflectance Microscopy, C= Control.

CRM differentiates human cellular from acellular brain tumor biopsies.

To test the ability of CRM to differentiate cellular tumor from acellular tissue samples in a clinical setting, we imaged two fresh human brain tumor biopsies; one yielding radiation necrosis tissue. Tissue samples were placed in ice-cold aCSF and imaged with CRM. Imaging time per sample was less than 2 minutes. Samples were then compared to final histpathological diagnosis.

Similar to our findings in rodent xenografts, we found that CRM contrasted cellular regions from acellular regions in human biopsies. Tissue samples identified as cellular with CRM were found to be cellular with proceeding standard histopathological assessment (Figure3 A,C). CRM failed to identify cellular regions in necrotic tissue samples (Figure3 B,D).

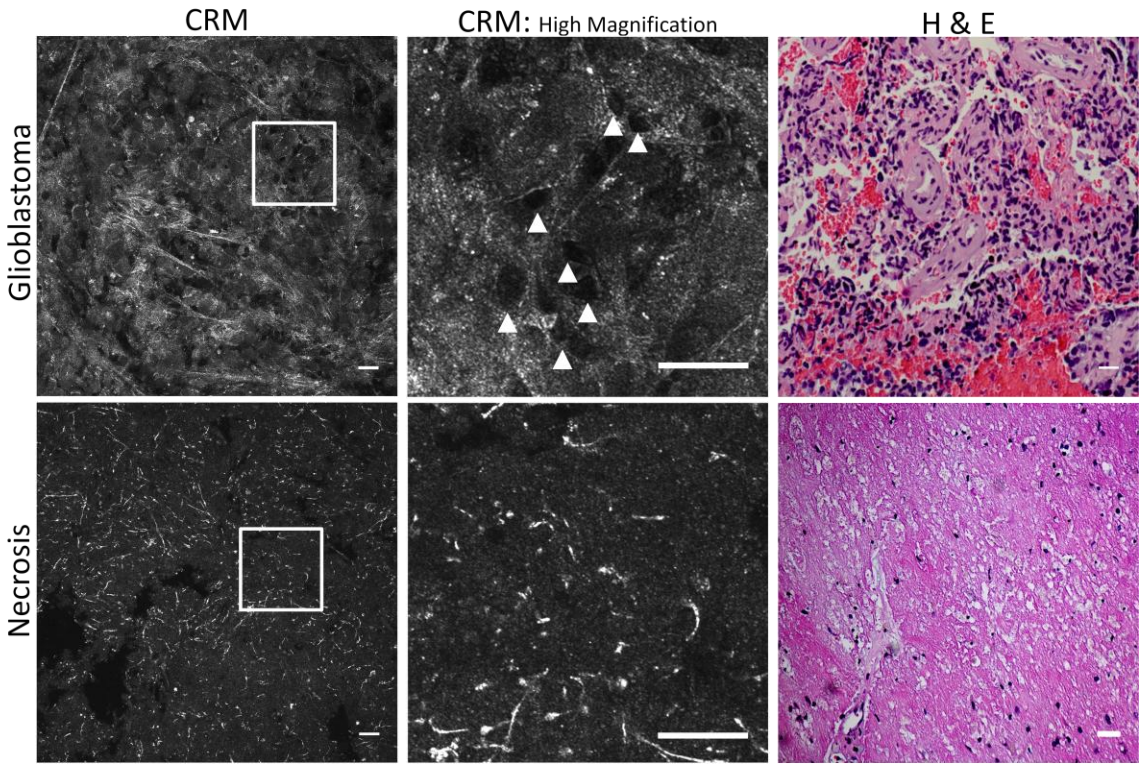

Figure3: Reflectance imaging immediately identifies cellular and necrotic fresh human brain tumor biopsies. (A-C) Glioblastoma. A) Low magnification CRM image of *ex vivo* human GBM biopsy imaged with CRM. B) High magnification of cellular region identified from inset of A, note arrowheads identifying cells within region. C) Corresponding H&E image. (D-F) Necrotic sample. D) Low magnification image of *ex vivo* necrotic biopsy imaged with CRM. E) High magnification inset from D. Note lack of distinct cells. F) H&E from corresponding section. Scale bar equals 20*um*.

Discussion:

Our data illustrate confocal reflectance microscopy's utility as a safe and rapid technique for identifying the cellularity of glioma tissue prior to biobanking. This imaging modality can be immediately utilized on fresh tissue samples without application of exogenous contrast agents and without altering the molecular characteristics of examined tissue. CRM can provide a much needed tool for neurosurgery-neuropathology teams by maximizing the quality of tissue samples collected during surgical resection. Although other imaging modalities may provide excellent images, their greater energy input and the possible need to use exogenous fluorophores could affect future molecular analysis of the tissue (Liao, Tsytsarev et al. 2013).

We found CRM did not alter the DNA, RNA, or protein that could be extracted and quantified from tissue biopsies screened up to 2 hours after resection. CRM images collected from these samples could be digitally stored and potentially recalled with biobanked specimens. We found CRM may have diagnostic utility, as many images revealed distinct morphological details such as; cellularity, vasculature, and necrosis (Figures 1and 3) typically identified with traditional histopathological H & E staining.

Many translational neuro-oncology studies rely on human GBM tissue samples that appropriately represent an original tumor. Unintentional utilization of necrotic or non-representative tissue samples in studies can lead to erroneous results that will not improve our knowledge of the disease. In studies that advance to clinical trials, patient biopsies are often screened to determine eligibility for a targeted clinical trial. CRM's nondestructive tissue assessment can ensure patients are not mistakenly excluded from potential life-prolonging treatments, particularly when standard therapy has failed.

Screening for high quality tissue specimens with CRM can facilitate the advancement of our knowledge of gliomagenisis, and can ensure qualified patients receive potential life-prolonging therapies (Rainov and Heidecke 2011).

Current limitations of CRM include limited imaging depth penetration. With our imaging parameters, CRM could assess tissue from the surface to 200-300 microns within. However, we did not find this limitation altered the accuracy of tissue assessment in our studies. Additionally, few pathology departments currently contain the imaging hardware or personnel required to screen tissue biopsies with CRM. Modernization of pathology departments may include addition of confocal microscopes and other systems capable of CRM that will allow the screening of samples within two-hours time. Lastly, *ex vivo* CRM is limited by the ability to only assess tissue that is intraoperatively selected to represent tumor. A hand held intraoperative CRM device could potentially overcome human sampling error and allow assessment of tissue samples prior to resection.

CRM technology has shown utility in providing cellular and subcellular detail, specifically in diagnosing dermatological conditions, identifying neoplastic tissue and margins, and assessing diseased and normal liver tissue (Rajadhyaksha, Gonzalez et al. 1999, White, Tearney et al. 2000, Campo-Ruiz, Ochoa et al. 2002, Clark, Gillenwater et al. 2003, Drezek, Richards-Kortum et al. 2003, Gonzalez, Swindells et al. 2003, Hicks, Swindells et al. 2003, Curiel-Lewandrowski, Williams et al. 2004, Campo-Ruiz, Lauwers et al. 2005). Our study is the first to assess human brain tumor biopsies with CRM for biobanking purposes. By quantifying DNA, RNA, and protein, we also demonstrate for the first time CRM's ability to assess tissue cytoarchitecture without altering tissue

molecular integrity, meaning that no part of the tissue to be banked needs to be discarded in the assessment process.

Conclusion

Confocal reflectance microscopy can screen brain tumor tissue cellularity for inclusion into biobanks while preserving the molecular integrity of tissue samples. CRM provides a rapid imaging modality that can accurately provide *ex vivo* morphological information in animal models and fresh human biopsies. In comparison to traditional histopathological methods, this technique does not rely on exogenous dyes or fixation and sectioning. Furthermore, this technique preserves the DNA, RNA, and protein characteristics of tissues, allowing further analysis of imaged specimens. Future technical developments of CRM include utilization of a handheld confocal endomicroscope for imaging, which would allow rapid and safe histopathological assessments *in vivo*. Further applications of CRM may include rapid *ex vivo* and *in vivo* examination of brain tumors in addition to glioblastoma. This technique ensures that high quality specimens are biobanked for future molecular studies of tumor samples and for assessing patient eligibility for clinical trials based on tumor characteristics.

References

Campo-Ruiz, V., G. Y. Lauwers, R. R. Anderson, E. Delgado-Baeza and S. Gonzalez (2005). "In vivo and ex vivo virtual biopsy of the liver with near-infrared, reflectance confocal microscopy." Mod Pathol **18**(2): 290-300.

Campo-Ruiz, V., E. R. Ochoa, G. Y. Lauwers and S. Gonzalez (2002). "Evaluation of hepatic histology by near-infrared confocal microscopy: a pilot study." Hum Pathol **33**(10): 975-982.

Clark, A. L., A. M. Gillenwater, T. G. Collier, R. Alizadeh-Naderi, A. K. El-Naggar and R. R. Richards-Kortum (2003). "Confocal microscopy for real-time detection of oral cavity neoplasia." Clin Cancer Res **9**(13): 4714-4721.

Curiel-Lewandrowski, C., C. M. Williams, K. J. Swindells, S. R. Tahan, S. Astner, R. A. Frankenthaler and S. Gonzalez (2004). "Use of in vivo confocal microscopy in malignant melanoma: an aid in diagnosis and assessment of surgical and nonsurgical therapeutic approaches." Arch Dermatol **140**(9): 1127-1132.

Dolecek, T. A., J. M. Propp, N. E. Stroup and C. Kruchko (2012). "CBTRUS statistical report: primary brain and central nervous system tumors diagnosed in the United States in 2005-2009." Neuro Oncol **14 Suppl 5**: v1-49.

Drezek, R. A., R. Richards-Kortum, M. A. Brewer, M. S. Feld, C. Pitris, A. Ferenczy, M. L. Faupel and M. Follen (2003). "Optical imaging of the cervix." Cancer **98**(9 Suppl): 2015-2027.

Fleige, S. and M. W. Pfaffl (2006). "RNA integrity and the effect on the real-time qRT-PCR performance." Mol Aspects Med **27**(2-3): 126-139.

Furnari, F. B., T. Fenton, R. M. Bachoo, A. Mukasa, J. M. Stommel, A. Stegh, W. C. Hahn, K. L. Ligon, D. N. Louis, C. Brennan, L. Chin, R. A. DePinho and W. K. Cavenee (2007). "Malignant astrocytic glioma: genetics, biology, and paths to treatment." Genes Dev **21**(21): 2683-2710.

Gonzalez, S., K. Swindells, M. Rajadhyaksha and A. Torres (2003). "Changing paradigms in dermatology: confocal microscopy in clinical and surgical dermatology." Clin Dermatol **21**(5): 359-369.

Hicks, S. P., K. J. Swindells, M. A. Middelkamp-Hup, M. A. Sifakis, E. Gonzalez and S. Gonzalez (2003). "Confocal histopathology of irritant contact dermatitis in vivo and the impact of skin color (black vs white)." J Am Acad Dermatol **48**(5): 727-734.

Lefranc, F., J. Brotchi and R. Kiss (2005). "Possible future issues in the treatment of glioblastomas: special emphasis on cell migration and the resistance of migrating glioblastoma cells to apoptosis." J Clin Oncol **23**(10): 2411-2422.

Liao, L. D., V. Tsytsarev, I. Delgado-Martinez, M. L. Li, R. Erzurumlu, A. Vipin, J. Orellana, Y. R. Lin, H. Y. Lai, Y. Y. Chen and N. V. Thakor (2013). "Neurovascular coupling: in vivo optical techniques for functional brain imaging." Biomed Eng Online **12**: 38.

Mohyeldin, A. and E. A. Chiocca (2012). "Gene and viral therapy for glioblastoma: a review of clinical trials and future directions." Cancer J **18**(1): 82-88.

Rainov, N. G. and V. Heidecke (2011). "Clinical development of experimental therapies for malignant glioma." Sultan Qaboos Univ Med J **11**(1): 5-28.

Rajadhyaksha, M., S. Gonzalez, J. M. Zavislan, R. R. Anderson and R. H. Webb (1999). "In vivo confocal scanning laser microscopy of human skin II: advances in instrumentation and comparison with histology." J Invest Dermatol **113**(3): 293-303.

Stupp, R., W. P. Mason, M. J. van den Bent, M. Weller, B. Fisher, M. J. Taphoorn, K. Belanger, A. A. Brandes, C. Marosi, U. Bogdahn, J. Curschmann, R. C. Janzer, S. K. Ludwin, T. Gorlia, A. Allgeier, D. Lacombe, J. G. Cairncross, E. Eisenhauer, R. O. Mirimanoff, R. European Organisation for, T. Treatment of Cancer Brain, G. Radiotherapy and G. National Cancer Institute of Canada Clinical Trials (2005). "Radiotherapy plus concomitant and adjuvant temozolomide for glioblastoma." N Engl J Med **352**(10): 987-996.

Tilli, M. T., M. C. Cabrera, A. R. Parrish, K. M. Torre, M. K. Sidawy, A. L. Gallagher, E. Makariou, S. A. Polin, M. C. Liu and P. A. Furth (2007). "Real-time imaging and characterization of human breast tissue by reflectance confocal microscopy." J Biomed Opt **12**(5): 051901.

White, W. M., G. J. Tearney, B. Z. Pilch, R. L. Fabian, R. R. Anderson and R. D. Gaz (2000). "A novel, noninvasive imaging technique for intraoperative assessment of parathyroid glands: confocal reflectance microscopy." Surgery **128**(6): 1088-1100; discussion 1100-1081.

CHAPTER 4

RAPID AND SPECIFIC DIAGNOSIS OF HUMAN ASTROCYTIC BRAIN TUMORS BY IMMEDIATE EX VIVO IMAGING WITH SULFORHODAMINE 101

Brain tumor resection is guided by intraoperative diagnostics. However, current histopathological techniques lack the specificity and speed required to be effective intraoperative diagnostic tools. Here we show that imaging of fresh human brain tumors rapidly labeled with the physiological fluorophore sulforhodamine 101 (SR101) can differentiate astrocytic tumors, reactive astrocytes and tumor margins from non-astrocytic brain tumors and normal brain. Acute slices from orthotopic human glioma (n=8) and lymphoma (n=6) xenografts were incubated with SR101 or its fixabale analog and imaged with confocal microscopy. A subset of slices (n=18 slices) were respectively counter-immunostained with GFAP and CD20 for stereological assessment of SR101 co-localization. Additionally, sixty-five undiagnosed fresh human samples were examined by quickly incubating with SR101, immediately imaging, and comparing to final pathological diagnosis. SR101 differentiated astrocytic tumor cells from reactive astrocytes and lymphoma cells. In acute slices, SR101 labeled 86.50% (+/-1.86; $p<0.0001$) of astrocytoma cells and 2.19% (+/-0.47; $p<0.0001$) of lymphoma cells. In human biopsies, SR101 rapidly labeled reactive astrocytes and selectively identified 12 of 13 astrocytomas without labeling non-astrocytic tumors. SR101 rapidly and selectively labels human astrocytic tumors and astrocytes in a time frame that supports intraoperative decision-making. This is the first reported use of a functional dye on living human brain tumor tissue to provide a clinically meaningful immediate histopathological diagnosis.

Clinical application of SR101 could improve intraoperative decision-making, ultimately improving patient care.

Introduction

Intraoperative histopathological diagnosis guides the surgical resection strategy for numerous cancers, including intrinsic brain tumors such as astrocytomas. However, frozen-section analysis, the method of choice for obtaining such diagnoses, often produces artifacts and provides only limited nonspecific information about tissue based on its morphology and cellular architecture (Gal 2005, Lechago 2005). When an accurate intraoperative diagnosis cannot be obtained, clinical teams must wait for postoperative antibody staining of biopsied tissue to identify its specific molecular markers, a process that often requires 24-72 hours. Consequently, the inability of the frozen section to consistently provide rapid and specific information can limit definitive intraoperative surgical planning. Furthermore, while rapid identification of the tumor core is important for diagnosis, identification of the tumor margin is most critical for guiding astrocytoma resection.

Glioblastoma multiforme (GBM), grade IV astrocytoma, is the most common subtype of astrocytoma with a median survival of 12-15 months (Wen and Kesari 2008). Length of survival is directly related to extent of GBM tumor resection, which is based on frozen-section analysis of biopsied tissue to identify tumor margins (Lacroix, Abi-Said et al. 2001, Powell 2005, Pichlmeier, Bink et al. 2008). In contrast, definitive resection of the common central nervous system (CNS) tumor, CNS lymphoma, remains contraindicated; diagnostic biopsy alone is the most common reason for surgical

intervention. GBM and lymphoma have similar clinical presentations, and can be difficult to differentiate on diagnostic imaging (Ferreri, Reni et al. 2009, Ricard, Idbaih et al. 2012). Consequently, clinical decision-making depends on tissue biopsy and histopathological analysis. Furthermore, frozen-section analysis often fails to be diagnostic, necessitating the need for postoperative antibody staining of resected brain tissue. Glial fibrillary acidic protein (GFAP) is a useful immunohistochemical tool, which combined with cellular morphology assists in the diagnosis of astrocytomas. GFAP positivity supports the diagnosis of GBM, whereas CD20 positivity supports a diagnosis of CNS B-cell lymphoma. Although effective, such postoperative staining requires 24 hours to obtain a diagnosis—too slow to guide intraoperative decision-making.

Although its underlying mechanism is incompletely understood, SR101 is a red fluorescent dye used in neuroscience research for the rapid and specific labelling of astrocytes (Nimmerjahn, Kirchhoff et al. 2004, Kafitz, Meier et al. 2008). Similar to GFAP, SR101 labels astrocytic cells, and it has been used to label rodent astrocytoma cells in culture (Lai, Bechberger et al. 2007). If SR101 also labels GBM and other cells of astrocytoma lineage, it could provide a clinical alternative to GFAP for differentiating GBM from lymphoma during intraoperative diagnosis. We hypothesized that the combined use of live-cell imaging with targeted fluorophores could improve the current standard of care by providing rapid and specific intraoperative diagnoses of astrocytic tumors. Specifically, we evaluated the utility of sulforhodamine 101 (SR101) to rapidly distinguish tumor type and neuropathological diagnosis of astrocytoma in cell culture, animal tumor models, and freshly resected human brain tumors.

Materials and Methods

Cell culture

We acquired human glioma cell line U251 and human CNS lymphoma cell line MC116 from American Type Culture Collection (ATCC). The cell lines were maintained in culture with Dulbecco's Modified Eagle Medium (DMEM) media supplemented with 10% fetal bovine serum, and Roswell Park Memorial Institute Medium (RPMI**)** 1640 media supplemented with 20% FBS (all from Invitrogen, Grand Island, NY). Cells were grown at 37°C in a humidified incubator under 5% CO_2.

In Vitro SR101 labeling

U251 glioma cells were labeled by incubating 100,000 cells on a collagen-coated glass-bottom dish (MatTek). After 24 hours, the medium was replaced with artificial cerebrospinal fluid (aCSF) containing 2 μM SR101 (Sigma) for 20 minutes, followed by two 5-minute washes with standard aCSF.

Animals

Fifteen male Crl:NIH-Foxn1^{rnu} rats (5 weeks age) were obtained from The Charles River Laboratories International, Inc. (Wilmington, MA). Experiments were performed in accordance with the guidelines and regulations set forth by the National Institutes of Health Guide for the Care and Use of Laboratory Animals and were approved by the Institutional Animal Care and Use Committee of the Barrow Neurological Institute of St. Joseph's Hospital and Medical Center, Phoenix, Arizona.

Intracranial implantation

The rats were anesthetized by intramuscular injection of a mixture of 10 mg/kg xylazine and 80 mg/kg ketamine (Wyeth, Madison, NJ) and placed in a small animal stereotactic headframe (Model 900, David Kopf Instruments, Tujunga, CA). A 10-mm incision was made starting between the animal's eyes to expose bregma. A bur hole was made 3.5 mm lateral to bregma. U251 (n=9 rats) or MC116 cells (n=6 rats) were infused at a depth of 4.5 mm below the surface of the brain after the syringe (Hamilton) was advanced 5.0 mm to create a 0.5-mm pocket. The cell suspension was infused using a UMP3-1 UltraMicroPump microinjector (WPI, Sarasota, FL) set to a volume of 10 µL with an infusion rate of 3.00 µL/minute. The needle was withdrawn 2 minutes after the injection to minimize backflow of the cell suspension. The bur hole was covered with bone wax, the skin incision was sutured, and the rats were allowed to recover.

Acute slices

Twenty-eight days after implantation, rats were deeply anesthetized using the xylazine/ketamine mixture as described previously. They were immediately decapitated, and their brains were removed. Immediately, coronal slices (350 µm thick) were cut from the cerebral cortex on a Leica VT1200 vibratome in aCSF containing the following (in mM): 126 NaCl, 26 $NaHCO_3$, 2.5 KCl, 1.25 NaH_2PO_4, 2 $MgSO_4$, 2 $CaCl_2$ and 10 glucose, pH 7.4. Slices were then incubated at room temperature in aCSF containing 2µM SR101 for 20 minutes followed by a 10-minute wash in aCSF. A two-tailed paired t-test with alpha set to 0.05 was used to compare mean fluorescence intensity (MFI) between tumor cells and reactive astrocytes.

Co-labeling

SR101 is not amenable to fixation; we therefore used a fixable version of SR101(Texas Red Hydrazide) for these experiments. The staining pattern of fixable SR101 fluorophore mimics the staining pattern of the standard nonfixable SR101 (Nimmerjahn, Kirchhoff et al. 2004, Kafitz, Meier et al. 2008). For clarity, the use of the fixable version of SR101 is clearly indicated by the term "fixable SR101" throughout the text. Fixable-SR101 and the nonfixable version had similar staining patterns, but the intensity and cellular staining of the fixable version was weaker than that of the standard SR 101.

Acute xenograft slices were incubated with the fixable version of SR101 (Texas Red Hydrazide; Sigma), washed at room temperature, and fixed with 4% paraformaldehyde for 12 hours at 4° C. The sections were rinsed in phosphate-buffered saline, permeabilized with 0.3% triton, and blocked with CAS block (Invitrogen) (Beeman, Georges et al. 2013). The GBM xenograft slices (9 slices from 3 animals) were incubated in anti-GFAP primary antibody (Millipore; 1:500) for 12 hours, and the lymphoma sections (9 slices from 3 animals) were incubated in anti-CD20 primary antibody (Millipore; 1:250) for 12 hours. Sections were then rinsed and incubated with AlexaFluor488 secondary antibody (Invitrogen), followed by DAPI (Invitrogen) nuclear counterstain and mounted on slides with vectashield (Vector labs) and No 1.5 coverslips (VWR).

Stereology

We adapted standard stereology approaches to quantify tumor cells labeled with fixable- SR101 and GFAP or CD20 antibodies (Mouton 2002, Kim, Lee et al. 2010). We selected one rostral, midline, and caudal acute slice from each brain containing tumor incubated with fixable SR101. Glioma slices were immunofluorescently stained for GFAP, and slices containing lymphoma were stained for CD20. In each slice, 10 randomly selected region of tumor (150 μm^2) were optically sectioned to 50 μm with a Zeiss 710LSM. The first 5 μm of each image stack was discarded to minimize counts from cells damaged during sectioning. A maximum intensity projection image was generated from the remaining 45 μm, and a stereology dissector was overlaid onto the image. Cells within the dissector and those in contact with its left and bottom edges were counted for either GFAP or CD20 positivity and for SR101 positivity.

The percent overlap between immunostaining and SR101 positivity was calculated. Two-tailed t-tests with alpha levels of 0.05 were used to determine statistical differences. A paired t-test was used to determine if staining localization between antibody- and SR101-labeling differed between cell types. An unpaired t-test was used to compare fixable-SR101 staining between glioma and lymphoma models.

Human Samples

This research was approved by the Institutional Review Board of St. Joseph's Hospital and Medical Center and Barrow Neurological Institute, Phoenix, Arizona, where all surgery was performed. Preoperatively, 65 patients with one of 11 common brain tumors (Table 1) signed an informed consent for participation. Samples (mean size, 4 x 2

x 2 mm) were obtained at the time of craniotomy from within the tumor mass at a location determined to be safe by the surgeon. The diagnosis was determined by traditional immunohistochemistry and paraffin-embedded hematoxylin and eosin staining. For the purpose of comparisons, the histopathological diagnosis made by a board-certified neuropathologist was accepted as the final diagnosis.

Tissue samples were placed in ice-cold aCSF containing 2 μM of SR101 and were transported from the operating room to the laboratory. There, the samples were rinsed with aCSF (10 minutes), and imaged within 30 to 40 minutes of biopsy. Investigators conducting imaging experiments were unaware of the pathological diagnosis.

Imaging

SR101-labeled samples were placed in uncoated No.1.5 glass-bottom dishes and positioned on the stage of a Zeiss 710 laser scanning confocal microscope equipped with a 40x/1.2NA water emersion objective. We imaged SR101 by exciting the fluorophore with a 561-nm diode laser and collecting 595-nm to 625-nm emissions. The confocal aperture was set to Airy unit for all imaging. The laser and gain values were set to fill the dynamic range of the photomultiplier tube, and the frame size was set to sample at Nyquist. Images were collected in 8- and 12-bit format absent of nonlinear processing. An unstained adjacent tissue sample was imaged with each sample. In some cases, large field-of-view tiled and optically sectioned images were rapidly acquired using a Zeiss line-sweeping confocal microscope. For this system the frame size was fixed at 512 x 512 by a linear charged-coupled device array.

Results

SR101 labels human astrocytoma cells and reactive astrocytes

To investigate the potential of SR101 for identifying human astrocytoma cells, we used differential interference contrast (DIC) with fluorescence overlay to image human astrocytoma cell line U251 after incubation in SR101 (n=6 cultures). The fluorophore filled the cytoplasm of the cultured cells and clearly delineated cell nuclei (Figs. 1A, B).

Next, human astrocytoma cells (U251 cell line) were implanted into the caudate-putamen of 5 nude rats and allowed to grow for 4 weeks before the rats were sacrificed. This orthotopic xenograft model consistently produced astrocytic tumors as previously characterized (Michaud, Solomon et al. 2010, Buckingham, Campbell et al. 2011). Live cell confocal images of acute slices from the cerebral cortex of the implanted animals (Fig. 1C) treated with SR101 showed cells in the tumor core markedly labeled with the fluorophore. The cells were easily distinguished from low level background staining (Figs. 1D, E, F).

Confocal microscopy imaging of the acute slices treated with SR101 also showed distinct tumor margins that contained SR101-positive astrocytoma cells and reactive astrocytes (Figs. 1G, H). The fluorescence intensity from the astrocytoma cells and reactive astrocytes was quantified. The mean fluorescence intensity did not differ between the two cell types (Fig. 1I). However, reactive astrocytes were easily distinguished based on their distinct morphology (Fig. 1H). Therefore, SR101 can rapidly identify astrocytes and astrocytoma cells in cell culture and animal models, and it can effectively define tumor margins in an animal model.

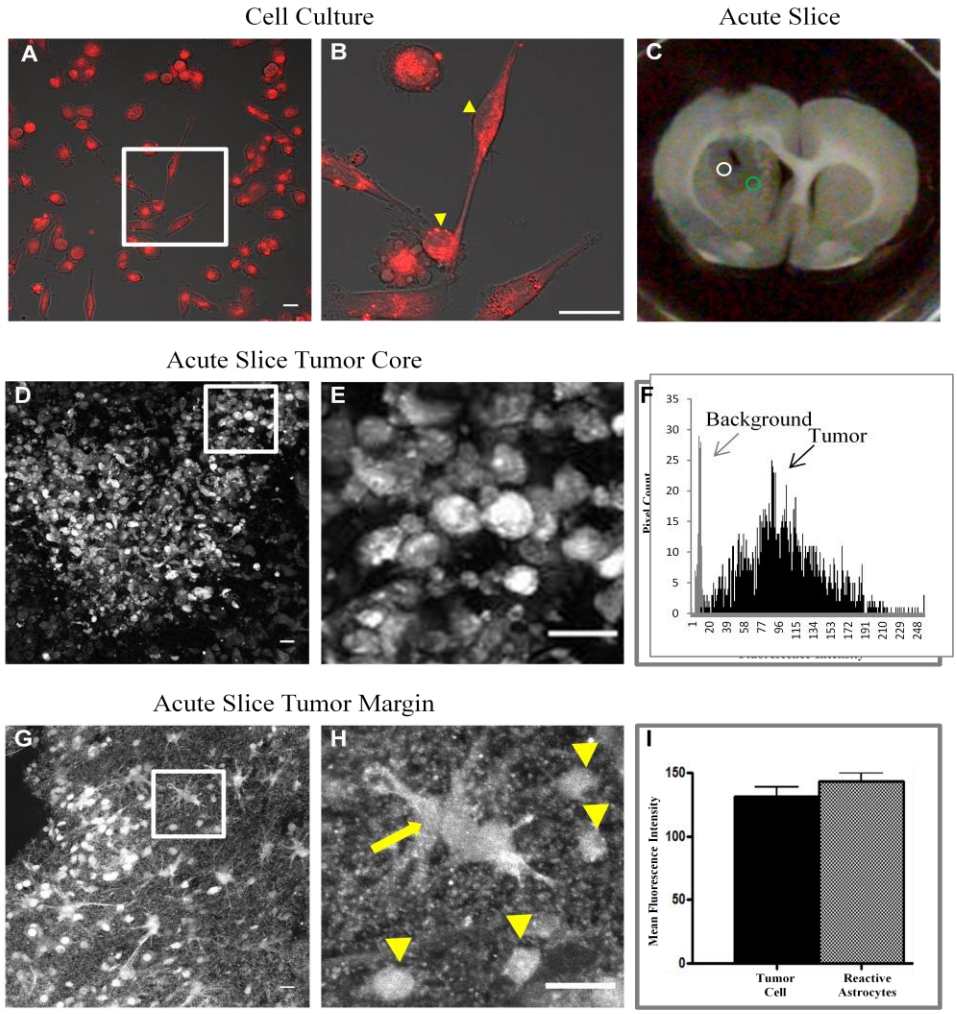

Figure1: Non-fixable SR101 labels human astrocytoma cells in culture and identifies tumor core and margin in rodent xenografts. U251 Astrocytoma Cell Culture (A-B). (A) DIC image with fluorescent overlay of human U251 astrocytoma cells incubated with SR101. (B) Inset showing cytoplasmic filling of cells and delineation of cell nuclei (arrowheads). Acute slices from rodents intracranially implanted with U251 cells (C-H). (C) Acute slice containing U251 derived tumor. Representative core and margin regions identified by white circle and green circle respectively. (D) Confocal fluorescence image of SR101-labeled tumor core. (E) High magnification of inset showing typical morphology of U251cells. (F) Histogram of SR101 fluorescence distribution in E between tumor core and background. Note the clear distinction in mean fluorescence intensity (MFI) between tumor (102.84) and background (8.74). (G) Image of tumor margin with SR101 labeled cells. (H) Inset of morphologically identified reactive astrocyte (arrow) surrounded by glioma cells (arrowheads) near the tumor margin. (I) Mean fluorescence intensity of U251 cells and reactive astrocytes normalized to background (n=9 optical sections from 3 acute slices). Note no statistically significant difference in MFI between the two cell types. Scale bar equals 20*um*

Fixable SR101 labels GFAP-positive human astrocytoma cells and reactive astrocytes

We used confocal microscopy to compare the efficacy and localization of SR101 and GFAP staining. Confocal images from the tumor core regions showed numerous cells simultaneously filled with fixable-SR101 and labeled by GFAP (Fig. 2A-D). In general, GFAP and SR101 labeled the same cells, although fixable-SR101 stained some cellular processes less intensely than GFAP (Figs. 2A, B, D). Merged images from the tumor core showed that most cells were positive for both fixable SR101 and GFAP, indicating that SR101 effectively labels astrocytic tumor cells.

We compared the staining pattern of fixable-SR101 and GFAP to determine if reactive astrocytes could be differentiated from neoplastic astrocytes to help identify tumor borders. Imaging of rat brain regions adjacent to human astrocytoma cells showed that the staining patterns of fixable-SR101and GFAP were similar (Figs. 2E, F). However, GFAP labeled membrane processes more thoroughly than the fixable-SR101. Cells in the peripheral regions contained extensive membrane projections that could be readily differentiated from cells within the tumor core that lacked this feature. When additional cells in these regions were stained with 4',6-diamidino-phenylindole (DAPI) (Fig. 2G), groups of cells were negative for both fixable-SR101 and GFAP (Figs. 2G, H, arrows). These findings suggest a mixed cell population of tumor cells and nontumor brain cells typical of regions outside the tumor core. Together, the data indicate that SR101-positive cells are the GFAP-positive astrocytoma cell population. Furthermore, fixable-SR101 provides morphological information that appears to differentiate astrocytoma cells from reactive astrocytes.

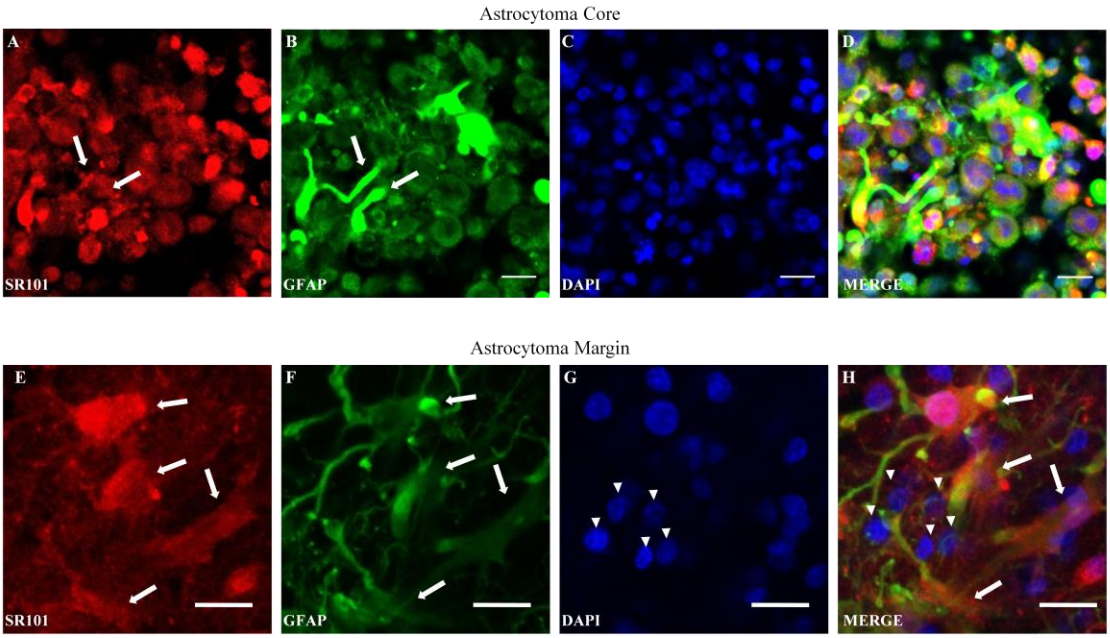

Figure 2: Fixable SR101 colocalizes with the astrocytic marker GFAP. Confocal imaging of rodent xenograft acute slices incubated in the fixable version of SR101. Following incubation slices were fixed and stained with GFAP and Dapi. Images taken from the core of the astrocytoma (A-D). Fixable SR101 fills the cell bodies of GFAP-positive cells in the tumor core, and weakly fills astrocytic processes (arrows). Note the significant overlap of GFAP, DAPI and SR101 in the merged image. Images taken from the margin of the astrocytoma (E-H) . Fixable SR101 fills cell bodies of GFAP-positive cells at the tumor margin. Solid arrows identify SR101 and GFAP positive cells. Note the appearance of DAPI positive cells (arrowheads) unlabeled by SR101 or GFAP that are selectively observed at the astrocytoma margin. Scale bar equals 20*um*.

SR101 differentiates astrocytoma from lymphoma

In contrast to the findings from astrocytoma cells, confocal imaging indicated minimal SR101 signal from the human CNS lymphoma cell line MC116 (Supplemental Fig. 1). In acute slices from astrocytoma and CNS lymphoma animal models incubated with fixable-SR101, we quantified co-localized GFAP for astrocytoma slices and CD20 for lymphoma slices. In astrocytoma tumor regions, fixable-SR101 labeled the majority of cells (Figs. 3A-D, I). The frequency of co-localization of SR101 and GFAP was 86.50% (Fig. 3K, Table 2), with a mean of 22.30 SR101-positive cells and 20.58 GFAP-positive cells per stereology dissector region of interest (Lacroix, Abi-Said et al.) ($p=0.0004$, Fig. 3I, Table 2). In contrast, fixable SR101 labeled only a very small number of cells from ROIs in CNS lymphoma acute slices (Fig. 3E). SR101 and CD20 co-localized poorly (2.19%), and there were significantly more CD20-positive cells than fixable-SR101-positive cells ($p<0.0001$) (Fig. 3J, Table 2). However, SR101 labeled a small number of cells in CNS lymphoma tissue that were not CD20-positive and that morphologically resembled reactive astrocytes (Figs. 3E, F; arrow). SR101 distinguished astrocytoma from lymphoma tissue and co-localized with GFAP more frequently than CD20 (Fig. 3K). This finding demonstrates the strong relationship of SR101 to GFAP-positive cells in astrocytoma, and the ability of SR101 to differentiate it from a non-astrocytic tumor such as CNS lymphoma.

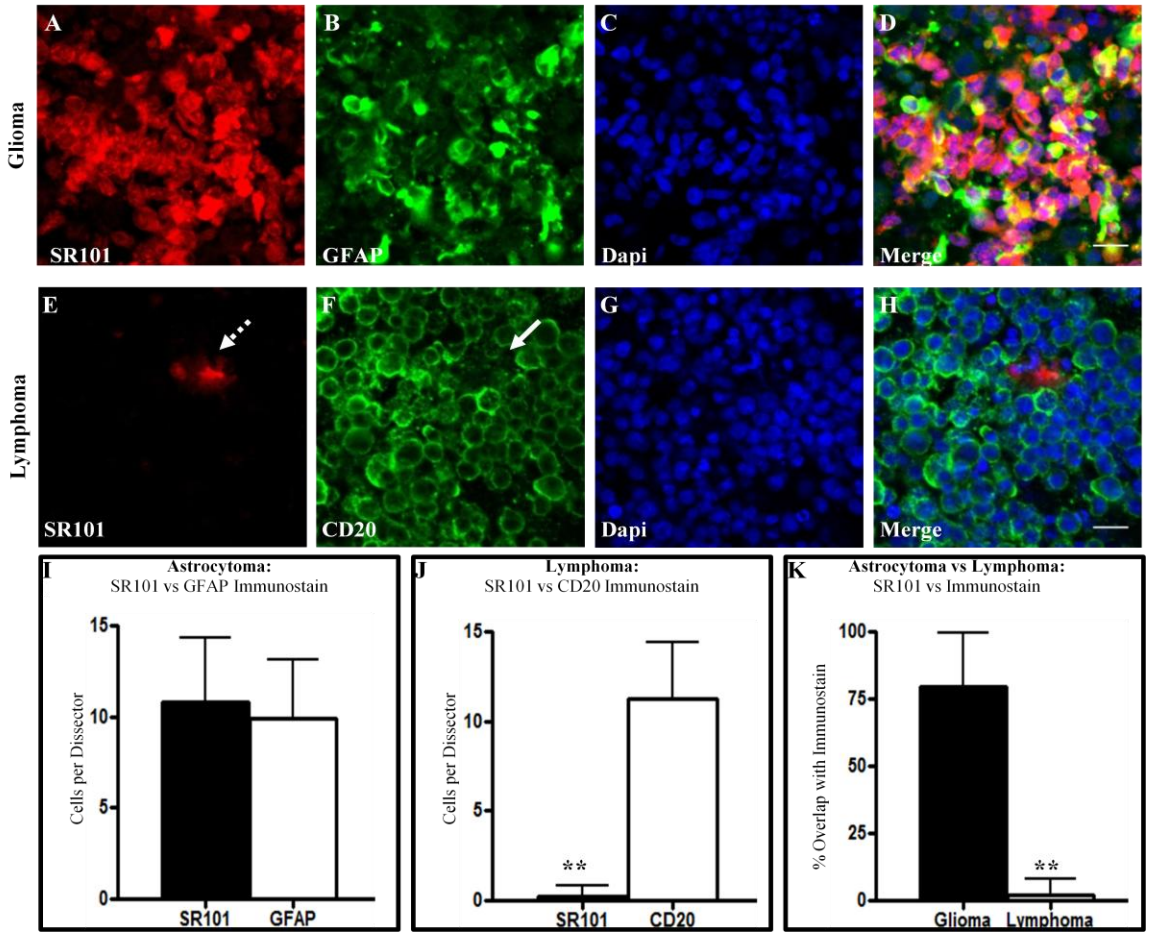

Figure 3: SR101 rapidly differentiates human astrocytoma from CNS lymphoma in rodent xenografts. Confocal imaging of acute slices taken from xenograft animals implanted with astrocytoma cells (U251)(van Dam, Themelis et al.) or lymphoma cells (MC116)(Middle). Slices were stained with fixable SR101 and specific markers for Astrocytoma (GFAP) or Lymphoma (CD20) . Nuclei were counterstained with DAPI. Top: Region from U251 astrocytoma acute slice incubated with fixable SR101 and counterstained with GFAP and DAPI (A-D). Middle: (E) SR101 labels a single cell (dashed arrow) in a MC116 xenograft lymphoma region. (F) CD20 immunostaining labels lymphoma cells, but does not label region containing SR101-positive cell (solid arrow). (G) DAPI counterstain of cell nuclei in field of view. (H) Merged lymphoma image indicating poor colocalization of SR101 and CD20. Scale bar equals 20*um*. Bottom: Confocal stereology of acute slices (see Methods). (I) Number of SR101 and GFAP-positive cells present in U251 xenograft astrocytoma regions are not statistically different ($p<0.01$). (J) Number of SR101 and CD20 -positive cells present in MC116 xenograft lymphoma regions are highly statistically different ($P<0.01$*). (K) SR101 significantly overlaps with GFAP positive astrocytoma cells (79.6%) compared with CD20 lympoma cells (1.97%)($p<0.01$).

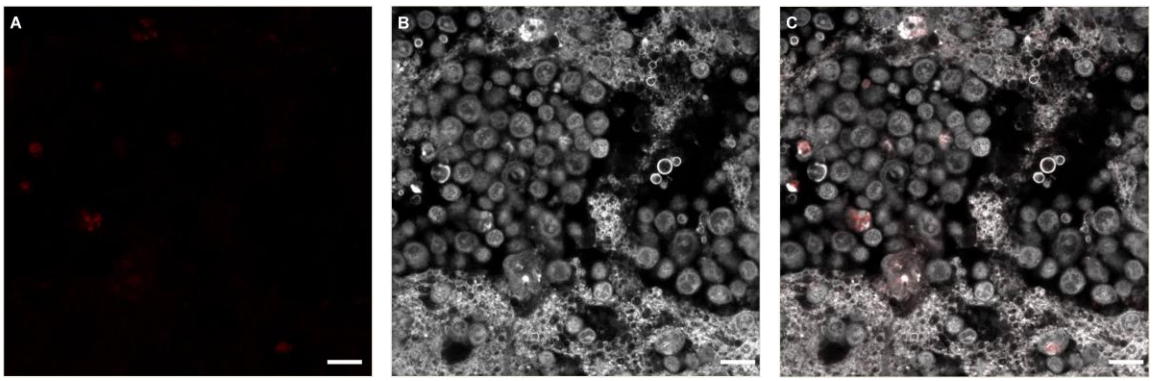

Supplemental 1: Non-Fixable SR101 does not label human lymphoma cells in rodent xenografts. (Verkman, Hara-Chikuma et al.) SR101 labeled acute slices prepared from rodent CNS lymphoma xenografts. (A) SR101 sparsely labels a minimal number of cells within the tumor region. (B) Non-specific acridine orange staining reveals a hypercellular tumor region. (C) Overlay image shows incomplete cytoplasmic filling of cells with SR101 staining. Scale bar equals 20*um*.

SR101 intraoperatively differentiates human astrocytoma from other human CNS neoplasms

We studied the utility of SR101 as a broad-spectrum neurosurgical intraoperative diagnostic agent by intraoperative identification of astrocytic brain tumors with fluorescence imaging of fresh human brain tumor biopsies labeled with SR101. In brain without tumor, SR101 filled the cytoplasm of cells that morphologically resembled astrocytes (Fig. 4A). In astrocytic tumor cores, SR101 stained cytoplasm, was excluded from most cell nuclei, and distinguished nuclear atypia (Fig. 4C, D). The fluorescence detected in astrocytes and astrocytoma cells was not endogenous autofluorescence (Supplemental Fig. 2). In non-astrocytic tumor samples, SR101 exclusion outlined the location of cell bodies but did not fill cytoplasm (Figs. 4E-I). One GBM case did not stain with SR101. Final neuropathological diagnosis of this case indicated the examined tissue consisted mostly of radiation treatment effect and not cellular GBM.

Interestingly, SR101 did not label most oligodendroglioma samples, although these tumors are often positive for GFAP. This finding suggests that SR101 also may be helpful for distinguishing oligodendrogliomas from other gliomas (Fig. 4H). SR101 failed to stain human lymphoma but labeled reactive astrocytes within the tissue, supporting the findings from our CNS lymphoma animal model (Fig. 4I, Supplemental Fig. 3).

Together, these data show that SR101 exhibits marked specificity for human astrocytes, astrocytomas, and reactive astrocytes. SR101 staining coupled with confocal microscopy allowed human astrocytic tumors and margins as well as reactive astrocytes to be identified within a time frame that supports intraoperative decision-making.

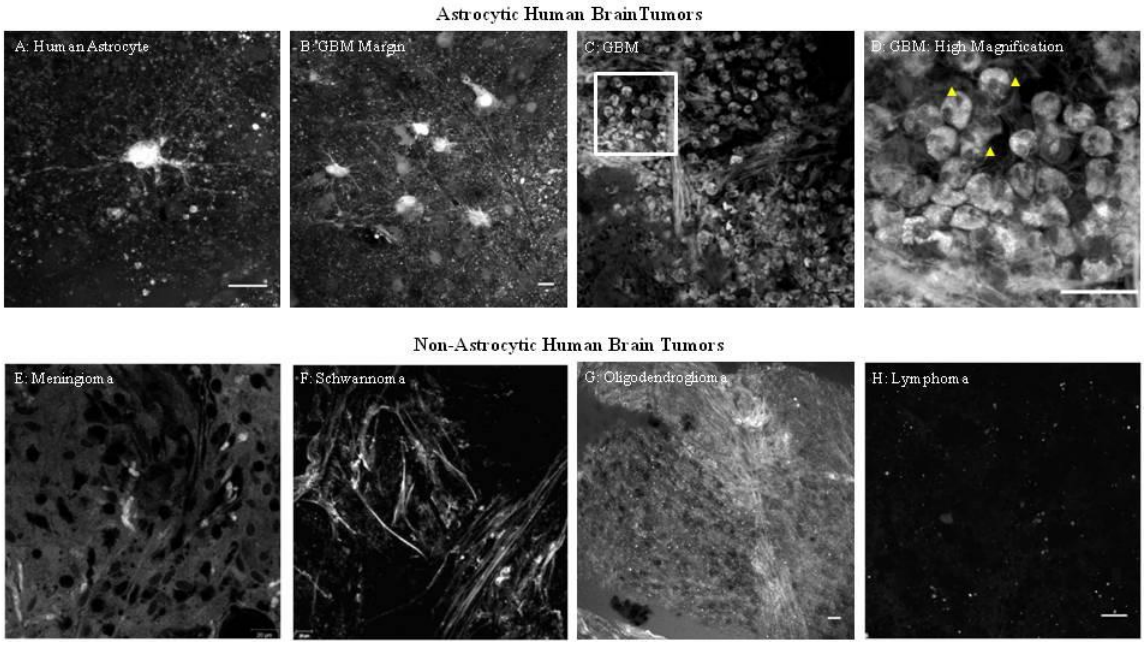

Figure 4: SR101 selectively labels human astrocytes and astrocytic brain tumors. Human brain tumor biopsies rapidly stained with SR101 and imaged with a confocal microscope. (A) Cell with astrocytic morphology from human brain labeled with SR101. (B) GBM margin with morphologically distinct tumor cells and reactive astrocytes (C) Grade IV astrocytoma. (D) Inset from C; hypercellularity and nuclei (arrowheads) are evident . (E-G) Non-astrocytic tumors absent of cells cytoplasmically filled with SR101. Dark regions in tissue indicate location of cell bodies. (G) Oligodendroglioma does not stain with SR101. (H) Lymphoma is negative for SR101 staining. Scale bar equals 20*um*

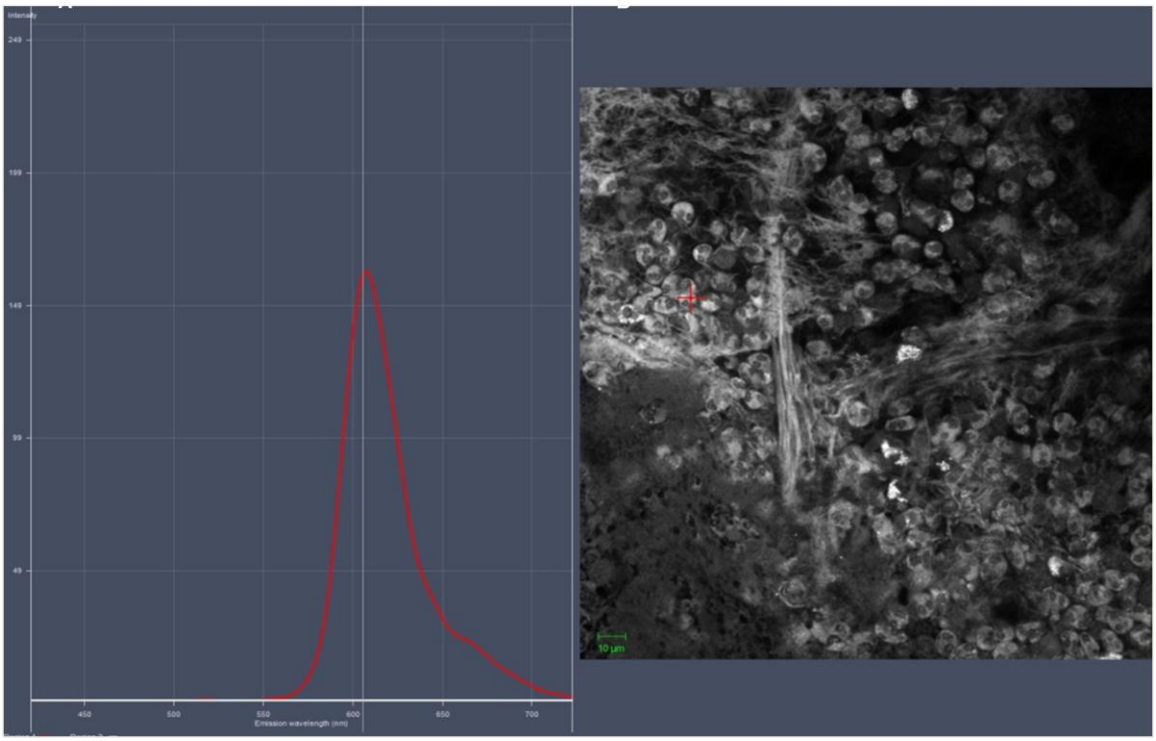

Supplemental 2: Endogenous fluorophores in human ex vivo tissue do not contribute to SR101 fluorescence. (A) Spectral imaging of human samples stained with SR101 generates a single emission profile unique to SR101. Note absence of additional emission spectra suggesting minimal contribution of endogenous fluorophores to the overall fluorescence signal. (B) Red crosshairs indicate SR101 positive cell selected for spectral analysis.

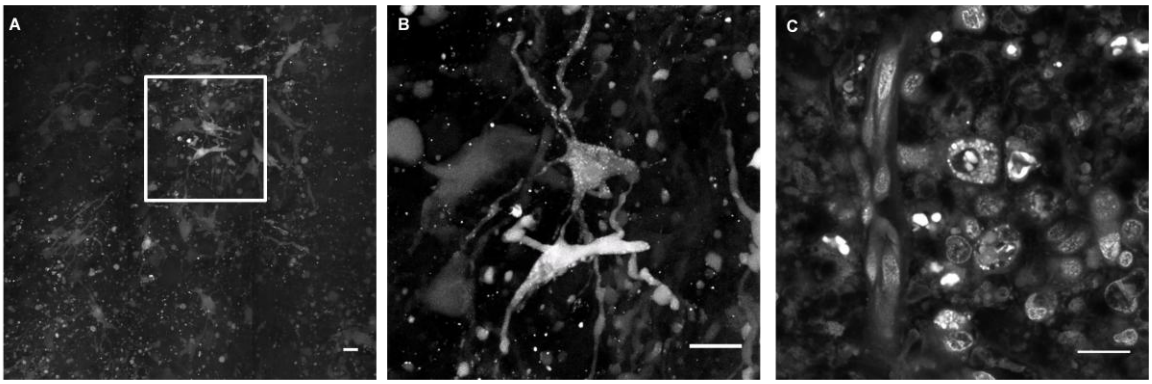

Supplemental 3: SR101 identifies reactive astrocytes in a human lymphoma biopsy. (A) Tiled image of human CNS lymphoma composed of 53 500um^2 optical sections contains SR101 positive cells with extensive processes. (B) High magnification inset morphologically clarifies SR101 positive cells as reactive astrocytes. Note lack of additional cell morphologies positive for SR101. (C) Non-specific acridine orange staining from adjacent biopsied region shows hypercellular tissue containing a heterozygous cell population. Scale bar equals 20*um*.

Discussion

We have demonstrated a technique for identifying the most common primary brain tumor, astrocytoma, by ex vivo exposure to the fluorescent dye SR101. This technique can provide specific cellular and molecular information necessary for diagnosis during surgery. We tested the specificity of SR101 in human cell culture, orthotopic rodent xenografts, and human tumor samples. Compared to the current standard of immunocytochemistry and final pathological paraffin-embedded diagnoses, SR101 provided more rapid and equally accurate identification of astrocytic tumors in all model systems. In human samples, SR101 provided effective visualization and differentiation of astrocytic tumors and, most importantly, their margins.

Improvements in timely and accurate intraoperative diagnoses are profoundly needed in clinical neurosurgery. Current diagnostic techniques rely on visualization of tissue with standard light microscopes and conventional contrast agents, a process that has evolved little over the last century (Gal 2005, Lechago 2005). Here, we have shown that fluorescent labeling of ex vivo tissue coupled with confocal imaging provide clear diagnostic benefits compared with current techniques. Our technique allows visualization of pathological tissue without freezing, fixing, or sectioning with their attendant artifacts and tissue loss (Supplemental Fig. 4). Images from tissue can provide a diagnosis within minutes—well within a time frame required to effectively guide a surgical approach and influence a patient's care while surgery is still in progress.

We envision that fluorescence imaging of ex vivo tissue will become a common technique in pathology departments in the near future. Our results here have clearly indicated the potential utility of SR101 for meeting the important clinical need of

differentiating high-grade astrocytoma from CNS lymphoma. Although the macroscopic appearance of these tumors is similar intraoperatively, their treatment plans are markedly distinct (Ricard, Idbaih et al. 2012). Astrocytomas require maximal safe resection to provide survival benefits to patients, while lymphomas are best biopsied and treated with adjuvant therapy. Differentiating these tumors requires a surgical biopsy followed by a minimum of 24 hours for diagnostic processing. We found these tumors could be differentiated by SR101 staining and confocal microscopy within 30 minutes of biopsy. This information could allow rapid modification of a surgical plan with consequent improvement of clinical outcomes.

GBM contains a heterozygous population of cells that vary in terms of GFAP expression (Bonavia, Inda et al. 2011). SR101 labeled slightly more tumor cells in GBM xenografts than GFAP. This finding resembles data from normal brain showing that SR101 identifies subtypes of astrocytes and precursor cells that are GFAP negative (Kimelberg 2004, Kafitz, Meier et al. 2008). Future studies on SR101 are required to identify and characterize GBM precursor cells that uptake SR101. Furthermore, a direct comparison of the sensitivity of SR101 and GFAP in human brain tumors is warranted.

Probes and devices that allow microscopic visualization and diagnosis of deep in vivo structures are under development (Michalet, Pinaud et al. 2005, Rivera, Brown et al. 2011, Kircher, de la Zerda et al. 2012). Some in vivo fluorescence imaging instruments have already been tested clinically (Eschbacher, Martirosyan et al. 2012). Safety concerns, however, may preclude some fluorophores and imaging modalities from ever being approved for in vivo clinical use. Nonetheless, rapid ex vivo diagnostics could

complement in vivo imaging by providing information from tissues processed with techniques that may not be safe for in vivo clinical use.

There are important considerations to diagnostic use of SR101. Staining with this agent requires tissue to be alive and relatively healthy when it is incubated with the dye. Damaged cells have been reported to uptake the dye (Masamoto, Tomita et al. 2012, Nimmerjahn and Helmchen 2012). However, we encountered no significant false positives in our experiments. A practical limitation to the widespread use of SR101 includes the need for immediate incubation of resected tissue in the operating room. Furthermore, immediate ex vivo imaging using specific fluorescent probes is not yet part of clinical pathological practice. Therefore, few pathology laboratories have confocal microscopes. Modernization of pathology departments would be needed to overcome these limitations.

Conclusion

SR101 rapidly and selectively labels human astrocytic tumors and astrocytes. To our knowledge, our results represent the first use of a functional dye on living human brain tumor tissue to provide a clinically meaningful immediate ex vivo histopathological diagnosis. There is compelling reason to believe that this method is only the first foray into a broad new area of pathology that has become possible because of the rapid and dramatic advances in fluorescence probes and fluorescence imaging techniques. Application of this technique to other tumors and diseases will only be limited by the identification of specific molecular targets and the development of targeted fluorophores.

These imaging techniques may have profound implications for improving patient diagnosis, clinical outcomes, and our understanding of human tumor pathophysiology.

Table 1. Distribution of human biopsies stained with SR101 and final diagnosis. SR101 selectively stained 12 of 11 astrocytoma cases and oligodendroglioma. SR101 did not stain necrotic tissue or tumors cells from additionally sampled CNS neoplasms.

Tumor Diagnosis	Number of Cases	Number SR101 Positive
Astrocytoma/GBM	13	12
Cavernous malformation	4	0
Chordoma	1	0
Ependymoma	2	0
Fibrous dysplasia	1	0
Meningioma	17	0
Metastasis	6	0
Necrosis	3	0
Oligodendroglioma	6	1
Pituitary Adenoma	5	0
Schwannoma	5	0
Subependymoma	2	0

Table 2. Stereology counts/region of interest. We quantified colabeling of fixable-SR101 and antibody staining in tumors with 18 acute slices from 6 rodent xenografts. Images were collected from 10 randomly selected 55 μM^2 regions of interest optically sectioned to 50 μM.

Tumor	Immunostain Positive	SR101 positive	Percent Overlap	Total Cells Counted
Astrocytoma	20.58 ±3.26	22.30±3.55	86.50±1.86	1316
Lymphoma	25.61±4.05	1.58±0.32	2.20±0.47	1657

References

Beeman, S. C., J. F. Georges and K. M. Bennett (2013). "Toxicity, biodistribution, and ex vivo MRI detection of intravenously injected cationized ferritin." Magn Reson Med **69**(3): 853-861.

Bonavia, R., M. M. Inda, W. K. Cavenee and F. B. Furnari (2011). "Heterogeneity maintenance in glioblastoma: a social network." Cancer Res **71**(12): 4055-4060.

Buckingham, S. C., S. L. Campbell, B. R. Haas, V. Montana, S. Robel, T. Ogunrinu and H. Sontheimer (2011). "Glutamate release by primary brain tumors induces epileptic activity." Nat Med **17**(10): 1269-1274.

Eschbacher, J., N. L. Martirosyan, P. Nakaji, N. Sanai, M. C. Preul, K. A. Smith, S. W. Coons and R. F. Spetzler (2012). "In vivo intraoperative confocal microscopy for real-time histopathological imaging of brain tumors." J Neurosurg **116**(4): 854-860.

Ferreri, A. J., M. Reni, M. Foppoli, M. Martelli, G. A. Pangalis, M. Frezzato, M. G. Cabras, A. Fabbri, G. Corazzelli, F. Ilariucci, G. Rossi, R. Soffietti, C. Stelitano, D. Vallisa, F. Zaja, L. Zoppegno, G. M. Aondio, G. Avvisati, M. Balzarotti, A. A. Brandes, J. Fajardo, H. Gomez, A. Guarini, G. Pinotti, L. Rigacci, C. Uhlmann, P. Picozzi, P. Vezzulli, M. Ponzoni, E. Zucca, F. Caligaris-Cappio, F. Cavalli and G. International Extranodal Lymphoma Study (2009). "High-dose cytarabine plus high-dose methotrexate versus high-dose methotrexate alone in patients with primary CNS lymphoma: a randomised phase 2 trial." Lancet **374**(9700): 1512-1520.

Gal, A. A. (2005). "The centennial anniversary of the frozen section technique at the Mayo Clinic." Arch Pathol Lab Med **129**(12): 1532-1535.

Kafitz, K. W., S. D. Meier, J. Stephan and C. R. Rose (2008). "Developmental profile and properties of sulforhodamine 101--Labeled glial cells in acute brain slices of rat hippocampus." J Neurosci Methods **169**(1): 84-92.

Kim, J. H., J. E. Lee, S. U. Kim and K. G. Cho (2010). "Stereological analysis on migration of human neural stem cells in the brain of rats bearing glioma." Neurosurgery **66**(2): 333-342; discussion 342.

Kimelberg, H. K. (2004). "The problem of astrocyte identity." Neurochem Int **45**(2-3): 191-202.

Kircher, M. F., A. de la Zerda, J. V. Jokerst, C. L. Zavaleta, P. J. Kempen, E. Mittra, K. Pitter, R. Huang, C. Campos, F. Habte, R. Sinclair, C. W. Brennan, I. K. Mellinghoff, E. C. Holland and S. S. Gambhir (2012). "A brain tumor molecular imaging strategy using a new triple-modality MRI-photoacoustic-Raman nanoparticle." Nat Med **18**(5): 829-834.

Lacroix, M., D. Abi-Said, D. R. Fourney, Z. L. Gokaslan, W. Shi, F. DeMonte, F. F. Lang, I. E. McCutcheon, S. J. Hassenbusch, E. Holland, K. Hess, C. Michael, D. Miller

and R. Sawaya (2001). "A multivariate analysis of 416 patients with glioblastoma multiforme: prognosis, extent of resection, and survival." J Neurosurg **95**(2): 190-198.

Lai, C. P., J. F. Bechberger, R. J. Thompson, B. A. MacVicar, R. Bruzzone and C. C. Naus (2007). "Tumor-suppressive effects of pannexin 1 in C6 glioma cells." Cancer Res **67**(4): 1545-1554.

Lechago, J. (2005). "The frozen section: pathology in the trenches." Arch Pathol Lab Med **129**(12): 1529-1531.

Masamoto, K., Y. Tomita, H. Toriumi, I. Aoki, M. Unekawa, H. Takuwa, Y. Itoh, N. Suzuki and I. Kanno (2012). "Repeated longitudinal in vivo imaging of neuro-glio-vascular unit at the peripheral boundary of ischemia in mouse cerebral cortex." Neuroscience **212**: 190-200.

Michalet, X., F. F. Pinaud, L. A. Bentolila, J. M. Tsay, S. Doose, J. J. Li, G. Sundaresan, A. M. Wu, S. S. Gambhir and S. Weiss (2005). "Quantum dots for live cells, in vivo imaging, and diagnostics." Science **307**(5709): 538-544.

Michaud, K., D. A. Solomon, E. Oermann, J. S. Kim, W. Z. Zhong, M. D. Prados, T. Ozawa, C. D. James and T. Waldman (2010). "Pharmacologic inhibition of cyclin-dependent kinases 4 and 6 arrests the growth of glioblastoma multiforme intracranial xenografts." Cancer Res **70**(8): 3228-3238.

Mouton, P. R. (2002). Principles and Practices of Unbiased Stereology: An Introduction For Bioscientists. Baltimore, The Johns Hopkins University Press.

Nimmerjahn, A. and F. Helmchen (2012). "In vivo labeling of cortical astrocytes with sulforhodamine 101 (SR101)." Cold Spring Harb Protoc **2012**(3): 326-334.

Nimmerjahn, A., F. Kirchhoff, J. N. Kerr and F. Helmchen (2004). "Sulforhodamine 101 as a specific marker of astroglia in the neocortex in vivo." Nat Methods **1**(1): 31-37.

Pichlmeier, U., A. Bink, G. Schackert, W. Stummer and A. L. A. G. S. Group (2008). "Resection and survival in glioblastoma multiforme: an RTOG recursive partitioning analysis of ALA study patients." Neuro Oncol **10**(6): 1025-1034.

Powell, S. Z. (2005). "Intraoperative consultation, cytologic preparations, and frozen section in the central nervous system." Arch Pathol Lab Med **129**(12): 1635-1652.

Ricard, D., A. Idbaih, F. Ducray, M. Lahutte, K. Hoang-Xuan and J. Y. Delattre (2012). "Primary brain tumours in adults." Lancet **379**(9830): 1984-1996.

Rivera, D. R., C. M. Brown, D. G. Ouzounov, I. Pavlova, D. Kobat, W. W. Webb and C. Xu (2011). "Compact and flexible raster scanning multiphoton endoscope capable of imaging unstained tissue." Proc Natl Acad Sci U S A **108**(43): 17598-17603.

van Dam, G. M., G. Themelis, L. M. Crane, N. J. Harlaar, R. G. Pleijhuis, W. Kelder, A. Sarantopoulos, J. S. de Jong, H. J. Arts, A. G. van der Zee, J. Bart, P. S. Low and V. Ntziachristos (2011). "Intraoperative tumor-specific fluorescence imaging in ovarian cancer by folate receptor-alpha targeting: first in-human results." Nat Med **17**(10): 1315-1319.

Verkman, A. S., M. Hara-Chikuma and M. C. Papadopoulos (2008). "Aquaporins--new players in cancer biology." J Mol Med **86**(5): 523-529.

Wen, P. Y. and S. Kesari (2008). "Malignant gliomas in adults." N Engl J Med **359**(5): 492-507.

CHAPTER 5

DISCUSSION

Infiltrative Margin

Tumor infiltration is detrimental to improving GBM patient care. Infiltrative cells undergo physiological changes which attenuate the effectiveness of current therapeutic agents (Horiuchi and Rosenblatt 1987, Wolf, Agnihotri et al. 2010, Wolf, Agnihotri et al. 2011). Neurosurgery provides a treatment option, with increased extent of tumor resection correlating with improved patient survival (Sanai and Berger 2008, Sanai and Berger 2009). However, the infiltrative nature of GBM prohibits maximal tumor cytoreduction. Developing means for clinically targeting GBM infiltration could improve patient survival by- (1) Preventing distal brain parenchymal tumor infiltration, (Barker, Prados et al.) allowing greater extent of surgical resection, and (Waring, Steinberg et al.) converting GBM into a more manageable chronic disease. Chapter 2 of this dissertation evaluates aqp-1 as a protein involved in GBM infiltration, chapter 3 develops a method for improving the quality of biobanked GBM patient biopsies, and chapter 4 identified an optical contrast agent for improving neurosurgical resection of GBM. Our work fills gaps in the current knowledge of GBM by identifying a targetable gene and protein which regulate GBM infiltration and developing optical imaging tools for improving GBM diagnostics.

AQP1 and Tumor Infiltration

Chapter 2 of this dissertation addressed aquaporin-1 and glioblastoma infiltration. Aqp1 is a membrane protein discovered by Peter Agre in 1991 (Agre 2006). This protein

belongs to a family of channel proteins that regulate cellular water transport. We discovered that over-expression of this protein in GBM correlates with decreased patient survival. Since the mechanistic role this gene and protein play in cellular motility is unknown, our studies address likely mechanisms underlying its prognostic power.

We implemented experiments with cultured human GBM cells, and found aqp1 enhanced the motility of GBM cells in culture without altering proliferation or survival of tumor cells. Next, we developed rodent xenografts from human GBM cells over-expressing AQP1, and found that tumors overexpressing aqp1 produce infiltrative tumor margins and decrease animal survival by nearly 20%. This suggests decreased survival in GBM patients overexpressing aqp1 is likely mediated by cellular motility.

AQP1 Water Transport and Tumor Motility

After observing aquaporin-1 enhanced tumor motility and infiltration in cell culture and animal models, we designed experiments testing the role water transport on aqp1 mediated GBM motility. We acquired a well-characterized aqp1 mutant (e17n)c with one point mutation that effectively prohibits water transport across aqp1's water channel, and generated human GBM cell lines overexpressing the mutant (Yool 2007). We found e17n-expressing GBM cells enhance motility similar to wild type aqp1. Our animal models confirmed e17n GBM cells produce infiltrative margins similar to wild type aqp1.

Our findings suggest aqp1 harbors a water transport-independent function that enhances tumor infiltration. This is significant to biomedical research as selective inhibitors of aqp1-mediated water transport are under development (Yool, Brown et al.

2010). Our findings suggest a region of the protein that does not regulate water transport must be targeted to modulate aqp1's role in GBM motility.

One potential target is aqp1's potassium ion transport function. The central pore of aqp1, which is created by assembly of 4 aqp1 monomers, transports potassium (Yool and Campbell 2012). Recent studies on GBM ion transport have shown that selective inhibition of K^+ decreases motility of GBM cells (Catacuzzeno, Aiello et al. 2011). We hypothesize that GBM motility could be attenuated if aqp1-mediated K^+ transport is inhibited. We are currently developing experiments to test this hypothesis.

Reflectance Imaging and Biobanking

We identified AQP1 overexpression in clinical biopsies by studying biobanked tissue. These tissues are collected and stored by immediately freezing intraoperative tumor biopsies (Botling and Micke 2011, Lim, Dickherber et al. 2011, Vaught, Henderson et al. 2012, Basik, Aguilar-Mahecha et al. 2013). However, many biobanked samples are poor quality (i.e. contain a large amount of necrotic tissue), or do not adequately represent the characteristics of the original tumor. This is partially due to poor histologic tissue assessment prior to biobanking (Georges, Zehri et al. 2014). We hypothesized that a rapid and reliable means for differentiating cellular from necrotic samples prior to biobanking could profoundly improve the quality of tissues stored for future research.

The third chapter of this dissertation develops patient biopsy assessment by confocal reflectance microscopy (CRM) prior to biobanking. CRM is an optical imaging modality that generates contrast by collecting backscattered photons from an imaged

sample. The photons pass through a pinhole that spatially filters photons originating outside the focal plane. Since the technique does not rely on a Stokes shift, it requires a small fraction of the light energy needed for standard fluorescence confocal imaging (Georges, Zehri et al. 2014).

Biospecimen analysis by CRM requires stability of tissue DNA, RNA, and protein. We generated a time course of samples examined by CRM immediately after biopsy to 2 hours post-biopsy. Samples imaged up to 2 hours post-resection had DNA, RNA, and protein characteristics similar to reference controls.

CRM and DAPI identified similar cellular boundaries in animal glioma models, and CRM differentiated cellular from necrotic samples in human biopsies. Interestingly, CRM identified several histopathological features utilized for intraoperative diagnoses, such as psammoma bodies in meningiomas and antoni A/B regions in schwannomas. We are currently testing CRM for intraoperative neuropathologic diagnostics.

Neurosurgery Cytoreduction

Surgical tumor cytoreduction is another means for increasing patient survival. Studies based on post-operative MRI show optimal survival benefits when at least 98% of the tumor is removed (Sanai and Berger 2008, Sanai and Berger 2009, Sanai and Berger 2011, Sanai, Polley et al. 2011).

Neurosurgeons rely on gross tumor appearance to guide resection during surgery. However, GBM is difficult to differentiate from non-neoplastic tissue due to its infiltrative nature, In non-eloquent brain regions, a surgeon may opt for a more aggressive resection, possibly resecting benign tissue, in effort to maximize GBM

cytoreduction (Sanai 2012). In more eloquent regions, a surgeon may choose a less aggressive course in effort to preserve neurological function. Neuropathologists examine frozen biopsy sections from presumed tumor margins intraoperatively to determine necessity for further resection. Unfortunately, frozen section contrast agents are not tumor-specific and may provide inconclusive feedback.

Studies with a tumor-specific contrast agent, 5 ALA, suggest that GBM extent of resection increases when neurosurgeons have means to distinguish neoplastic from normal brain tissue (Stummer, Novotny et al. 2000, Stummer, Pichlmeier et al. 2006). However, this contrast agent is not useful at the microscopic level, and literature suggests it may not be tumor-specific (Masubuchi, Kajimoto et al. 2013). We hypothesized that the fluorescent contrast agent Sulforhodamine 101 provides real-time intraoperative visualization of GBM and its infiltrative margins.

Sulforhodamine 101

Clinicians utilize frozen sections and GFAP immunohistochemistry to histopathologically diagnose glioblastoma. These histologic techniques were developed in the early 20th century, and are fundamentally the same since their inception (Gal and Cagle 2005, Powell 2005). Frozen sections are conducted intraoperatively, but can be inconclusive due to non-specific staining. GFAP immunohistochemistry provides specific staining of GBM, but requires 24-48 hours and is too slow for intraoperative diagnosis. In chapter 4 of this dissertation, we begin to develop a novel clinical fluorescent contrast agent - Sulforhodamine 101. We couple the agent with modern imaging techniques to provide immediate cellular visualization of GBM.

SR101 is commonly used in neuroscience research to rapidly label live astrocytic cells with GFAP-like specificity (Nimmerjahn, Kirchhoff et al. 2004, Nimmerjahn and Helmchen 2012). The work in this dissertation is the first test of SR101's clinical potential. Tested on cell culture, animal brain tumor models, and fresh human biopsies we found SR101 could rapidly label astrocytic tumors, such as GBM, with minimal labeling of non-astrocytic lesions. Our findings suggest significant clinical potential of this fluorescent contrast agent for rapid and specific intraoperative diagnosis. These methods could complement current neuropathologic techniques and provide much-needed information during surgical resection.

Conclusions

This dissertation uses interdisciplinary approaches to target the clinical problem of GBM infiltration. In chapter two we implemented cancer genomics plus molecular and cellular biology to investigate AQP1-mediated GBM patient survival. We began this work by analyzing biobanked human GBM biopsies and noticed many biobanked specimens lacked the cellularity to be utilized in research. This prompted us to successfully develop an optical imaging technique to screen biopsies prior to biobanking. Lastly, we identified and tested an intraoperative contrast agent that could improve neurosurgical resection of GBM.

GBM is the most common primary brain tumor. Despite decades of focused research, patient survival has only increased a few months (Salcman 1980, Georges, Zehri et al. 2014). The diffusely infiltrative nature of this tumor precludes effectiveness of current clinical approaches. By targeting a gene and protein that mediate infiltration,

and providing clinicians better tools for intraoperative visualization of GBM, we hope this dissertation is a foundation for future translational approaches aimed at improving GBM patient care.

REFERENCES

Agre, P. (2006). "The aquaporin water channels." Proc Am Thorac Soc **3**(1): 5-13.

Antonio Frigeri, G. P. N., Maria Svelto (2007). "Aquaporins as Targets for Drug Discovery." Current Pharmaceutical Design **13**(23): 2421-2427.

Bailey, O. T. (1985). "Genesis of the Percival Bailey-Cushing classification of gliomas." Pediatr Neurosci **12**(4-5): 261-265.

Barker, F. G., 2nd, M. D. Prados, S. M. Chang, P. H. Gutin, K. R. Lamborn, D. A. Larson, M. K. Malec, M. W. McDermott, P. K. Sneed, W. M. Wara and C. B. Wilson (1996). "Radiation response and survival time in patients with glioblastoma multiforme." J Neurosurg **84**(3): 442-448.

Basik, M., A. Aguilar-Mahecha, C. Rousseau, Z. Diaz, S. Tejpar, A. Spatz, C. M. Greenwood and G. Batist (2013). "Biopsies: next-generation biospecimens for tailoring therapy." Nat Rev Clin Oncol **10**(8): 437-450.

Berens, M. E., G. Bjotvedt, D. C. Levesque, M. D. Rief, J. R. Shapiro and S. W. Coons (1993). "Tumorigenic, invasive, karyotypic, and immunocytochemical characteristics of clonal cell lines derived from a spontaneous canine anaplastic astrocytoma." In Vitro Cell Dev Biol Anim **29A**(4): 310-318.

Bloch, O., S. J. Han, S. Cha, M. Z. Sun, M. K. Aghi, M. W. McDermott, M. S. Berger and A. T. Parsa (2012). "Impact of extent of resection for recurrent glioblastoma on overall survival: clinical article." J Neurosurg **117**(6): 1032-1038.

Boassa, D., W. D. Stamer and A. J. Yool (2006). "Ion channel function of aquaporin-1 natively expressed in choroid plexus." J Neurosci **26**(30): 7811-7819.

Botling, J. and P. Micke (2011). "Biobanking of fresh frozen tissue from clinical surgical specimens: transport logistics, sample selection, and histologic characterization." Methods Mol Biol **675**: 299-306.

Brooks, H. L., J. W. Regan and A. J. Yool (2000). "Inhibition of aquaporin-1 water permeability by tetraethylammonium: involvement of the loop E pore region." Mol Pharmacol **57**(5): 1021-1026.

Catacuzzeno, L., F. Aiello, B. Fioretti, L. Sforna, E. Castigli, P. Ruggieri, A. M. Tata, A. Calogero and F. Franciolini (2011). "Serum-activated K and Cl currents underlay U87-MG glioblastoma cell migration." J Cell Physiol **226**(7): 1926-1933.

Clarke, L. E. and B. A. Barres (2013). "Emerging roles of astrocytes in neural circuit development." Nat Rev Neurosci **14**(5): 311-321.

Colman, H., L. Zhang, E. P. Sulman, J. M. McDonald, N. L. Shooshtari, A. Rivera, S. Popoff, C. L. Nutt, D. N. Louis, J. G. Cairncross, M. R. Gilbert, H. S. Phillips, M. P. Mehta, A. Chakravarti, C. E. Pelloski, K. Bhat, B. G. Feuerstein, R. B. Jenkins and K. Aldape "A multigene predictor of outcome in glioblastoma." Neuro Oncol **12**(1): 49-57.

Daumas-Duport, C. (1992). "Histological grading of gliomas." Curr Opin Neurol Neurosurg **5**(6): 924-931.

Daumas-Duport, C., B. Scheithauer, J. O'Fallon and P. Kelly (1988). "Grading of astrocytomas. A simple and reproducible method." Cancer **62**(10): 2152-2165.

Daumas-Duport, C., B. W. Scheithauer and P. J. Kelly (1987). "A histologic and cytologic method for the spatial definition of gliomas." Mayo Clin Proc **62**(6): 435-449.

Di, C., A. K. Mattox, S. Harward and C. Adamson (2010). "Emerging therapeutic targets and agents for glioblastoma migrating cells." Anticancer Agents Med Chem **10**(7): 543-555.

DP Byar, S. G. a. T. S. (1983). Prognostic Factors For Malignant Gliomas. Oncology of the Nervous System. Boston, Martinus Nijoff.

Farina, M., J. B. Rocha and M. Aschner (2011). "Mechanisms of methylmercury-induced neurotoxicity: evidence from experimental studies." Life Sci **89**(15-16): 555-563.

Ferguson, S. and M. S. Lesniak (2005). "Percival Bailey and the classification of brain tumors." Neurosurg Focus **18**(4): e7.

Foersch, S., A. Heimann, A. Ayyad, G. A. Spoden, L. Florin, K. Mpoukouvalas, R. Kiesslich, O. Kempski, M. Goetz and P. Charalampaki (2012). "Confocal laser endomicroscopy for diagnosis and histomorphologic imaging of brain tumors in vivo." PLoS One **7**(7): e41760.

Gal, A. A. and P. T. Cagle (2005). "The 100-year anniversary of the description of the frozen section procedure." JAMA **294**(24): 3135-3137.

Georges, J., A. Zehri, E. Carlson, J. Nichols, M. A. Mooney, N. L. Martirosyan, L. Ghaffari, M. Y. Kalani, J. Eschbacher, B. Feuerstein, T. Anderson, M. C. Preul, K. Van Keuren-Jensen and P. Nakaji (2014). "Contrast-free microscopic assessment of glioblastoma bioposy specimens prior to biobanking." Neurosurg Focus **36**(2): E8.

Gonen, T. and T. Walz (2006). "The structure of aquaporins." Q Rev Biophys **39**(4): 361-396.

Hart, M. G., R. Garside, G. Rogers, K. Stein and R. Grant (2013). "Temozolomide for high grade glioma." Cochrane Database Syst Rev **4**: CD007415.

Hegi, M. E., A. C. Diserens, T. Gorlia, M. F. Hamou, N. de Tribolet, M. Weller, J. M. Kros, J. A. Hainfellner, W. Mason, L. Mariani, J. E. Bromberg, P. Hau, R. O. Mirimanoff, J. G. Cairncross, R. C. Janzer and R. Stupp (2005). "MGMT gene silencing and benefit from temozolomide in glioblastoma." N Engl J Med **352**(10): 997-1003.

Horiuchi, N. and M. Rosenblatt (1987). "Evaluation of a parathyroid hormone antagonist in an in vivo multiparameter bioassay." Am J Physiol **253**(2 Pt 1): E187-192.

Kandel, E. R., J. H. Schwartz and T. M. Jessell (2000). Principles of neural science. New York ; London, McGraw-Hill Health Professions Division.

Lacroix, M., D. Abi-Said, D. R. Fourney, Z. L. Gokaslan, W. Shi, F. DeMonte, F. F. Lang, I. E. McCutcheon, S. J. Hassenbusch, E. Holland, K. Hess, C. Michael, D. Miller and R. Sawaya (2001). "A multivariate analysis of 416 patients with glioblastoma multiforme: prognosis, extent of resection, and survival." J Neurosurg **95**(2): 190-198.

Lim, M. D., A. Dickherber and C. C. Compton (2011). "Before you analyze a human specimen, think quality, variability, and bias." Anal Chem **83**(1): 8-13.

Loitto, V. M., T. Karlsson and K. E. Magnusson (2009). "Water flux in cell motility: expanding the mechanisms of membrane protrusion." Cell Motil Cytoskeleton **66**(5): 237-247.

Louis, D. N., Deutsches Krebsforschungszentrum Heidelberg., International Agency for Research on Cancer., World Health Organization. and ebrary Inc. (2007). WHO classification of tumours of the central nervous system. World Health Organization classification of tumours. Geneva, Switzerland, Distributed by WHO Press, World Health Organization,**:** 309 p.

Mahaley, M. S., Jr., C. Mettlin, N. Natarajan, E. R. Laws, Jr. and B. B. Peace (1990). "Analysis of patterns of care of brain tumor patients in the United States: a study of the Brain Tumor Section of the AANS and the CNS and the Commission on Cancer of the ACS." Clin Neurosurg **36**: 347-352.

Masubuchi, T., Y. Kajimoto, S. Kawabata, N. Nonoguchi, T. Fujishiro, S. Miyatake and T. Kuroiwa (2013). "Experimental study to understand nonspecific protoporphyrin IX fluorescence in brain tissues near tumors after 5-aminolevulinic acid administration." Photomed Laser Surg **31**(9): 428-433.

Mattox, A. K., J. Li and D. C. Adamson (2012). "Stopping cancer in its tracks: using small molecular inhibitors to target glioblastoma migrating cells." Curr Drug Discov Technol **9**(4): 294-304.

McCoy, E. and H. Sontheimer "MAPK induces AQP1 expression in astrocytes following injury." Glia **58**(2): 209-217.

McCoy, E. and H. Sontheimer (2007). "Expression and function of water channels (aquaporins) in migrating malignant astrocytes." Glia **55**(10): 1034-1043.

McCoy, E. and H. Sontheimer (2010). "MAPK induces AQP1 expression in astrocytes following injury." Glia **58**(2): 209-217.

Mooney, M. A., A. H. Zehri, J. F. Georges and P. Nakaji (2014). "Laser scanning confocal endomicroscopy in the neurosurgical operating room: a review and discussion of future applications." Neurosurg Focus **36**(2): E9.

Nimmerjahn, A. and F. Helmchen (2012). "In vivo labeling of cortical astrocytes with sulforhodamine 101 (SR101)." Cold Spring Harb Protoc **2012**(3): 326-334.

Nimmerjahn, A., F. Kirchhoff, J. N. Kerr and F. Helmchen (2004). "Sulforhodamine 101 as a specific marker of astroglia in the neocortex in vivo." Nat Methods **1**(1): 31-37.

Orringer, D., D. Lau, S. Khatri, G. J. Zamora-Berridi, K. Zhang, C. Wu, N. Chaudhary and O. Sagher (2012). "Extent of resection in patients with glioblastoma: limiting factors, perception of resectability, and effect on survival." J Neurosurg **117**(5): 851-859.

Powell, S. Z. (2005). "Intraoperative consultation, cytologic preparations, and frozen section in the central nervous system." Arch Pathol Lab Med **129**(12): 1635-1652.

Roberts, D. W., P. A. Valdes, B. T. Harris, A. Hartov, X. Fan, S. Ji, F. Leblond, T. D. Tosteson, B. C. Wilson and K. D. Paulsen (2012). "Glioblastoma multiforme treatment with clinical trials for surgical resection (aminolevulinic acid)." Neurosurg Clin N Am **23**(3): 371-377.

Salcman, M. (1980). "Survival in glioblastoma: historical perspective." Neurosurgery **7**(5): 435-439.

Sanai, N. (2012). "Emerging operative strategies in neurosurgical oncology." Curr Opin Neurol **25**(6): 756-766.

Sanai, N. and M. S. Berger (2008). "Glioma extent of resection and its impact on patient outcome." Neurosurgery **62**(4): 753-764; discussion 264-756.

Sanai, N. and M. S. Berger (2009). "Operative techniques for gliomas and the value of extent of resection." Neurotherapeutics **6**(3): 478-486.

Sanai, N. and M. S. Berger (2011). "Extent of resection influences outcomes for patients with gliomas." Rev Neurol (Paris) **167**(10): 648-654.

Sanai, N., J. Eschbacher, G. Hattendorf, S. W. Coons, M. C. Preul, K. A. Smith, P. Nakaji and R. F. Spetzler (2011). "Intraoperative confocal microscopy for brain tumors: a feasibility analysis in humans." Neurosurgery **68**(2 Suppl Operative): 282-290; discussion 290.

Sanai, N., M. Y. Polley, M. W. McDermott, A. T. Parsa and M. S. Berger (2011). "An extent of resection threshold for newly diagnosed glioblastomas." J Neurosurg **115**(1): 3-8.

Schneider, T., C. Mawrin, C. Scherlach, M. Skalej and R. Firsching (2010). "Gliomas in adults." Dtsch Arztebl Int **107**(45): 799-807; quiz 808.

Stummer, W., A. Novotny, H. Stepp, C. Goetz, K. Bise and H. J. Reulen (2000). "Fluorescence-guided resection of glioblastoma multiforme by using 5-aminolevulinic acid-induced porphyrins: a prospective study in 52 consecutive patients." J Neurosurg **93**(6): 1003-1013.

Stummer, W., U. Pichlmeier, T. Meinel, O. D. Wiestler, F. Zanella, H. J. Reulen and A. L.-G. S. Group (2006). "Fluorescence-guided surgery with 5-aminolevulinic acid for resection of malignant glioma: a randomised controlled multicentre phase III trial." Lancet Oncol **7**(5): 392-401.

Sutton, D. J. and P. B. Tchounwou (2006). "Mercury-induced externalization of phosphatidylserine and caspase 3 activation in human liver carcinoma (HepG2) cells." Int J Environ Res Public Health **3**(1): 38-42.

Teodorczyk, M. and A. Martin-Villalba (2010). "Sensing invasion: cell surface receptors driving spreading of glioblastoma." J Cell Physiol **222**(1): 1-10.

Tonn, J. C., N. Thon, O. Schnell and F. W. Kreth (2012). "Personalized surgical therapy." Ann Oncol **23 Suppl 10**: x28-32.

Udovich, J. A., D. G. Besselsen and A. F. Gmitro (2009). "Assessment of acridine orange and SYTO 16 for in vivo imaging of the peritoneal tissues in mice." J Microsc **234**(2): 124-129.

Vaught, J. B., M. K. Henderson and C. C. Compton (2012). "Biospecimens and biorepositories: from afterthought to science." Cancer Epidemiol Biomarkers Prev **21**(2): 253-255.

Verkman, A. S., M. Hara-Chikuma and M. C. Papadopoulos (2008). "Aquaporins--new players in cancer biology." J Mol Med **86**(5): 523-529.

Waring, G. O., 3rd, E. B. Steinberg and L. A. Wilson (1985). "Slit-lamp microscopic appearance of corneal wound healing after radial keratotomy." Am J Ophthalmol **100**(1): 218-224.

Wirth, D., M. Snuderl, S. Sheth, C. S. Kwon, M. P. Frosch, W. Curry and A. N. Yaroslavsky (2012). "Identifying brain neoplasms using dye-enhanced multimodal confocal imaging." J Biomed Opt **17**(2): 026012.

Wolf, A., S. Agnihotri and A. Guha (2010). "Targeting metabolic remodeling in glioblastoma multiforme." Oncotarget **1**(7): 552-562.

Wolf, A., S. Agnihotri, J. Micallef, J. Mukherjee, N. Sabha, R. Cairns, C. Hawkins and A. Guha (2011). "Hexokinase 2 is a key mediator of aerobic glycolysis and promotes tumor growth in human glioblastoma multiforme." J Exp Med **208**(2): 313-326.

Yool, A. J. (2007). "Dominant-negative suppression of big brain ion channel activity by mutation of a conserved glutamate in the first transmembrane domain." Gene Expr **13**(6): 329-337.

Yool, A. J., E. A. Brown and G. A. Flynn (2010). "Roles for novel pharmacological blockers of aquaporins in the treatment of brain oedema and cancer." Clin Exp Pharmacol Physiol **37**(4): 403-409.

Yool, A. J. and E. M. Campbell (2012). "Structure, function and translational relevance of aquaporin dual water and ion channels." Mol Aspects Med **33**(5-6): 553-561.

Zhang, J., M. F. Stevens and T. D. Bradshaw (2012). "Temozolomide: mechanisms of action, repair and resistance." Curr Mol Pharmacol **5**(1): 102-114.

APPENDIX A

CIRRICULUM VITAE

CIRRICULUM VITAE (THROUGH MAY 2014)

EDUCATION

August 2006 – May 2014
Arizona College of Osteopathic Medicine
· Doctor of Osteopathic Medicine

August 2008 – May 2014
Arizona State University & Barrow Neurological Institute
· Doctor of Philosophy: Neuroscience
· Dissertation: Evaluating and Controlling Glioblastoma Infiltration

August 1999 – December 2003
Arizona State University
· Bachelor of Science: Kinesiology

POSITIONS, AWARDS, & PROFESSIONAL DEVELOPMENT

Teaching Assistant Positions and Employment:

2013- 2014	Neurosurgery Research Fellow, Barrow Neurological Institute Phoenix, Arizona
2011-2013	Supervisor of Barrow Neurological Institute Microscopy Core, Phoenix, Arizona
May 2012	Analytical and Quantitative Light Microscopy, Woods Hole, MA
Fall 2011	Molecular and Cellular Biology for graduate students; *Advanced Fluorescence Microscopy: Theory and Technique*, Arizona State University, Tempe, Arizona
Fall 2009	Biology for Majors, Arizona State University, Tempe, Arizona
Spring 2009	Cell Biotechnology Arizona State University, Tempe, Arizona
2007-2009	Gross Anatomy, Arizona College of Osteopathic Medicine, Phoenix, Arizona
Summer 2006	Human Anatomy and Physiology, Arizona State University, Tempe, Arizona
Spring 2006	ECG Interpretation, Arizona State University, Tempe, Arizona

Mentored Students:

2012-2014	Aqib H. Zehri (MS1): University of Arizona College of Medicine **Project:** Rapid Screening of Brain Tumor Biospecimens with Confocal Reflectance Microscopy **Recognition:** Project awarded AANS summer research fellowship

Fellowships and Awards:

2013-2014	Robert F. Spetzler Neurosurgery Research Fellow
2012	Rookie of the Year Teaching Assistant at Woods Hole; **Analytical and Quantitative Light Microscopy.**
2010	Chroma Cube Award at **Quantitative Fluorescence Microscopy** for overall best student project and presentation
2010	Molecular Imaging Fellowship; Carl Zeiss, Inc

2008-2009 Neuroscience Research Fellowship; Barrow Neurological Institute
2008 Welch Grant Scholar; American Osteopathic Association

Scientific Development Courses:

April 2014 Cold Spring Harbor Laboratory; **Neuronal Circuits**
May 2011 Marine Biological Laboratory (Woods Hole); **Analytical and Quantitative Light Microscopy**
June 2010 Mount Desert Island Biological Laboratories; **Quantitative Fluorescence Microscopy**
April 2010 Jackson Laboratories; **Colony Management; principles and practices**
July 2009 Cold Spring Harbor Laboratory; **Imaging Structure and Function in the Nervous System** (one week of lecture and lab covering confocal and multiphoton imaging)

PUBLICATIONS AND PRESENTATIONS

Publications:

1. **J.F. Georges***, X. Liu*, J. Eschbacher, J. Nichols, R. Spetzler, B.G. Feuerstein, M.C. Preul, K. Van Keuren-Jensen, T. Anderson, H. Yan*, P. Nakaji*. **Rapid *Ex Vivo* Identification of Central Nervous System Lymphoma with a Conformational Switching Aptamer**. Submitted to *Acta Neuropathologica* April 2014.
2. **J.F. Georges**, S. Flitman, J. Tobin. **Pseudotumor-like Headache with Normal Intracranial Pressure: A Case Series of 4 Patients.** Submitted to *Cephalalgia* April 2014.
3. **J.F. Georges***, A.H. Zehri*, E. Carlson, J. Eschbacher, J. Nichols, N. Martirosyan, R. Spetzler, M.Y.S. Kalani , B.G. Feuerstein, T. Anderson, M.C. Preul, K.Van Keuren-Jensen, P. Nakaji. **Contrast-Free Microscopic Assessment of Glioblastoma Biospecimens Prior to Biobanking.** *Journal of Neurosurgery: Neurosurgical Focus* February 2014.
4. M. Mooney, A.H. Zehri, **J.F. Georges**, P. Nakaji. **Laser Scanning Confocal Endomicroscopy in the Neurosurgical Operating Room: A Review and Discussion of Future Applications.** *Journal of Neurosurgery: Neurosurgical Focus* February 2014.
5. **J.F. Georges**, N. Martirosyan, J. Eschbacher, J. Nichols, M. Tissot, M Preul, B. Feuerstein, T. Anderson, R. Spetzler, P. Nakaji. **Rapid and Specific Diagnosis of Astrocytic Brain Tumors by Immediate Ex Vivo Confocal Imaging with Sulforhodamine 101.** *Journal of Clinical Neuroscience* March 2014.
6. M. Mooney, F.C. Albuquerque, D.A. Hardesty, K.K Almefty, A.H. Zehri, **J.F. Georges**, P. Nakaji. **Unusual Presentation of a Tentorial Dural Arteriovenous Fistula as a Pineal Mass: Case Report and Review of the Literature.** Submitted to *Journal of Neurosurgery* November 2013.
7. Seth Truran, Volkmar Weissig, Marina Ramirez-Alvarado, Daniel A. Franco, Camelia Burciu, **Joseph Georges**, Shishir Murarka, Winter Okoth, Parameswaran

Hari and Raymond Q. Migrino. **Nanoliposome Protection against AL Amyloid Light Chain Protein-Induced Endothelial Injury.** *Journal of Liposome Research* November 2013.

8. M. Behbahaninia, N.L. Martirosyan, **J.F. Georges,** J. Udovich, M.Y.S. Kalani, B.G. Fueurstein, P. Nakaji, R.F. Spetzler, M.C. Preul. **Intraoperative Fluorescent imaging of Intracranial Lesions: A Review.** *Clinical Neurology and Neurosurgery* May 2013.
9. N Martirosyan, **J Georges**, J Eschbaucher, DD Cavalcanti, MG Abdelwahab, AC Scheck, P. Nakaji, RF Spetzler, and MC Preul. **Handheld Confocal Endomicroscope Imaging in an Experimental Glioblastoma Model and Normal Brain: Utility of a Variety of Rapid Fluorescent Dyes.** *Journal of Neurosurgery: Neurosurgical Focus* February 2014.
10. S.A. Truran, A.E. Roher, T.G. Beach, C. Burciu, D.A. Franco, G. Serrano, C.L. Maarouf, **J.F. Georges**, P. Reaven, R.Q. Migrino. **Novel Human Microvascular Tissue Model to Study Alzheimers Disease.** Submitted to *Journal of Neuroscience Methods* December 2013.
11. S. Beeman, **J. Georges**, and K.M. Bennet. **An MRI Technique to Detect Microstructural Changes in Chronic Liver Disease.** *Magnetic Resonance in Medicine* February 2013.
12. E. Sulman*, **J. Georges***, G. Samuelson*, K. Aldape, K.M. Bennett, E. Mirvish, A. Misra, L. Hu, M. Kala, C. Schendel, B.F. Feuerstein. **Aquaporin-1 Mediated Effects in Human Malignant Glioma**. In revision to *Cancer Research**.
13. S. Beeman, **J. Georges**, and K.M. Bennett. **Toxicity, Biodistribution, and *Ex Vivo* MRI Detection of Intravenously Injected Cationic Ferritin**. *Magnetic Resonance in Medicine* April 2012.
14. C. Shi, J. Lu, W. Wu, F. Ma, **J. Georges**, H. Huang, J. Balducci, Y. Chang, Y. Huang. **Endothelial Cell-Specific Molecule 2 (ECSM2) Localizes to Cell-Cell Junctions and Modulates bFGF-directed Cell Migration via the ERK-FAK Pathway.** *PLoS ONE* June 2011.
15. Y. Tufail, A. Matyushov, N. Baldwin, M.L. Tauchmann, **J. Georges**, A. Yoshihiro, S.H. Tillery, and W.J. Tyler. **Transcranial Pulsed Ultrasound Stimulates Intact Mammalian Cortex.** *Neuron* June 2010.

Abstracts:

1. **J. Georges**, A. Zehri, E. Carlson, N.L. Martirosyan, J. Eschbacher, J. Nichols, A.M. Elhadi, G. Mendes, B.G. Feuerstein, R.F. Spetzler, T. Anderson, M.C. Preul, K. Jensen, P. Nakaji. **Contrast-Free Microscopic Assessment of Glioblastoma Biospecimens.** *American Association of Neurological Surgeons,* April 9th-14th, 2014, San Francisco, CA.
2. **J. Georges**, A. Zehri, E. Carlson, N.L. Martirosyan, J. Eschbacher, J. Nichols, A.M. Elhadi, G. Mendes, B.G. Feuerstein, R.F. Spetzler, T. Anderson, M.C. Preul, K. Jensen, P. Nakaji. **Immediate Screening of Glioblastoma**

Biospecimens with Confocal Reflectance Microscopy Improves Quality of Biobanked Specimens. In the annual meeting of the *Society for NeuroOncology*, Nov. 21st-24th, 2013, San Francisco, CA.

3. R.D. Bhardwaj, M. Chakravadhanul;a, V. Ozols, **J. Georges**, E. Carlson, C. Hamptom, W.K. Decker. **Autologous Dendritic Cell Vaccine to Combat Brain Tumors in Dogs and Mice.** In the annual meeting of the *Society for NeuroOncology*, Nov. 21st-24th, 2013, San Francisco, CA.
4. S. Truran, V. Wessig, M.R. Alvarado, D.A. Franco, C. Burciu, **J. Georges**, S. Murarka, W.A. Okoth, H. Parameswaran, R. Migrino. **Nanoliposome Protection Against AL Amyloid Light Chain Protein-Induced Endothelial Injury.** In the annual meeting of the *American Heart Association*, Nov. 17th-20th, 2013, Dallas, TX.
5. **J. Georges**, N.L. Martirosyan, J. Eschbacher, J. Nichols, M. Tissot, A.M. Elhadi, G. Mendes, M. McQuilkin, B.G. Feuerstein, R.F. Spetzler, T. Anderson, M.C. Preul, P. Nakaji. **Rapid and Specific Diagnosis of Human Astrocytic Brain Tumors by Immediate Imaging with Sulforhodamine 101.** *American Association of Neurological Surgeons*, April 27th-May 1st, 2013, New Orleans, LA.
6. S. Truran, M. Ramirez-Alvarado, A.C.DiCostanzo, D.A. Franco, C. Burcio, S. Murarka, A. Maltagliati, **J. Georges**, R.Q. Migrino. **Adipose Arteriole Endothelial Dysfunction Induced by Amyloid Proteins: A Novel Human Model to Study Protein Misfolding Disease.** *American Heart Association*, Nov 3rd-4th, 2012, Los Angeles, CA.
7. S. Pati, J.X. Yin, Y. Gan, **J. Georges**, F.D. Shi, M. Maalouf, D.M. Treiman. **Hypothermia Attenuates Neuro-glial Injury and Neuroinflammation in Prolonged Status Epilepticus.** In the *American Academy of Neurology*, April 21st-28th, 2012, New Orleans, LA.
8. **J. Georges**, G. Samuelson, A. Misra, A. Joy, M. McQuilkin, L. Butler, B.G. Feuerstein. **Aquaporin-1 Increases Invasion of Glioblastoma Multiforme.** In the annual meeting of the *Society for NeuroOncology*, Nov. 17th-20th, 2011, Orange County, CA.
9. D.P. Baluch*, **J. Georges***, P. Deviche, W.J. Tyler. **Estrogen Acts Through GPR-30 Receptors to Rapidly Increase Neurotransmitter Release from Hippocampal Excitatory Synapses.** In the annual meeting of *Society for Neuroscience*, Oct. 17th-21st, 2009, Chicago, Illinois.
10. Y. Tufail, A. Matyushov, N. Baldwin, M.L. Tauchmann, **J. Georges**, A. Yoshihiro, S.H. Tillery, and W.J. Tyler. **Transcranial Pulsed Ultrasound Stimulates Intact Mammalian Cortex.** In the annual meeting of *Society for Neuroscience*, Oct. 17th-21st, 2009, Chicago, Illinois.
11. **J. Georges**, K. McGraw, P. Nolan, P. Deviche, and L. Beard**. Carotenoids, Neurodevelopment, and Vocal Performance in the Zebra Finch, *Taeniopygia guttata*.** In the annual meeting of *Society of Integrative and Comparative Biology*, Jan. 3rd-7th, 2007, Phoenix, Arizona.

Presentations:

1. Arizona State University Neuroscience Seminar (February 2014) **Evaluating and Controlling Glioblastoma infiltration**
2. Barrow Neurological Institute Grand Rounds (June 2013) **Novel Contrast Agents for Rapid and Specific Diagnosis of Human Brain Tumors.**
3. American Association of Neurological Surgeons (April 2013) **Rapid and Specific Diagnosis of Human Astrocytic Brain Tumors by Immediate Ex Vivo Imaging.**
4. American Association for Cancer Research; State-of-the-Art Molecular Imaging in Cancer Biology and Therapy (February 2013) **Rapid and Specific Diagnosis of Human Astrocytic Brain Tumors by Immediate Ex Vivo Imaging.**
5. Barrow Neuroscience Symposium (September 2012) **Rapid and Specific Diagnosis of Human Astrocytic Brain Tumors by Immediate Ex Vivo Imaging.**
6. Stanford University; Irving Weissman Stem Cell and Regenerative Medicine Laboratory Conference (August 2011) **Aquaporin-1 Mediated Infiltration of Glioblastoma.**
7. Society for Neuro-Oncology (November 2011) **Aquaporin-1 Promotes Infiltration of Glioblastoma Multiforme and Predicts Patient Survival.**
8. Mount Desert Island Biological Laboratory (June 2010) **Three-Dimensional Microscopic Tracking of Human Glioma Cell Infiltration.**
9. Society of Integrative and Comparative Biology poster presentation (February 2007) **Carotenoids, Neurodevelopment, and Vocal Performance in the Zebra Finch, Taeniopygia guttata.**

Patents

- Sulforhodamine 101 as an intraoperative contrast agent for specific identification of reactive astrocytes and astrocytic tumors (pending).
- FRET-based aptamers for intraoperative visualization and diagnosis of central nervous system B-cell lymphoma (in preparation).

APPENDIX B

POSTER

SOCIETY FOR NEURO-ONCOLOGY

ANNUAL MEETING (2011)

AQUAPORIN-1 PROMOTES INFILTRATION OF GLIOBLASTOMA AND PREDICTS PATIENT SURVIVAL

Aquaporin-1 Promotes Infiltration of Glioblastoma Multiforme and Predicts Patient Survival

Joseph Georges1, Gay Samuelson1, Erik P. Sulman4, Kenneth D. Aldape4, Anjan Mitra4, Anna Joy1, Yao Hsiang1, Michelle McKinlin2, Anna Yoshikawa1, Darla Carpenter2, Lacy Butler2, Burt G. Feuerstein1,3
1Barrow Neurological Institute, Phoenix, AZ, 2Arizona State University, Tempe, AZ, 3University of Arizona College of Medicine – Phoenix, 4 Departments of Radiation Oncology and Pathology, the University of Texas M.D. Anderson Cancer Center, Houston, TX

Abstract

Glioblastoma (World Health Organization grade 4 glioma; GBM) are highly vascular, infiltrative tumors with 12-15 month median patient survival. Standard treatment provides modest survival benefit. Since GBM are infiltrative, local therapies do not remove all neoplastic elements, and appropriate therapeutic alternatives for infiltrative cells are not available. This project addresses a potential therapeutic target, the water channel protein aquaporin 1 (aqp1). Our clinical data indicate AQP1 RNAand Aqp1 protein are independently prognostic. We developed *in vitro* assays to model likely mechanisms underlying the clinical effects of AQP1. These results suggest that AQP1 alters the motility of GBM, but not cell proliferation and cell survival. Our results suggest that aqp1 protein is a viable therapeutic target.

Introduction

New brain tumors arise in more than 40,000 Americans each year [1]. They are the second most common cause of cancer death up to age 35, and are most common among middle-aged and older adults. About half of brain tumors are primary with grade IV (GBM) being the most common. Current standard GBM treatment is surgical resection followed by radiation and treatment with the alkylating agent, temozolomide [2]. Aggressive resection slightly improves survival. However, remaining infiltrative cells may lead to recurrence. Thus, controlling GBM infiltration could increase the extent of resection and improve patient survival. This project addresses a potential therapeutic target, the water channel protein aquaporin 1 (aqp1). Literature suggests expression of the aquaporin 1 (AQP1) gene correlates negatively with patient survival, and links it to cell movement . We developed *in vitro* and *in vivo* assays to model likely mechanisms underlying the clinical effects of aqp1These motility changes occur without effect to glioma cell proliferation or cell survival. Our results suggest that aqp1 protein is a viable therapeutic target. We are conducting further studies to determine aqp1's mechanistic role in GBM motility, and the therapeutic efficacy of targeting aqp1 function for the treatment of GBM.

This work was supported by:
-The Barrow Neurological Foundation (BGF, AJ, AM) and the Bruce T Halle Family Foundation (BGF).
-Welch Scholars Grant
-Arizona Biomedical Research Commission
-ASU School of Life Sciences
-NIH NO1
-American Brain Tumor Association
-American Society for Radiation Oncology (ASTRO)
-NIH K23-RR024149

Results

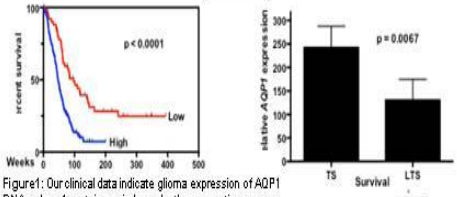

Figure1: Our clinical data indicate glioma expression of AQP1 RNAand aqp1 protein are independently prognostic.

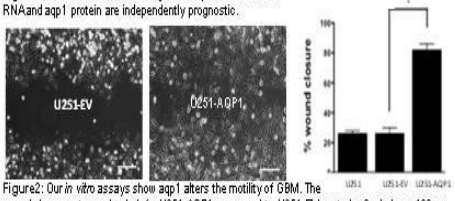

Figure2: Our *in vitro* assays show aqp1 alters the motility of GBM. The wound closure rate quadrupled for U251-AQP1 compared to U251-EV controls. Scale bar= 100*um*

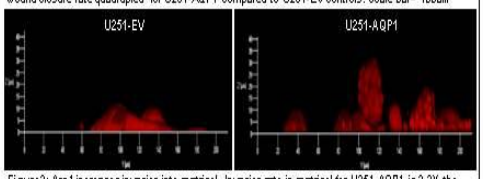

Figure3: Aqp1 increases invasion into matrigel. Invasion rate in matrigel for U251-AQP1 is 2-3X the rate of U251-EV after 24hr incubation .

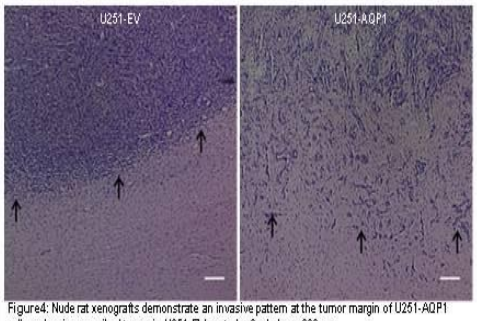

Figure4: Nude rat xenografts demonstrate an invasive pattern at the tumor margin of U251-AQP1 cells and a circumscribed tumor in U251-EV controls. Scale bar= 200*um*

Methods

- AQP1 protein and message assayed by IHC and qRT-PCR from 187 patient samples.
- AQP1 cDNA subcloned into retroviral expression vector pLXSN.
- Human glioma cell line U251 infected with pLXSN viral particles to produce Aqp1 overexpressing cells (U251-AQP1) and empty vector cells (U251-EV).
- Engineered cell lines screened In-vitro for proliferation, growth, cell adhesion, and motility.
- Orthotopic xenografts produced to study histology and survival.

Summary and Conclusions

- Aquaporin 1 protein and message gauge GBM patient outcome, and are independent prognostic factors in GBM patients (data not shown).
- AQP1 expression correlates directly with cell migration and invasion.
- Nude rodent model suggests a relationship between poor survival and aqp1 expression in human disease relates to aqp1's effects on tumor infiltration.
- Combined, the data suggest aqp1's clinical effects are related to its effects on motility, and not on cell growth or survival.
- Aqp1 is a likely candidate for therapeutic intervention.

References

1. *National Cancer Institute: Surveillance, Epidemiology and End Results (SEER) Database.*
2. Hegi, M.E., et al., *MGMT gene silencing and benefit from temozolomide in glioblastoma.* N Engl J Med, 2005. **352**(10): p. 997-1003.

APPENDIX C

POSTER

AMERICAN ASSOCIATION OF NEUROLOGICAL SURGEONS

ANNUAL MEETING (2013)

EX VIVO NEUROPATHOLOGY: IMMEDIATE AND SPECIFIC DIAGNOSIS OF HUMAN ASTROCYTIC BRAIN TUMORS

Ex Vivo Fluorescence Neuropathology: Immediate and Specific Diagnosis of Human Astrocytic Brain Tumors

BARROW Neurological Institute

Joseph F Georges,BS[1,2]; Nikolay L Martirosyan,MD[1]; Jennifer Eschbacher,MD[1]; Joshua Nichols,BS[3]; Maya Tissot,BS[1]; Aqib H Zehri,BS[3]; George AC Mendes, MD[1]; Anna Joy, PhD[1]; Ali Elhadi, MD[1]; Mark C Preul,MD[1]; Burt G Feuerstein,MD/PhD[3]; Robert F Spetzler, MD[1];Trent Anderson,PhD[3]; and Peter Nakaji, MD[1]

(1) Barrow Neurological Institute - St. Joseph's Hospital and Medical Center, Phoenix, Arizona. (2) Arizona College of Osteopathic Medicine - Midwestern University, Glendale, AZ. (3) Department of Basic Medical Sciences, University of Arizona - College of Medicine Phoenix, Phoenix, AZ

Introduction

Surgical resection of brain tumors is guided by intraoperative diagnostics. However, frozen section analysis, the method for obtaining these diagnoses, lacks the specificity to effectively differentiate some tumors with conflicting treatment plans (ie; astrocytoma and lymphoma). When specificity is required, clinical teams must typically wait 24-72 hours for a diagnosis from post-operative antibody staining of biopsied tissue. This timeframe precludes intraoperative feedback, and can result in additional surgeries for a patient if surgery is prematurely halted. Here we show that live cell imaging of fresh human brain tumors rapidly labeled with the physiological fluorophore Sulforhodamine 101 (SR101) can rapidly differentiate astrocytic tumors and reactive astrocytes from non-astrocytic brain tumors with antibody-like specificity in a time frame that supports intraoperative decision-making.

Methods

In Vitro Labeling: We acquired human glioma cell line U251 and human CNS lymphoma cell line MC116 from American Type Culture Collection (ATCC).U251 glioma cells were labeled by incubating 100,000 cells on a collagen-coated glass-bottom dish (MatTek). After 24 hours, the medium was replaced with artificial cerebrospinal fluid (aCSF) containing 2 μM SR101 (Sigma) for 20 minutes, followed by two 5-minute washes with standard aCSF.

Animals: Fifteen male Crl:NIH-Foxn1rnu rats (5 weeks age) were obtained from The Charles River Laboratories International, Inc. (Wilmington, MA). U251 (n=9 rats) or MC116 cells (n=6 rats) were implanted through a bur hole at a depth of 4.5 mm below the surface of the brain after the syringe (Hamilton). The cell suspension was infused using a UMP3-1 UltraMicroPump microinjector (WPI, Sarasota, FL) set to a volume of 10 μL with an infusion rate of 3.00 μL/minute. The bur hole was covered with bone wax, the skin incision was sutured, and the rats were allowed to recover. Experiments were performed in accordance with the guidelines and regulations set forth by the National Institutes of Health Guide for the Care and Use of Laboratory Animals and were approved by the Institutional Animal Care and Use Committee of the Barrow Neurological Institute of St. Joseph's Hospital and Medical Center, Phoenix, Arizona.

Acute slices: Twenty-eight days after implantation, rats were deeply anesthetized using the xylazine/ketamine mixture as described previously. They were immediately decapitated, and their brains were removed. Immediately, coronal slices (350 μm thick) were cut from the cerebral cortex on a Leica VT1200 vibratome in aCSF containing the following (in mM): 126 NaCl, 26 NaHCO3, 2.5 KCl, 1.25 NaH2PO4, 2 MgSO4, 2 CaCl2 and 10 glucose, pH 7.4. Slices were then incubated at room temperature in aCSF containing 2μM SR101 for 20 minutes followed by a 10-minute wash in aCSF. A two-tailed paired t-test with alpha set to 0.05 was used to compare mean fluorescence intensity (MFI) between tumor cells and reactive astrocytes

Co-labeling: Acute xenograft slices were incubated with the fixable version of SR101 (Texas Red Hydrazide; Sigma), washed at room temperature, and fixed with 4% paraformaldehyde for 12 hours at 4° C. The sections were rinsed in phosphate-buffered saline, permeabilized with 0.3% triton, and blocked with CAS block (Invitrogen). The GBM xenograft slices (9 slices from 3 animals) were incubated in anti-GFAP primary antibody (Millipore; 1:500) for 12 hours, and the lymphoma sections (9 slices from 3 animals) were incubated in anti-CD20 primary antibody (Millipore; 1:250) for 12 hours. Sections were then rinsed and incubated with AlexaFluor488 secondary antibody (Invitrogen), followed by DAPI (Invitrogen) nuclear counterstain and mounted on slides with vectashield (Vector labs) and No 1.5 coverslips (VWR).

Stereology: We selected one rostral, midline, and caudal acute slice from each brain containing tumor incubated with fixable SR101. Glioma slices were immunofluorescently stained for GFAP, and slices containing lymphoma were stained for CD20. In each slice, 10 randomly selected region of tumor (150 μm2) were optically sectioned to 50 μm with a Zeiss 710LSM. The first 5 μm of each image stack was discarded to minimize counts from cells damaged during sectioning. A maximum intensity projection image was generated from the remaining 45 μm, and a stereology dissector was overlaid onto the image. Cells within the dissector and those in contact with its left and bottom edges were counted for either GFAP or CD20 positivity, SR101 positivity, and DAPI positivity.

Human samples: Preoperatively, 65 patients with one of 11 common brain tumors signed an informed consent for participation. Samples were obtained at the time of craniotomy from within the tumor mass at a location determined to be safe by the surgeon. Tissue samples were placed in ice-cold aCSF containing 2 μM of SR101 and were transported from the operating room to the laboratory. There, the samples were rinsed with aCSF (10 minutes), and imaged within 30 to 40 minutes of biopsy. Investigators conducting imaging experiments were unaware of the pathological diagnosis. The diagnosis was determined by traditional immunohistochemistry and paraffin-embedded hematoxylin and eosin staining. For the purpose of comparisons, the histopathological diagnosis made by a board-certified neuropathologist was accepted as the final diagnosis.

1. Cell Culture: SR101 rapidly labels human astrocytoma cells in culture.

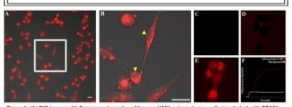

Figure1: (A) DIC image with fluorescent overlay of human U251 astrocytoma cells incubated with SR101. (B) Inset showing cytoplasmic filling of cells and delineation of cell nuclei (arrowheads). (C) Live cell imaging of cells before, (D) immediately after, and (E) 60 seconds after incubation with SR101. (F) Plot of change in fluorescence intensity in cultured astrocytoma cells after incubation with SR101. Scale bar equals 20um.

2. Rodent Xenografts: SR101 identifies tumor core and tumor margin in rodent xenografts.

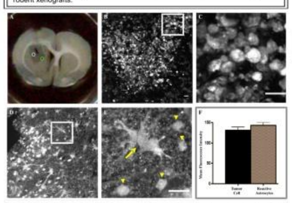

Figure2: (A) Acute slice containing U251 derived tumor. Representative core and margin regions identified by white circle and green circle respectively. (B) Confocal fluorescence image of SR101-labeled tumor core. (C) High magnification of inset showing typical morphology of U251cells. (D) Image of tumor margin with SR101 labeled cells. (E) Inset of morphologically identified reactive astrocyte (arrow) surrounded by glioma cells (arrowheads) near the tumor margin. (F) Mean fluorescence intensity of U251 cells and reactive astrocytes normalized to background. Note lack of statistical significance in MFI between the two cell types. Scale bar equals 20um.

3. Tumor Core vs Margin: SR101 morphologically differentiates astrocytoma cells from reactive astrocytes at the tumor margin.

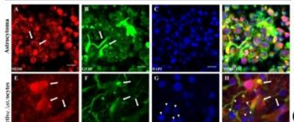

Figure 3: Images taken from the core of the astrocytoma (A-D). SR101 fills the cell bodies of GFAP-positive cells in the tumor core, and fills astrocytic processes (arrows). Note the significant overlap of GFAP, DAPI and SR101 in the merged image. **Images taken from the margin of the astrocytoma (E-H).** Fixable SR101 fills cell bodies of GFAP-positive cells at the tumor margin. Solid arrows identify SR101 and GFAP positive cells. Note the appearance of DAPI positive cells (arrowheads) unlabeled by SR101 or GFAP that are selectively observed at the astrocytoma margin. Scale bar equals 20um.

4. Astrocytoma vs Lymphoma: SR101rapidly differentiates human astrocytoma from CNS lymphoma in rodent xenografts

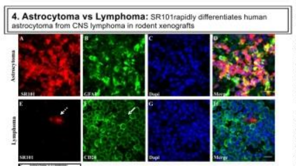

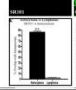

Figure 4:Confocal imaging of acute slices taken from xenograft animals implanted with astrocytoma cells (U251)(Top) or lymphoma cells (MC116)(Middle), and stained with SR101 and specific markers for Astrocytoma (GFAP) or Lymphoma (CD20). Top: Region from U251 astrocytoma acute slice incubated with fixable SR101 and counterstained with GFAP and DAPI (A-D). Middle: (E) SR101 labels a single cell (dashed arrow) in a MC116 xenograft lymphoma region. (F) CD20 immunostaining labels lymphoma cells, but does not label region containing SR101-positive cell (solid arrow). (G) DAPI counterstain of cell nuclei in field of view. (H) Merged lymphoma image indicating poor colocalization of SR101 and CD20. Scale bar equals 20um. Bottom: Confocal stereology of acute slices. (K) SR101 significantly overlaps with GFAP positive astrocytoma cells (86.53%) compared with CD20 lymphoma cells (1.58%) (p=0.0001).

5. Human Astrocytic BrainTumors vs Non-Astrocytic Brain Tumors

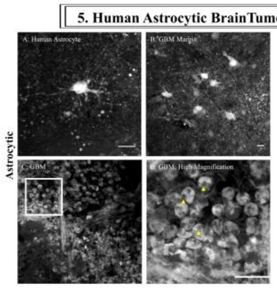

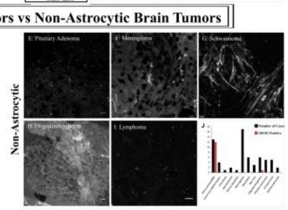

Figure 5: Human brain tumor biopsies rapidly stained with SR101 and imaged with a confocal microscope. SR101 selectively labels human astrocytes and astrocytic brain tumors (A-D). (A) Cell with astrocytic morphology from human brain labeled with SR101. (B) GBM margin with morphologically distinct tumor cells and reactive astrocytes (C) Grade IV astrocytoma. (D) Inset from C; hypercellularity and nuclei (arrowheads) are evident. **Non-astrocytic tumors absent of cells cytoplasmically filled with SR101 (E-I).** Dark regions in tissue indicate location of cell bodies. (E) Pituitary Adenoma, (F) Meningioma, (H) Oligodendroglioma and (I) Lymphoma are negative for SR101 staining. (J) Case distribution. Scale bar equals 20um.

Results

1. SR101 rapidly fills the cytoplasm of human astrocytoma cells in culture and delineates cell nuclei.
2.SR101 rapidly labels astrocytoma cells and reactive astrocytes in acute slices generated from rodent orthotopic astrocytoma xenografts
3. SR101 colocalizes with GFAP to selectively label astrocytoma cells and reactive astrocytes. Much like GFAP staining, SR101 morphologically differentiates astrocytoma cells from reactive astrocytes.
4. SR101 rapidly differentiates astrocytoma from CNS lymphoma in rodent orthotopic xenografts. In acute slices, SR101 labels 86.53% of astrocytoma cells and 2.17% lymphoma cells.
5. SR101 labeling and imaging of *ex vivo* human tissue could be completed in 30 minutes. SR101 rapidly labeled reactive astrocytes and selectively identified 12 of 13 astrocytomas. In non-astrocytic tumors, SR101 labeled cells that resembled reactive astrocytes but not tumor cells. SR101 did not label CNS lymphoma or the majority of oligodendroglioma biopsies.

Conclusions

We have demonstrated a technique for identifying the most common primary brain tumor, astrocytoma, by *ex vivo* exposure to the fluorescent dye SR101. This technique can provide specific cellular and molecular information necessary for diagnosis during surgery. We tested the specificity of SR101 in human cell culture, orthotopic rodent xenografts, and human tumor samples. Compared to the current standard of immunocytochemistry and final pathological paraffin-embedded diagnoses, SR101 provided more rapid and equally accurate identification of astrocytic tumors in all model systems. In human samples, SR101 provided effective visualization and differentiation of astrocytic tumors and, most importantly, their margins.

Improvements in timely and accurate intraoperative diagnoses are profoundly needed in clinical neurosurgery. Current diagnostic techniques rely on visualization of tissue with standard light microscopes and conventional contrast agents, a process that has evolved little over the last century. Here, we have shown that fluorescent labeling of *ex vivo* tissue coupled with confocal imaging provide clear diagnostic benefits compared with current techniques. Our technique allows visualization of pathological tissue without freezing, fixing, or sectioning. Images from tissue can provide a diagnosis within minutes—well within a time frame required to effectively guide a surgical approach and patient care while surgery is still in progress.

We envision that fluorescence imaging of *ex vivo* tissue will become a common technique in pathology departments in the near future. Our results here have clearly indicated the potential utility of SR101 for meeting the important clinical need of differentiating high-grade astrocytoma from CNS lymphoma. Although the macroscopic appearance of these tumors is similar intraoperatively, their treatment plans are markedly distinct. Astrocytomas require maximal safe resection to provide survival benefits to patients, while lymphomas are best biopsied and treated with adjuvant therapy. Differentiating these tumors requires a surgical biopsy followed by a minimum of 24 hours for diagnostic processing. We found these tumors could be differentiated by SR101 staining and confocal microscopy within 30 minutes of biopsy. This information could allow rapid modification of a surgical plan with consequent improvement of clinical outcomes.

There are important considerations to diagnostic use of SR101. Staining with this agent requires tissue to be alive and relatively healthy when it is incubated with the dye. Damaged cells have been reported to uptake the dye. However, we encountered no significant false positives in our experiments. A practical limitation to the widespread use of SR101 includes the need for immediate incubation of resected tissue in the operating room. Immediate *ex vivo* imaging using specific fluorescent probes is not yet part of clinical pathological practice. Therefore, few pathology laboratories have confocal microscopes. Modernization of pathology departments would be needed to overcome these limitations.

SR101 rapidly and selectively labels human astrocytic tumors and astrocytes. To our knowledge, our results represent the first use of a functional dye on living human brain tumor tissue to provide a clinically meaningful immediate *ex vivo* histopathological diagnosis. There is compelling reason to believe that this method is only the first foray into a broad new area of pathology that has become possible because of the rapid and dramatic advances in fluorescence probes and fluorescence imaging techniques. Application of this technique to other tumors and diseases will only be limited by the identification of specific molecular targets and the development of targeted fluorophores. These imaging techniques may have profound implications for improving patient diagnosis, clinical outcomes, and our understanding of human tumor pathophysiology.

References

1. Beeman SC, Georges JF, Bennett KM. Toxicity, biodistribution, and ex vivo MRI detection of intravenously injected cationized ferritin. Magn Reson Med. 2012.

2. Kafitz KW, Meier SD, Stephan J, Rose CR. Developmental profile and properties of sulforhodamine 101--Labeled glial cells in acute brain slices of rat hippocampus. J Neurosci Methods. 2008; 169:84-92.

3. Mouton PR. Principles and Practices of Unbiased Stereology: An Introduction for Bioscientists. Baltimore: The Johns Hopkins University Press; 2002.

4. Nimmerjahn A, Kirchhoff F, Kerr JN, Helmchen F. Sulforhodamine 101 as a specific marker of astroglia in the neocortex in vivo. Nat Methods. 2004;1:31-37.

5. Nimmerjahn A, Helmchen F. In vivo labeling of cortical astrocytes with sulforhodamine 101 (SR101). Cold Spring Harb Protoc. 2012;2012:326-334.

APPENDIX D

POSTER

AMERICAN ASSOCIATION OF NEUROLOGICAL SURGEONS

ANNUAL MEETING (2014)

CONTRAST-FREE MICROSCOPIC ASSESSMENT OF GLIOBLASTOMA BIOSPECIMEN CELLULARITY PRIOR TO BIOBANKING

Contrast-Free Microscopic Assessment of Glioblastoma Biospecimen Cellularity Prior to Biobanking

Joseph F Georges,BS*[1,2]; Aqib H Zehri,BS*[1,3]; Elizabeth Carlson[4], Jennifer Eschbacher,MD[1]; Joshua Nichols,BS[3]; Nikolay L Martirosyan,MD[1], Layla Ighaffari[4]; Burt G Feuerstein,MD/PhD[3]; Robert F Spetzler, MD[1];Trent Anderson,PhD[3]; Mark C Preul,MD[1]; Kendall Jensen, PhD[4]; and Peter Nakaji, MD[1]

(1) Barrow Neurological Institute - St. Joseph's Hospital and Medical Center, Phoenix, Arizona. (2) Arizona College of Osteopathic Medicine - Midwestern University, Glendale, AZ. (3) Department of Basic Medical Sciences, University of Arizona - College of Medicine Phoenix, Phoenix, AZ. (4) Translational Genomics Research Institute, Phoenix, AZ

Introduction

Glioblastoma (World Health Organization grade 4 glioma; GBM) is the most common primary brain tumor with a 12-15 month median patient survival. Improving patient survival includes better understanding the biological mechanisms of GBM tumorgenesis and seeking targeted molecular therapies. Central to furthering these advances is the collection and storage of surgical biopsies (biobanking) for research. Unfortunately, due to the necrotic feature of GBM and our inability to assess tissue prior to biobanking, the majority of biobanked GBM samples lack appropriate cellularity to be utilized in research. This work addresses an imaging modality (confocal reflectance microscopy; CRM) for safely screening GBM biopsies prior to biobanking to increase the quality of tissue provided for research and clinical trials. CRM is a light scattering imaging modality that can generate contrast from cells and tissue without exogenous contrast agents. Our data indicate that CRM can immediately identify cellularity of tissue biopsies from animal models of GBM. When screening fresh human biopsies, CRM can differentiate a cellular GBM biopsy from a necrotic biopsy. Compared to controls, CRM does not alter the DNA, RNA, or protein expression of sampled tissue. Our data illustrate CRM's potential for rapidly and safely screening clinical biopsies prior to biobanking. This information can augment data gained from resected tissue for molecular and translational research, and for determining the eligibility of GBM patients for enrollment into clinical trials. Secondly, this method provides a digital histological record of a biopsy that can be stored along with a biobanked specimen. Our data show CRM to be a robust screening technique that can improve the quality of tissue biobanked for glioblastoma patients.

Methods

Intracranial implantation: Nude rats (n=5) were anesthetized by intramuscular injection of a mixture of 10 mg/kg xylazine and 80 mg/kg ketamine (Wyeth, Madison, NJ) and placed in a small animal stereotactic headframe (Model 900, David Kopf Instruments, Tujunga, CA). An incision was made to expose bregma. A bur hole was made 3.5 mm lateral to bregma and human glioma cells (U251; ATCC) were infused at a depth of 4.5 mm below the surface of the brain. The bur hole was covered with bone wax, the skin incision was sutured, and the rats were allowed to recover.

Rodent tissue: Twenty-eight days after implantation, rodent xenografts were deeply anesthetized using xylazine and ketamine. They were immediately decapitated, and their brains were removed. Immediately, coronal slices (350 µm thick) were cut from the cerebrum on a Leica VT1200 vibratome and placed in artificial cerebrospinal fluid (aCSF). Slices were then fixed in 4% paraformaldehyde at 4 degrees Celsius overnight and washed three times with phosphate buffered saline (PBS). Three tumor containing slices per animal were incubated with DAPI for 45 minutes at room temperature, rinsed three times with PBS, and placed into number 1.5 glass bottom dishes (MatTek) for imaging. A coefficient of determination analysis was used to compare cells identified with CRM to cells labeled with DAPI. Rodents utilized for molecular experiments (n=2) were deeply anesthetized using xylazine and ketamine and rapidly decapitated. Whole brains were placed in ice cold aCSF and sectioned into 1mm coronal sections using a rodent brain block. The cerebrum from each section was blocked into 4 equivalent sections. Two sections were immediately frozen in liquid nitrogen (LN2) for reference. At 15, 30, 45, 60, 90, and 120 minutes two sections were placed into glass bottom dishes. At each time point, the cortex, corpus callosum, and caudate/putamen from one section was imaged with CRM. As a control, one section was simultaneously placed on the stage of the microscope but not imaged. Each section was frozen in LN2 and stored at -80° C for assessment of DNA, RNA, and protein.

Imaging: All samples were imaged in uncoated No.1.5 glass-bottom dishes (MatTek corp). CRM was conducted with a Zeiss inverted 710 laser scanning confocal microscope equipped with a 40x/1.2NA water emersion objective. A 633-nm diode laser was used for reflectance imaging. A 405-nm diode laser and 430-490nm emission collection was used for Dapi imaging. The confocal aperture was set to one Airy unit for all imaging. The laser and gain values were set to fill the dynamic range of the photomultiplier tube, and the frame size was set to sample at nyquist. Images were collected in 12-bit format absent of nonlinear processing.

DNA Isolation & Analysis: DNA was isolated from brain tissue using the QIAamp DNA Mini (Qiagen), per manufacter's instructions. DNA was quantified using the Nanodrop Spectrophotometer (Thermo Scientific). Samples were loaded in equal concentrations (100 ng) in a 1% agarose gel with ethidium bromide and imaged on an Alpha Imager (Alpha Imager).

RNA Isolation and Analysis: Tissue was homogenized in 500 ul Ambion's Cell Disruption Buffer (Life Technologies) and subsequently isolated using Ambion's mirVana kit (Life Technologies), per manufacturer's instructions. RNA concentrations were determined using the Nanodrop Spectrophotometer (Thermo Scientific) and provided information for the dilutions necessary to remain within the dynamic range of the Bioanalyzer. The integrity of the RNA was assessed using Agilent 2100 Bioanalyzer Nanochips (Agilent Technologies).

Western Blot Analysis: Frozen tissue was sectioned on dry ice and protein lysate was made by placing brain sections into 750 ul Ambion's Cell Disruption Buffer (Life Technologies). Protein concentrations were quantified by BCA (Pierce, Thermo Scientific) and 18 ug/lane was loaded in 4-12% NuPage Bis-Tris gels (Invitrogen) and run using NuPage electrophoresis reagents (Invitrogen). Protein was transferred onto Novex nitrocellulose membrane (Invitrogen). Blots were probed for AKT and GAPDH.

Statistical Analysis: Coefficient of correlation (R^2 value) was determined between DAPI stained nuclei and nuclei detected by RCM using Graphpad Prism. Differences were considered statistically significant for probability of less than .05. The Agilent 2100 Bioanalyzer provided an RNA integrity number (RIN) calculated algorithmically by including the 28s/18s ribosomal RNA bands, the region before the peaks, signal areas, and intensities. An elevated threshold baseline and a decreased 28s:18s ratio are both indicative of RNA degradation while high 28S and 18S ribosomal RNA peaks as well as a small amount of 5s RNA or a RNA number 10 greater than 7.5 are indicative of intact RNA. Image J was used to determine density (intensity) of bands on a western blot.

Clinical Samples: This research was approved by the Institutional Review Board of St. Joseph's Hospital and Medical Center and Barrow Neurological Institute, Phoenix, Arizona, where all surgery was performed. Preoperatively, patients signed an informed consent for participation. Samples were obtained at the time of craniotomy from within the tumor mass at a location determined to be safe by the surgeon. Tissue samples were placed in ice-cold aCSF and transported from the operating room to the pathology-based CRM system. Final diagnosis was determined by traditional immunohistochemistry and paraffin-embedded hematoxylin and eosin staining of the sampled tissue. For the purpose of comparisons, the histopathological diagnosis made by a board-certified neuropathologist was accepted as the final diagnosis.

1. Normal Brain: Confocal reflectance microscopy contrasts normal brain histological features.

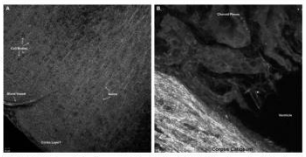

Figure1: Normal brain acute slices (A&B). (A) Rodent cortex. Confocal reflectance microscopy contrasts cell bodies, axons, and blood vessels in normal brain. Cell bodies appear as multiple hypointense circular regions within the tissue; note typical lack of cell bodies contrasted in layer 1 of the cortex. Myelinated axons are visualized as hyperintense fibers extending from cell bodies. **(B) Ventricle and corpus callosum.** White matter tracts in the corpus callosum generate a hyperintense reflectance signal. Individual cell bodies are contrasted in the choroid plexus. A lack of signal is appreciated from the fluid-filled ventricle.

2. Xenograft Brain: Confocal reflectance microscopy identifies cellular tumor in rodent brain slices.

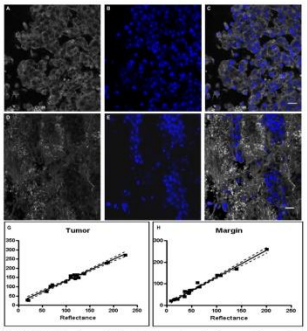

Figure2: Cellular Tumor (A-C). (A) Reflectance image of rodent xenograft tumor region; note shading of cell nuclei. (B) Dapi stain of identical tumor region identifies all cells in the field of view. (C) Overlay shows location of cells contrasted by reflectance to cells labeled with dapi. **Cellular tumor and acellular tissue interface (D-F).** (D) Reflectance image of cellular tumor and adjacent acellular region from rodent xenograft; note isolated cell populations. (E) Fluorescence confocal image of identical region labeled with dapi. (F) Overlay of reflectance and fluorescence images from tumor and peritumoral tissue interface. (G) Plot of coefficient of determination and confidence intervals for cells identified by reflectance imaging in tumor regions. r^2=0.97. (H) Plot of coefficient of determination and confidence intervals for cells identified by reflectance imaging at tumor and acellular tissue interface. r^2= 0.98. Scale bar equals 20um

3. Molecular Effects: Confocal reflectance microscopy does not alter the molecular characteristics of examined tissue.

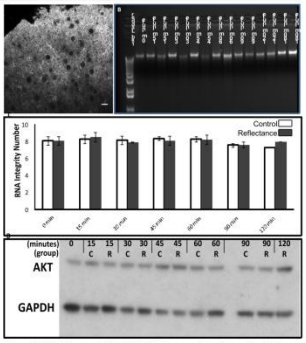

Figure 3: CRM does not alter DNA, RNA, or protein of examined tissue. A) CRM image of fresh brain tissue at cerebral cortex 90 minutes post-excision. Scale bar equals 20um. **B)** Gel electrophoresis of genomic DNA extracted from control and CRM imaged biopsies; note similar bands across time course. C=control and R= CRM. between imaged and control biopsies. **C)** Time course comparison of RNA integrity for all imaged and control samples; note similar RNA integrity for all samples. **D)** Western blot analysis showing expression of AKT over 120-minute time course. Protein signal did not degrade over time course or when exposed to CRM. R= Confocal Reflectance Microscopy, C= Control.

4. Clinical Application: CRM differentiates a cellular human GBM biopsy from a necrotic sample.

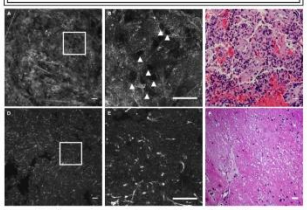

Figure 4: Reflectance imaging immediately identifies cellular and necrotic fresh human brain tumor biopsies. (A-C) Glioblastoma. A) Low magnification CRM image of *ex vivo* human GBM biopsy imaged with CRM. B) High magnification of cellular region identified from inset of A, note arrowheads identifying cells within region. C) Corresponding H&E image. **(D-F) Necrotic sample.** D) Low magnification image of *ex vivo* necrotic biopsy imaged with CRM. E) High magnification inset from D. Note lack of distinct cells. F) H&E from corresponding section. Scale bar equals 20um.

Results

1. Confocal reflectance microscopy contrasts cell bodies, blood vessels, and myelinated fibers in normal brain.
2. CRM can identify cellular regions in animal models of GBM.
3. Used within 120 minutes of biopsy, CRM does not alter the DNA, RNA, or Protein integrity of sampled tissue.
4. CRM can differentiate a cellular human GBM biopsy from a necrotic sample.

Conclusions

Our data illustrate the utility of confocal reflectance microscopy as a safe and rapid technique for identifying the cellularity of glioma tissue prior to biobanking. This imaging modality can be immediately utilized on fresh tissue samples without application of exogenous contrast agents, and without altering the molecular characteristics of examined tissued. CRM can provide a much needed tool for neurosurgery-neuropathology teams by maximizing the quality of tissue samples collected during surgical resection.

We found CRM did not alter the DNA, RNA, or protein that could be extracted and quantified from tissue biopsies screened up to 2 hours after resection. CRM images collected from these samples could be digitally stored and potentially recalled with biobanked specimens. We found CRM may have diagnostic utility, as many images revealed distinct morphological details such as; cellularity, vasculature, and necrosis (Figures 1,3, and Supplementary) typically identified with traditional histopathological H & E staining.

Many translational neuro-oncology studies rely on human GBM tissue samples that appropriately represent an original tumor. Unintentional utilization of necrotic or non-representative tissue samples in studies can lead to erroneous results that will not improve our knowledge of the disease. In studies that advance to clinical trials, patient biopsies are often screened to determine eligibility for a targeted clinical trial. CRM's nondestructive tissue assessment can ensure patients are not mistakenly excluded from potential life-prolonging treatments, particularly when standard therapy has failed. Screening for high quality tissue specimens with CRM can facilitate the advancement of our knowledge of gliomagenisis, and can ensure qualified patients receive potential life-prolonging therapies.

Current limitations of CRM include limited imaging depth of penetration. With our imaging parameters, CRM could assess tissue from the surface to 200-300 microns within. However, we did not find this limitation altered the accuracy of assessment of tissues in our studies. Additionally, few pathology departments contain the imaging hardware or personnel required to screen tissue biopsies with CRM. Modernization of pathology departments may include addition of confocal microscopes and other systems capable of CRM that will allow the screening of samples within two-hours time. Lastly, *ex vivo* CRM is limited by the ability to only assess tissue that is intraoperatively selected to represent tumor. A hand held intraoperative CRM device could potentially overcome human sampling error and allow assessment of tissue samples prior to resection.

CRM technology has shown utility in providing cellular and subcellular detail, specifically in diagnosing dermatological conditions, identifying neoplastic tissue and margins, and assessing diseased and normal liver tissue. Our study is the first to assess human brain tumor tissue solely with CRM. By quantifying DNA, RNA, and protein, we also demonstrate for the first time CRM's ability to assess tissue cytoarchitecture without altering tissue molecular integrity, meaning that no part of the tissue to be banked needs to be discarded in the assessment process.

References

1. Mouton PR. Principles and Practices of Unbiased Stereology: An Introduction for Bioscientists. Baltimore: The Johns Hopkins University Press; 2002.

2. Tilli MT, Cabrera MC, Parrish AR, Torre KM, Sidawy MK, Gallagher AL, Makariou E, Polin SA, Liu MC, Furth PA. Real-time imaging and characterization of human breast tissue by reflectance confocal microscopy. J Biomed Opt. 2007 Sep-Oct;12(5):051901.

3. Snuderl M, Wirth D, Sheth SA, Bourne SK, Kwon CS, Ancukiewicz M, Curry WT, Frosch MP, Yaroslavsky AN. Dye-enhanced multimodal confocal imaging as a novel approach to intraoperative diagnosis of brain tumors. Brain Pathology. 2013 Jan;23(1):73-81.